ANATOMY AND ASSEMBLY OF THE MCDOOGLE PLUTON NEAR SAWMILL LAKE, CENTRAL SIERRA NEVADA, CALIFORNIA

by

Michael Andrew Stearns

A thesis submitted to the faculty of
The University of Utah
in partial fulfillment of the requirements for the degree of

Master of Science

in

Geology

Department of Geology and Geophysics

The University of Utah

August 2009

THE UNIVERSITY OF UTAH GRADUATE SCHOOL

SUPERVISORY COMMITTEE APPROVAL

of a thesis submitted by

Michael Andew Stearns

This thesis has been read by each member of the following supervisory committee and by majority vote has been found to be satisfactory.

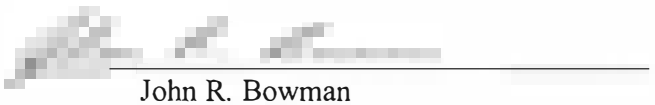

John R. Bowman

Barbara Nash

THE UNIVERSITY OF UTAH GRADUATE SCHOOL

FINAL READING APPROVAL

To the Graduate Council of the University of Utah:

I have read the thesis of Michael Andrew Stearns in its final form and have found that (1) its format, citations, and bibliographic style are consistent and acceptable; (2) its illustrative materials including figures, tables, and charts are in place; and (3) the final manuscript is satisfactory to the supervisory committee and is ready for submission to The Graduate School.

M. Bartley
ir: Supervisory Committee

Approved for the Major Department

Peter Associate Chair
Marjorie A. Chan
Chair/Dean

Approved for the Graduate Council

David S.
Dean of The Graduate School

ABSTRACT

This study examined the internal anatomy and assembly processes of the xenolith-rich (~30 vol %) McDoogle pluton of the John Muir Intrusive Suite (JMIS), part of the Sierra Nevada batholith. The McDoogle pluton is interpreted to have grown incrementally as a plexus of dikes emplaced synkinematically into the steep Sawmill Lake shear zone. The best exposed portion of the pluton near Sawmill Lake was investigated using detailed geologic and bulk magnetic susceptibility (BMS) mapping (1:3000 scale), structural analysis, and high-precision U-Pb geochronology.

The pluton is composed of five composite sheets of three different lithologic types arranged in mirror symmetry. The oldest, most heterogeneous, central phase grew antitaxially, meaning increments were added at the intrusive margins. Antitaxial growth preserves abundant in-situ wall-rock screens which are interpreted to mark contacts between increments. Folding patterns of the wall-rock screens suggest that the central phase grew from east to west. The younger intermediate and border phases were emplaced on both sides of the central phase, thus creating the mirror symmetry. The outer increments grew syntaxially, meaning increments were added at the centers of previous increments. The central phase terminates bluntly in the map area whereas the border phases continue southward and terminate as dike tips.

The McDoogle pluton rapidly intruded the Sawmill Lake shear zone at 95 Ma.

Three samples were processed for high-precision U-Pb zircon dating and produced ages that overlap within error (±0.1 Ma). The minimum permissible wall-rock displacement rate is 4 mm/yr, which exceeds normal local tectonic dilation rates of ~1 mm/yr. Data from the Bishop Pass phase of the Lamarck granodiorite, located further north in the JMIS, define a similar duration and minimum rate of growth.. Magmatic overpressure may account for the rapid dilation rate.

BMS mapping can distinguish and communicate subtle petrologic variations that traditional geologic mapping cannot. However, it is necessary to investigate what controls the BMS signal before large BMS surveys. The Sawmill Lake BMS map reflects the geologic map, but contains areas of high and low values that define tabular bodies which follow folded wall-rock screens, supporting structural interpretations. The correlation between BMS and color index (CI) was tested in nine samples. Ilmenite has much lower bulk susceptibility than magnetite, and therefore a rock that contains ilmenite in place of magnetite has a lower BMS for a given CI. Though, removing samples with significant ilmenite proportions did not improve the correlation between CI and BMS.

CONTENTS

ACKNOWLEDGMENTS

First, I would like to thank my advisor John Bartley, with whom I thoroughly enjoyed working and doing fieldwork. My committee members John Bowman and Barbara Nash have been very helpful, providing useful insight and feedback during the entire research process. Kristopher Clemons has provided enough moral, field, and scientific support to almost warrant authorship on this thesis. He has been a great friend through this entire endeavor. I would also like to thank Drew Coleman and Allen Glazner for their many thought provoking and helpful conversations. Jesse Davis, Michael Tappa, and Ayumi Shimokawa have been extremely helpful for all things U-Pb related. Denise Waterbury at the Owens Valley Lab was extremely helpful during all of my field seasons. Michael Dorais provided indispensable guidance during the EMPA analyses. Sarah Mazza, thank you for the SEM work for a person you had never met. Thanks to my fellow graduate students Matthew Heumann, Keith Beisner, Michele Mary, Ben Johnson, Jess Allen, and Rick Urash for very useful advice and discussion, geologic or not. This work is the product of my parents support that is too large to describe here. Funding for this project was provided by the National Science Foundation, the Geological Society of America Student Grant, the White Mountain Research Station Student Grant, and the University of Utah Department of Geology and Geophysics.

CHAPTER 1

INTRODUCTION

Our understanding of the fundamental processes that control pluton emplacement has changed very little in the last 30 years. Only recently have long-standing ideas been reexamined and challenged. These processes are critical to our understanding of how continental crust is made and how magmatic systems operate.

Several questions concerning the emplacement of plutons have yet to be definitively answered. First, how does the magma ascend from the source region, and second, how is space made in the crust? Traditionally, ascent and space making were thought to be accomplished by diapirism (Ramberg, 1970; Marsh, 1982), stoping (Culey and Joplin, 1937; Pignotta and Paterson, 2007), and to a lesser extent diking (including sills) (Pitcher and Berger, 1972; Hutton, 1982; Clemens and Mawer, 1992, Glazner and Bartley, 2006). Diapirism and stoping have been reexamined, and cannot significantly contribute to either the ascent or space-making process (Clemens and Mawer, 1992; Clemens, 1998). Diking may be a far more important ascent and space making mechanism than previously thought (Hutton, 1992; Petford et al., 2000; Bartley et al., 2008).

Third, what role do wall-rock tectonic processes play in the ascent and emplacement of plutons? It has become increasingly recognized that ductile shear-zones are conduits for magma and control emplacement of at least some plutons (Hutton et al., 1990; Tikoff and Teyssier, 1992; Saint Blanquat and Tikoff, 1997; Mahan et al., 2003; Clemons and Bartley, 2008).

Fourth, how long does pluton assembly take and what are the typical growth rates? Some large plutons have been recognized to grow over millions of years (Coleman et al., 2004; Glazner et al., 2004), whereas smaller plutons assembled by processes have grown over shorter time periods (Gracely, 2007). This suggests that plutons may grow at fairly uniform rates, but for drastically different lengths of time.

Fifth, what is the internal anatomy of a pluton and how can we recognize incremental growth? Understanding the anatomy of a pluton is critical to inferences about the ascent, assembly, and growth duration of the pluton. Wall-rock distribution within the pluton is one diagnostic feature of incremental growth. In crack-seal growth, different anatomies are predicted, depending on where increments are added. Syntaxial growth refers to addition at the center of the growing intrusion. Antitaxial growth refers to addition at the margins of the intrusion. Antitaxial growth predicts the presence of wall-rock screens because of the irregular nature of cracks. Perturbations in the dike's path isolates bodies of wall rock between two dikes. It is important to understand that, in this model, wall-rock screens were never completely engulfed in magma, but rather were isolated in situ by intrusion on one side, then the other. Wall-rock screens therefore are interpreted to mark contacts between increments.

Finally, what controls the lithologic variation of plutons that grow via diking? Plutons that grow by amalgamation of dikes have a relatively small volume of liquid magma at any stage of construction. This limits the effects, at the emplacement level, of magmatic differentiation processes such as side-wall fractionation, wall-rock contamination, and magma mixing (Glazner et al., 2004).

There are several reasons that the McDoogle pluton in the central Sierra Nevada, California, is an ideal place to address these questions. Exposure of the full width of the pluton allows for a detailed study of its anatomy. The recent alpine glaciation permits detailed outcrop examination. The preservation of abundant wall-rock screens that mark contacts between individual increments offers an opportunity to understand the anatomy at the increment scale. The abundance and pattern of lithologic variation allows examination of differentiation processes that affected the pluton over time.

It is an ideal laboratory because the Sierra Nevada is among the best studied magmatic arcs in the world. The regional mapping of Moore (1963) and mapping of the McDoogle pluton by Mahan (2000) enabled this study to focus on the detailed aspects of the best exposed portions of the pluton. Without the previous work, the detailed mapping would not have been practical. This study utilized geologic mapping at the 1:3000 scale, structural analysis, bulk magnetic susceptibility mapping, and high precision U-Pb zircon geochronology to investigate the best exposed areas of the McDoogle pluton.

Geologic setting

The western margin of North America has been shaped by a long and complex history. During the Proterozoic, the North American craton grew southwestward by accretion of several arcs (Hoffman, 1988; Dalziel, 1991). Late Proterozoic rifting of the western margin of the craton formed an ocean basin and, by the late Cambrian, a passive margin developed several hundred kilometers east of the current margin (Burchfiel et al., 1992). During the Paleozoic, passive-margin sedimentation continued until east-dipping subduction and collision of island arcs began in the Late Devonian (Poole et al., 1992). The collisions emplaced several large allochthons as far as 200 km onto the continent at the current latitude of the northern Sierra Nevada (Burchfiel et al., 1992). Subduction and arc collision continued during the Mesozoic, developing fold and thrust belts and volcanic arcs from Mexico to Alaska (Saleeby et al., 1992; Burchfiel et al., 1992). By the late Cretaceous, the major thrusting activity had propagated eastward as far as central Utah (Burchfiel et al., 1992). The Sierra Nevada batholith represents major magmatism produced by long-lived subduction along the continental margin and ranges in age from Triassic to late Cretaceous. Sierran magmatism ceased by 80 Ma (e.g., Glazner and Coleman, 1997) whereas foreland thrusting persisted until the Eocene (Burchfiel et al., 1992).

Sierra Nevada batholith

The Sierra Nevada batholith is a northwest-trending (N25W) magmatic arc constructed of hundreds of plutons. Magmatic activity occurred between 220 Ma and 80

Ma (Triassic to Cretaceous), with two voluminous episodes around 165 Ma and 100 Ma (Stern et al., 1981; Chen and Moore, 1982; Bateman, 1992). Jurassic plutons are more abundant in the western area of the batholith (Bateman, 1992). During the Cretaceous, plutonism migrated from west to east at a rate of 2.7 km/m.y. (Chen and Moore, 1982). Most plutons are thought to have intruded at a depth between 7 and 15 km (Ague and Brimhall, 1988; Bateman, 1992; Renne et al., 1993). Several intrusive suites exist within the batholith. These are groups of plutons that are spatially and temporally linked, and seem to be cogenetic (Chen and Moore, 1982; Bateman, 1992). The three biggest from north to south are the Tuolumne, John Muir, and Whitney Intrusive Suites (Figure 1.1). The John Muir Intrusive Suite stretches from the Mammoth Lakes to Mount Baxter, and includes the Cretaceous Rock Creek granite, Lamarck granodiorite, Inconsolable granodiorite, Mono Creek granite, Lake Edison pluton, Mount Givens pluton, and the McDoogle pluton (Figure 1.2). The Mount Givens pluton is temporally and spatially related to the JMIS, but was not originally included as part of the intrusive suite. During intrusion of the JMIS subduction of the Farallon plate under North America was dextral oblique (Engebretson et al., 1985; Umhoefer, 2003).

Mount Pinchot 15' Quadrangle

The Mount Pinchot 15' Quadrangle is located south of Big Pine, California, in the east-central Sierra Nevada (Figure 1.3). It was first mapped by Moore (1963) at the 1:62,500 scale and contains all or parts of more than 20 plutons. The plutonic rocks vary in composition from leucogranite to gabbro. Several plutons within the quadrangle have

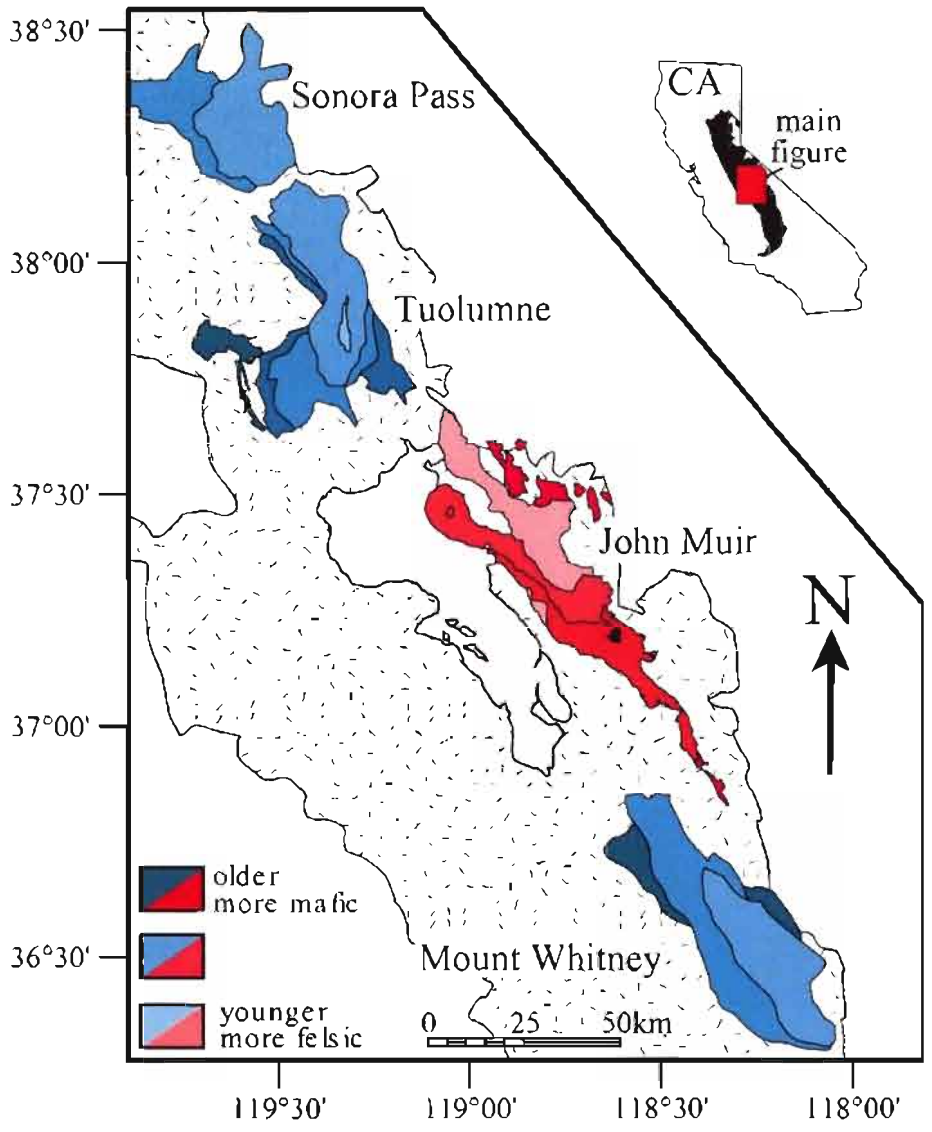

Figure 1.1: Regional map of the central Sierra Nevada, California. The major intrusive suites are colored blue and the John Muir Intrusive Suite (JMIS) pink. Older and mafic plutons are colored darker than younger felsic plutons. Figure adapted from Gracely (2007).

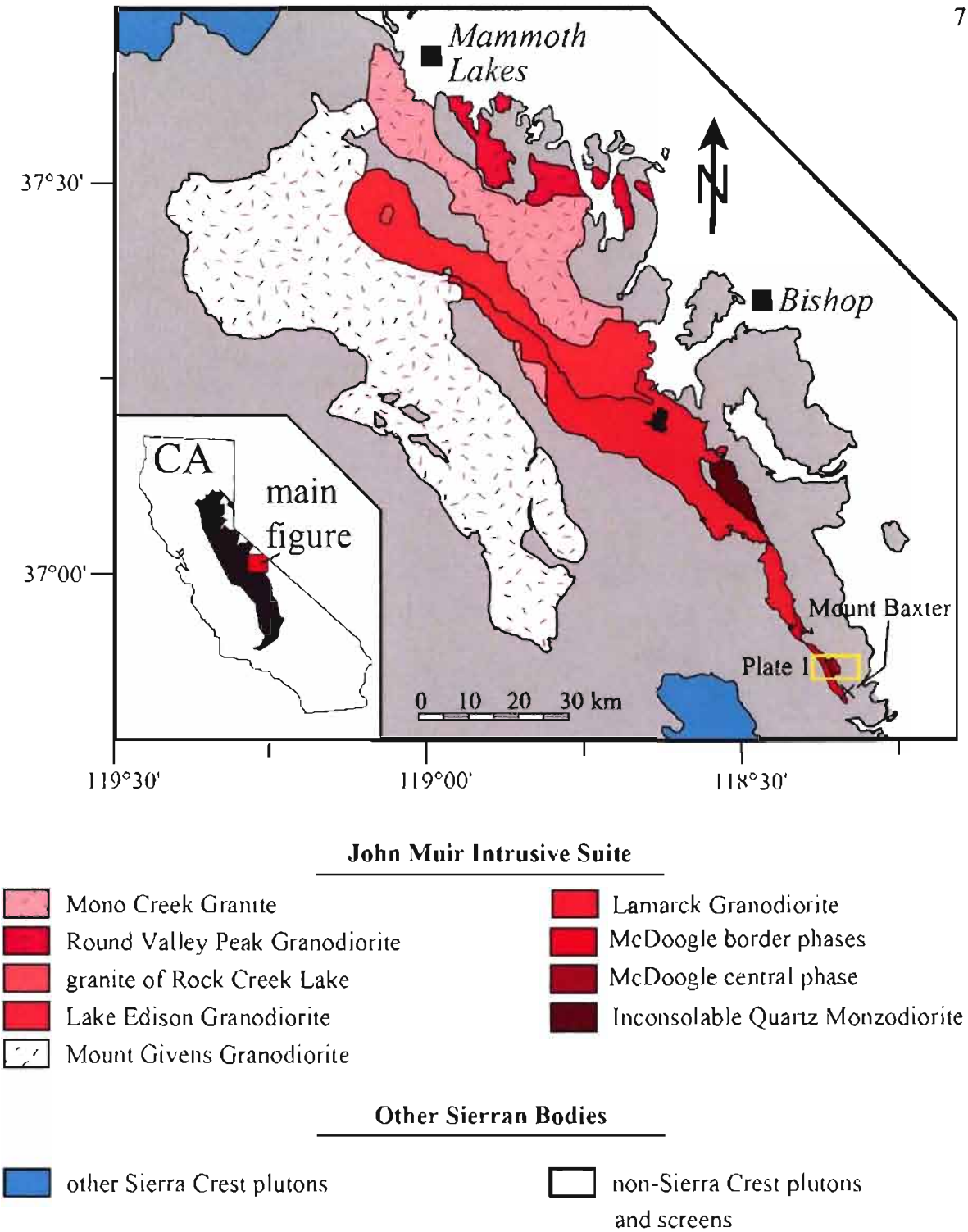

Figure 1.2: Simplified lithologic map of the John Muir Intrusive Suite (JMIS). The map area is located in the yellow box at the southern end of the JMIS. Figure adapted from Gracely (2007).

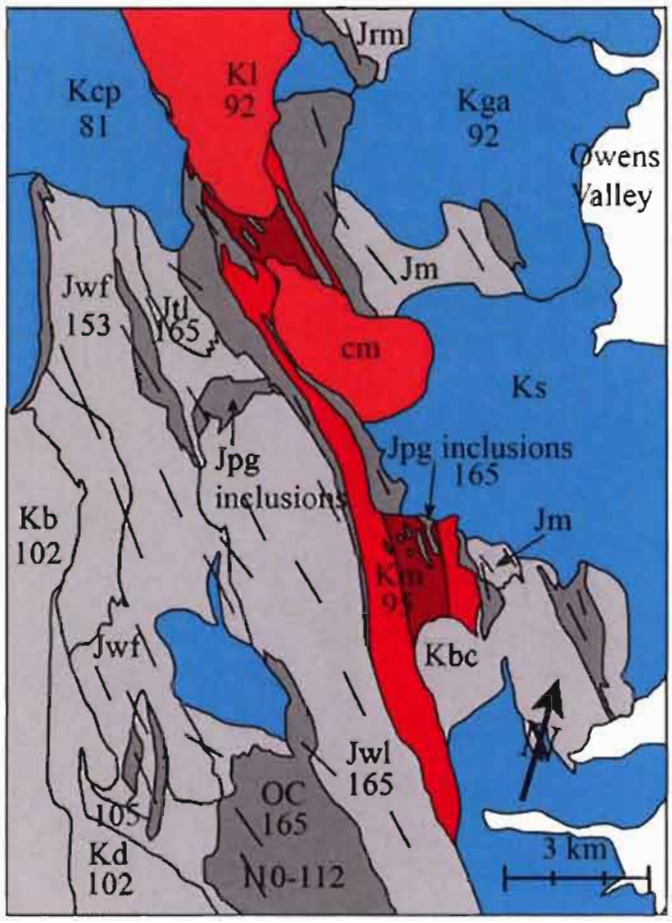

Figure 1.3: Lithologic map of the McDoogle pluton and nearby units. Other plutons included in the John Muir intrusive suite are colored pink. U-Pb zircon ages are included where available. Kcp, Cartridge Pass pluton; Kga, Goodale and Siberian plutons, and Aberdeen mafic complex; Ks, Spook pluton; Kl, Lamarck granodiorite; Kmc and Kmb, central and border phases of the McDoogle pluton; Kb, Bullfrog pluton; Kd, Dragon pluton; Jwf, White Fork pluton; Jtl, Twin Lakes pluton; Jwl, Woods Lake pluton; Jm, Mule Lake pluton; Jrm, Red Mountain Creek pluton. Other labels are OC, Oak Creek pendant; cm, Colosseum Mountain mass of the Lamarck granodiorite. The full width of the McDoogle is exposed near the ends of the pluton. Figure adapted from Moore (1963) and Mahan (2000).

been dated using the U-Pb zircon method, and range in age from Jurassic to Cretaceous (Figure 1.3). The White Fork (~156 Ma), Diamond (~160), Woods Lake (165±1 Ma), and Twin Lakes (165±2 Ma) plutons are Jurassic. These plutons, as well as the Red Mountain Creek and Mule Lake, are extensively intruded by the west- to northwest-striking 148 Ma Independence Dike Swarm (IDS) (Moore and Hopson, 1961; Carl and Glazner, 2002). Dated Cretaceous plutons in the quadrangle include the Lamarck granodiorite (92 Ma, Coleman et al., 1995), Cotter (~92 Ma; Carl, 2000), Goodale granodiorite (~92 Ma; Bradford, 1995), Bullfrog (102 Ma; Chen and Moore, 1982), Dragon (102±1 Ma; Saleeby et al., 1990), and McDoogle (94.8±0.6 Ma; Mahan, 2000) plutons. There are several mafic complexes in the area as well. The Aberdeen (Bradford, 1995) and Black Canyon mafic complexes are located east and directly south of the McDoogle pluton, respectively. The Aberdeen mafic complex is commingled with 92 Ma granodiorite and intruded by Cretaceous mafic dikes (Carl, 2000). The Black Canyon mafic complex also appears to be Cretaceous, but is likely complicated and may also contain Jurassic mafic rocks.

Nonplutonic wall-rocks in the area consist of Paleozoic metasedimentary and Jurassic through Cretaceous metavolcanic units. The metavolcanic rocks were studied by Longiaru (1987) in the Oak Creek pendant, which is located 4 km to the southwest of Sawmill Lake. The metasedimentary rocks have been correlated to the stratigraphic section of the White and Inyo Mountains to the east (Bateman, 1992). The wall rocks have a solid-state fabric acquired during penetrative deformation in the Cretaceous (Longiaru, 1987). Several studies have tried to establish the depth of exposure, with

mixed results. It is generally estimated to be less than 15 km in this area (Renne et al., 1993). Wall-rocks commonly contain andalusite ± sillimanite, but never kyanite. Thermobarometry using the garnet-biotite-plagioclase-aluminosilicate-quartz mineral assemblage in a sample from near Taboose Creek (~10 km from Sawmill Lake) yielded a pressure of 2.1±0.3 kbar and a temperature of 704±20 °C (Sisson et al., 1996). Mahan's (2000) aluminum in hornblende measurements also produced pressure estimates consistent with Sisson et al. (1996).

Mahan (2000; Mahan et al., 2003) remapped the McDoogle pluton and its wall rocks at 1:10,000 scale. He observed that the McDoogle pluton contained significant lithologic variations and abundant wall-rock screens. Mahan (2000) also observed that the pluton intruded a steep tabular shear zone that he named the Sawmill Lake shear zone. The McDoogle pluton intruded as an amalgamation of dikes during the later stages of motion across the shear zone. Despite the scope and detailed map scale of 1:10,000, Mahan (2000; Mahan et al., 2003) was unable to characterize all of the variations within the pluton. Questions still remained about the detailed anatomy and assembly processes of the McDoogle pluton.

For the purpose of this study, several terms must be defined. An intrusive suite is a group of plutons that are spatially and temporally related, and are thought to be cogenetic. A pluton is an accumulation of spatially contiguous igneous rocks that are sufficiently similar to be mapped as a single body. An increment is an addition of magma during the process of assembling a pluton (e.g., incremental assembly, or incremental emplacement), and may have any geometric form. Increments are sometimes marked by

intrusive contacts within the pluton. A phase is a part(s) of a pluton that can be distinguished and/or grouped at the map scale by some lithologic criteria.

CHAPTER 2

DESCRIPTION OF GEOLOGIC MAP UNITS

Introduction

This chapter overviews the mapping area and describes in detail the thirteen map units. The work builds on previous mapping by Moore (1963) and Mahan (2000). Lithology, map distribution, contact relations, and ages are organized according to rock type and known or inferred age.

Overview of map area

The study focuses on a ~2 km^2 area between Sawmill Lake and Sawmill Pass in the southeast portion of the Mt. Pinchot 15' Quadrangle (Figure 2.1; Plate 1, in pocket). The area was chosen because the full width of the McDoogle pluton is preserved, and recent glaciation provides good exposure. Part of the mapping area is obscured by Quaternary deposits, including talus, moraine, and a rock glacier, that were grouped into one map unit. The area was mapped at 1:3000 scale, and contains roughly 630 m of relief between Mule Lake (2980 m) and an unnamed peak (3610 m) at the southern edge of the field area. Brittle faults mapped in the area represented on Moore (1963) have been

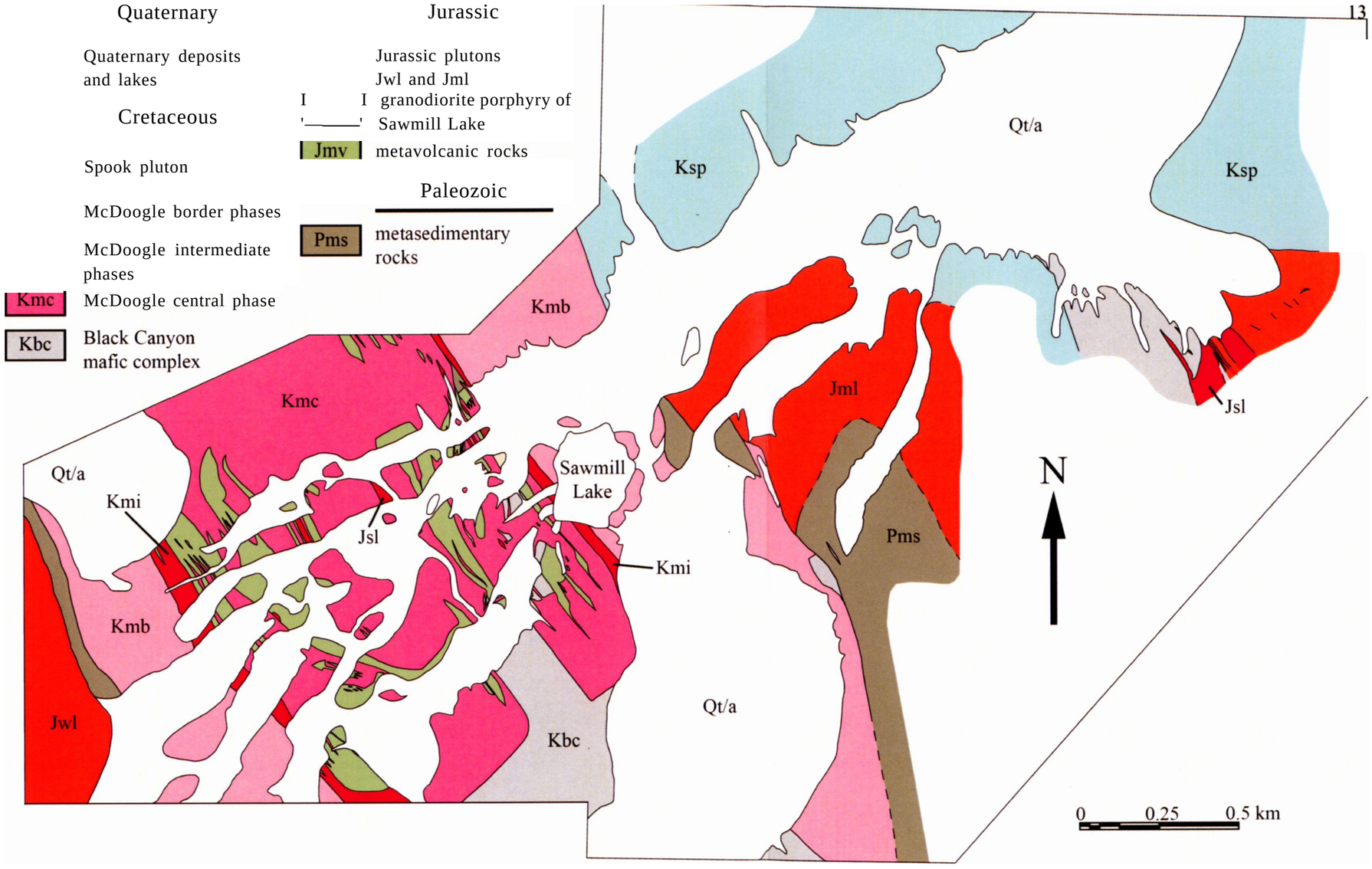

Figure 2.1: Simplified geologic map of the McDoogle pluton and its wall rocks near Sawmill Lake and Sawmill Meadow. Map scale is -1:15,000. The detailed geolog map is on Plate 1 (in pocket)

omitted because the faults do not have appreciable offset and were not the focus of this study.

The McDoogle pluton is a NNW-striking sheeted complex that intrudes the Sawmill Lake shear zone (Mahan, 2000). It consists of five lithologically distinct sheets with mirror symmetry across the strike of the pluton. The five sheets are grouped into three map units called the border phase (Kmb), intermediate phase (Kmi), and central phase (Kmc) (Figure 2.1). The pluton is reversely zoned with more felsic rocks at the margins and more mafic rocks in the center (Mahan, 2000): the central phase ranges in composition from quartz monzodiorite to quartz monzonite. The border phase ranges from granodiorite to granite.

The McDoogle pluton intrudes several different rock units and contains roughly 35% (by area) wall-rock xenoliths (Figure 2.2). Xenoliths commonly have aspect ratios between 2 and 20 and range in width from centimeters to tens of meters. In the Sawmill Lake area, the external contacts on both sides of the pluton are marked by metamorphic wall-rock screens that separate the McDoogle pluton from Jurassic intrusions. Internal contacts with xenoliths generally dip steeply to the east and strike concordantly with the overall trend of the pluton. Wall rocks in the area contain amphibolite-facies metamorphic mineral assemblages (Mahan, 2000). Protoliths include siliciclastic and carbonate sedimentary rocks, intermediate to felsic volcanic rocks, and granitic rocks.

The granodiorite porphyry of Sawmill Lake (Jsl) is strongly deformed, with fabrics ranging from protomylonitic to mylonitic. Mahan (2000) first described the unit and reported a U-Pb zircon age of 164±4 Ma. The granodiorite porphyry of Sawmill Lake

Figure 2.2 Distribution of wall rock in the McDoogle pluton near Sawmill Lake. The central phase contains abundant wall rocks screens, and the border phases contain almost none. The wall-rock screens are generally tabular bodies concordant with the overall strike and magmatic fabric of the pluton.

is the only Jurassic intrusive rock included within the McDoogle pluton. The Woods Lake pluton (Jwl) to the west and the Mule Lake pluton (Jml) to the east are relatively undeformed. They contain thin mylonitic shear zones (1-5 cm wide), which locally exceed 5 m in width (Carl, 2000). The 148 Ma Independence Dike Swarm (IDS) (Moore and Hopson, 1961) extensively intruded the Jurassic Plutons and older metamorphic rocks. Independence dikes are deformed with the wall rocks in this area. A small number of mafic dikes intrude Cretaceous units. Other younger dikes in the region that intrude Jurassic and Triassic plutons are between 90 and 94 Ma (Coleman et al., 2000; Carl, 2000). Cretaceous mafic dikes have a large range of strikes that overlaps with the WNW strike of most Independence dikes.

Description of lithologic units

Cretaceous units

McDoogle pluton (Kmb, Kmc, and Kmi)

Outcrop geometry and appearance

The McDoogle pluton contains five distinct sheets, grouped into three lithologic phases: the border phase, central phase, and intermediate phase. Mahan (2000) reported that the border phases range from granodiorite to granite and have a color index of 16-27 (Figure 2.3). The border phase contains few mafic enclaves or wall-rock screens, and has a massive, blocky outcrop appearance (Figure 2.4). The central phase ranges in composition from quartz monzodiorite to quartz monzonite, and commonly has a color index of 16-36. The central phase contains very abundant mafic enclaves and wall-rock

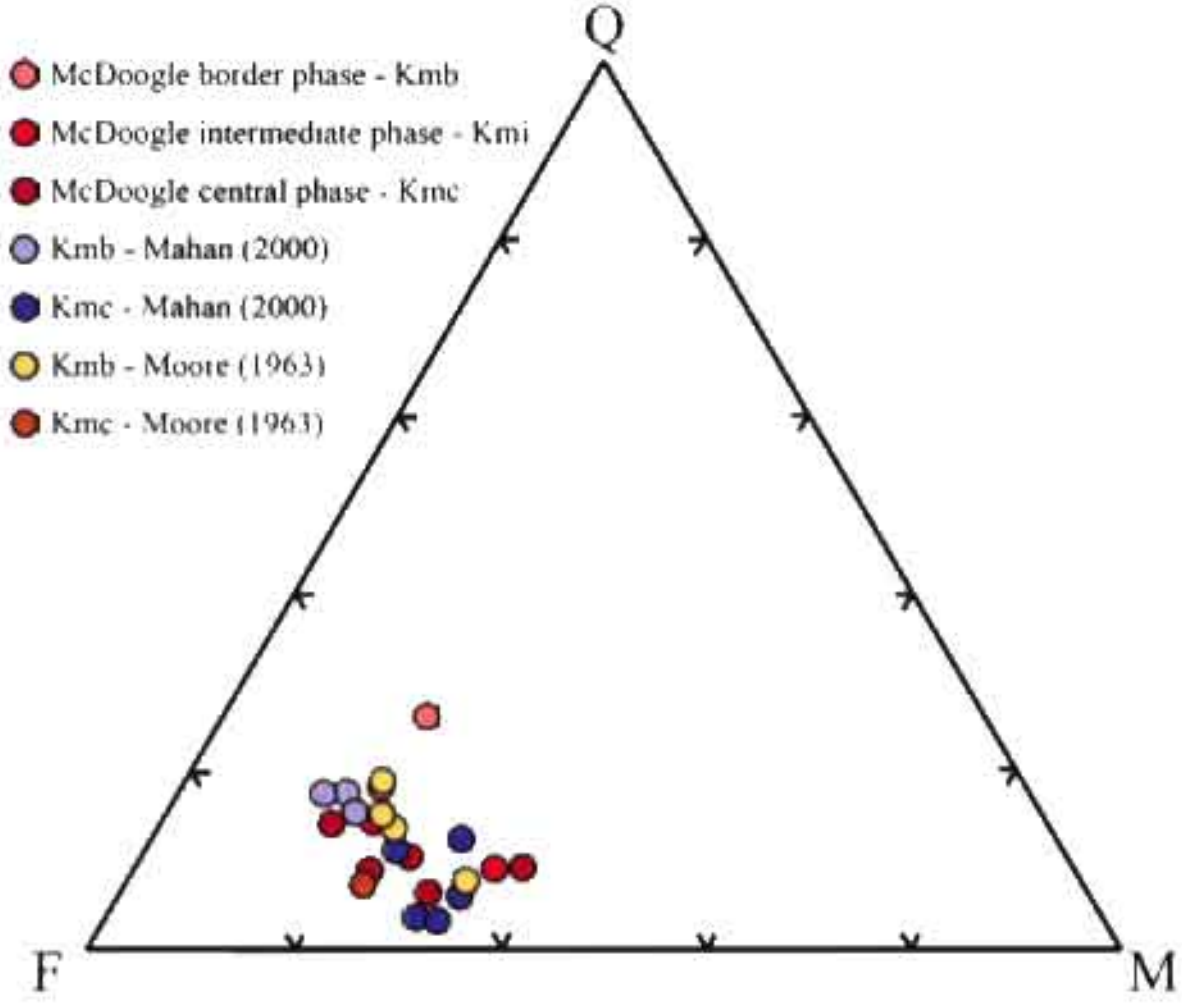

Figure 2.3 Nine samples from the central, eastern intermediate, and eastern border phases shown on a quartz-feldspar-mafic mineral plot. Additional data from Moore (1963) and Mahan (2000). The color of the data corresponds to the author and intrusive phase of the pluton

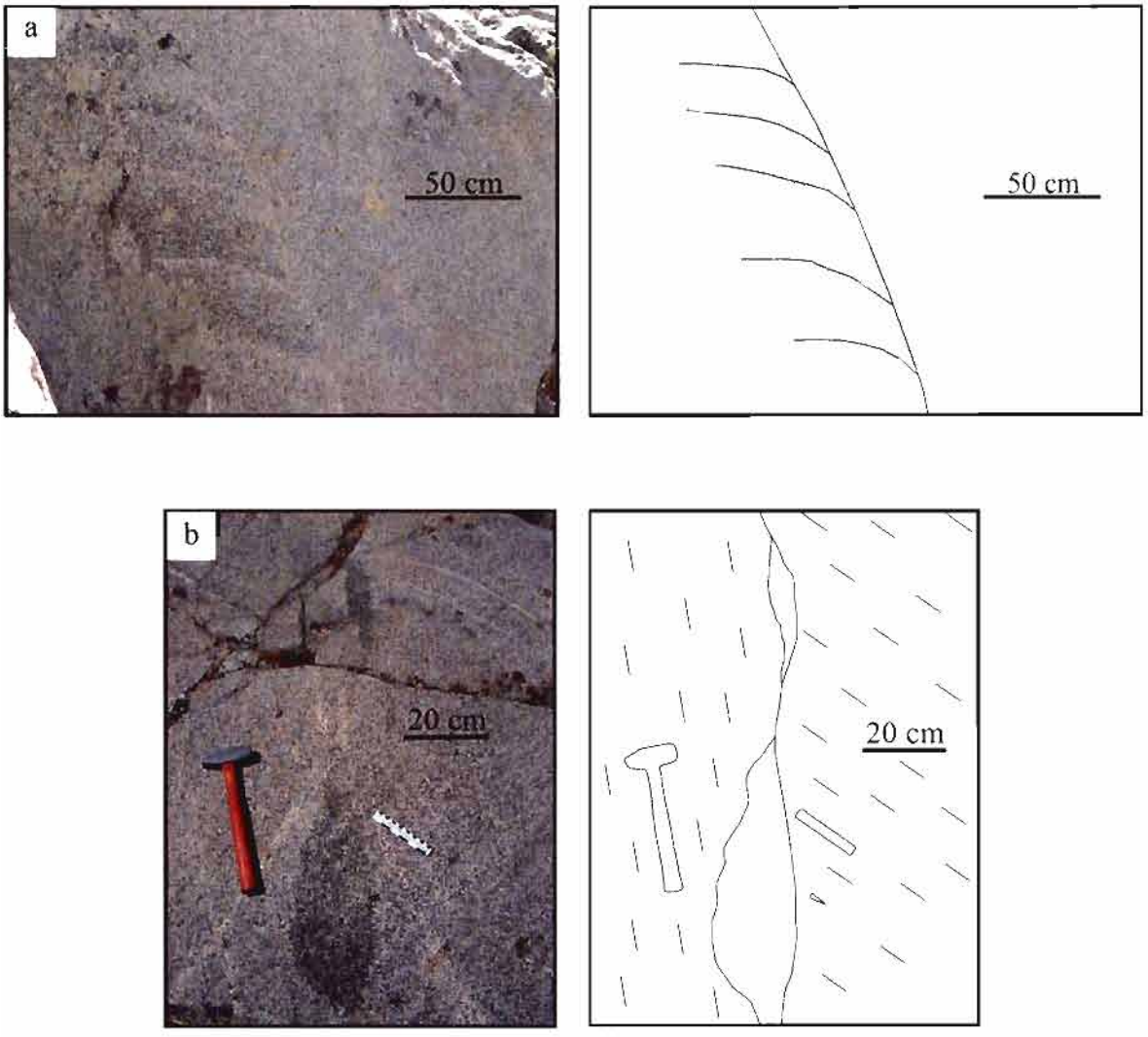

Figure 2.4: Wall-rock screens are uncommon in both border phases, and outcrops commonly contain internal intrusive contacts. a) Modal layering within the western border phase cross cut by an internal intrusive contact. b) Mafic enclave cut by an internal intrusive contact in the eastern border phase. Hammer and scale card approximate the magmatic fabric on either side of the contact.

screens. On average the wall-rock screen abundance is ~35%, but locally increases up to 50-60% by volume (Figure 2.2). Mahan (2000) observed that the central phase weathers more easily than the border phase and forms broken outcrops of alternating dikes and wall-rock screens (Figure 2.5). Dikes lack chilled margins and vary in thickness from 2 cm to 10's of meters. Wall-rock screens also vary in thickness from 2 cm to 10's of meters.

The newly defined intermediate phase spans the compositional range between border and central phase compositions and shares characteristics with each. It contains a stronger magmatic fabric and darker appearance than the border phase, but contains far fewer wall-rock screens than the central phase. The eastern and western contacts between the intermediate and central phases are marked by unusually thick wall-rock screens (>>10 m thick). This unit may represent a wide gradational contact between the central and border phases. In this area the entire pluton is 1900 m wide, including the wall-rock screens. Below is Table 2.1 lists each phase's width excluding wall rock screens.

TABLE 2.1: DIMENSIONS OF THE MCDOOGLE PLUTON NEAR SAWMILL LAKE

lithologic phase	border phases	intermediate phase	central phase
eastern width (m)	414	12	x
western width (m)	311	78	x
entire width (m)	725	90	1100

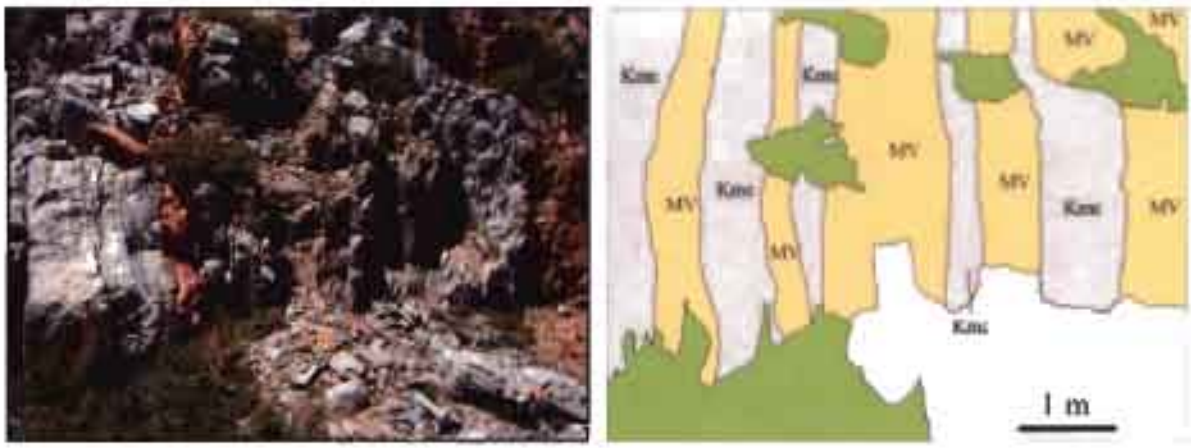

Figure 2.5 Wall-rock screens are abundant in the central phase (avg ~35%, but locally up to ~60-75% by vol.). The photo and corresponding line drawing, looking north, show several McDoogle dikes intruding metavolcanic wall rocks along foliation planes. Dike thickness varies from ~10 cm to 10 m.

Texture and composition

All three phases have medium- to coarse-grained, equigranular granitic textures. The border and intermediate phases have a moderate to no preferred orientation of hornblende, biotite, and mafic enclaves. Locally, the central phase has a very strong preferred orientation of the same minerals. Modal percentages were obtained from nine border-, intermediate-, and central-phase samples by point counting ~575 points from two thin sections per sample (see Figure 2.6 and Table 2.2).

Age and contact relations

The intrusive contact between the border phase and intermediate phase is gradational across 1-3 m. The intrusive contacts between the central phase and intermediate phase dips steeply, but commonly these contacts are marked by wall-rock screens. None of the units have chilled margins at intrusive contacts. In the southern portion of the mapping area near Sawmill Lake, the central phase terminates bluntly where it abuts older hornblende granodiorite (Khg). The contact between the central phase and hornblende granodiorite strikes ENE. The border phases continue southward beyond the mapping area. There are no clear cross-cutting relationships between the phases. Mahan (2000) suggested that the central phase was older than the border phase based on the observation that the central phase is more abundantly cut by aplite dikes than the border phase, but no direct cross-cutting relationships were observed. New U-Pb dates of both the border phase (94.9±0.1 Ma) and central phase (95.0±0.1 Ma) did not

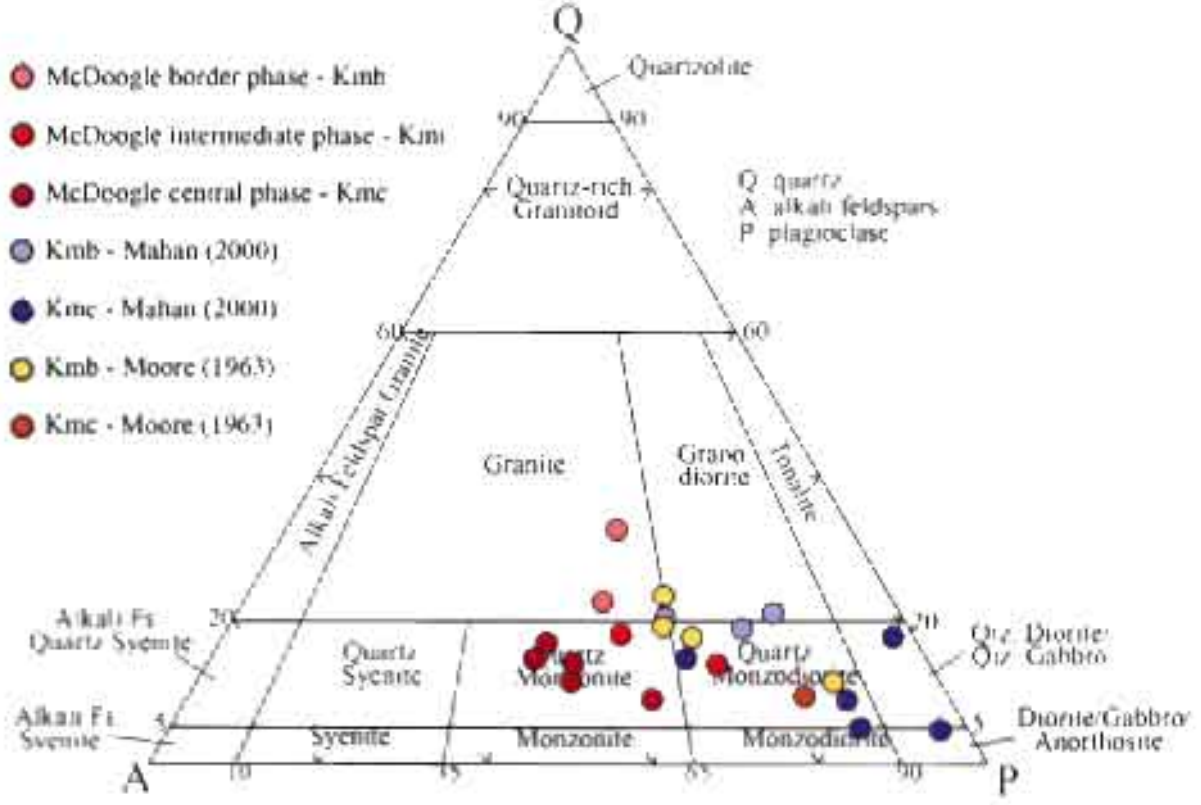

Figure 2.6 Quartz-alkali feldspar-plagioclase feldspar mineral modes, plotted with IUGS classifications, show the significant lithologic variation within the pluton. Additional data from Moore (1962) and Mahan (2000). The color of the data corresponds to the author and intrusive phase of the pluton.

TABLE 2.2: MODAL COMPOSITIONS FOR SELECTED SAMPLES

Sample*	quartz	alkali feldspar	plagioclase	biotite	hornblende	pyroxene	opaque accessories	titanite	color index	n
Kmb										
MS07-F2	26.0	22.3	31.5	11.3	8.3	0.0	0.0	0.6	19.6	470
MS07-F3	17.9	27.7	34.1	8.2	8.9	0.7	1.2	1.2	19.0	574
average	22.0	25.0	32.8	9.7	8.6	0.3	0.6	0.9	19.3	522
Kmi										
MS07-122	14.2	27.6	37.4	11.4	7.0	0.3	1.6	0.5	20.3	572
MS07-123	8.8	16.3	39.2	17.8	14.5	0.8	1.3	1.3	34.4	613
average	11.5	22.0	38.3	14.6	10.8	0.6	1.4	0.9	27.4	593
Kmc										
MS07-F4	13.8	36.5	31.9	7.9	7.3	0.3	0.7	1.6	16.2	573
MS07-F6	8.5	33.3	33.6	9.2	11.8	0.2	1.0	2.3	22.3	574
MS07-F7	10.3	31.5	32.2	13.4	9.6	0.9	2.1	0.2	25.9	575
MS07-F8	9.0	29.0	23.7	18.3	15.8	1.6	1.4	1.2	37.1	569
MS07-F9	6.1	24.5	38.3	13.2	13.4	0.3	2.3	1.9	29.2	575
average	9.5	30.9	31.9	12.4	11.6	0.7	1.5	1.4	26.1	573

NOTES: Modal analyses were conducted on an optical microscope
* Kmb, McDoogle pluton-border phases; Kmi, McDoogle pluton-intermediate phases; Kmc, McDoogle pluton-central phase
n = number of points counted from two thin sections per sample

yield resolvable age differences within uncertainty, but are consistent with Mahan's (2000) interpretation (see Ch 5 for full description of new data).

Mafic enclaves

There are several types of mafic enclaves in the McDoogle pluton. Most are porphyritic diorite to granodiorite(?) with a fine grained (~0.5-2 mm) dark groundmass that consists of biotite, hornblende, quartz and feldspar. The phenocrysts are euhedral plagioclase crystals that range in size from 0.5 to 2 cm. Other enclaves have very high color index and consist of equigranular hornblende and biotite, and euhedral plagioclase crystals. These diorite to gabbroic enclaves locally are spatially associated with modal layering. All phases of the McDoogle pluton contain mafic enclaves, but they are especially prevalent in the central phase. Locally they are very abundant, concentrated in swarms up to 60% by volume. The swarms are locally crosscut by internal intrusive contacts or focused near the margins of wall-rock screens (Figure 2.7).

Mafic dikes

The McDoogle pluton contains sparse mafic dikes. The IDS pervasively intrudes and is deformed with the wall rocks. A few Cretaceous mafic dikes are observed to intrude the McDoogle pluton in the Sawmill Lake area. These Cretaceous dikes strike WNW and dip steeply, and thus are subparallel to the 148 Ma IDS and are difficult to distinguish from it where they do not cross-cut Cretaceous rock units.

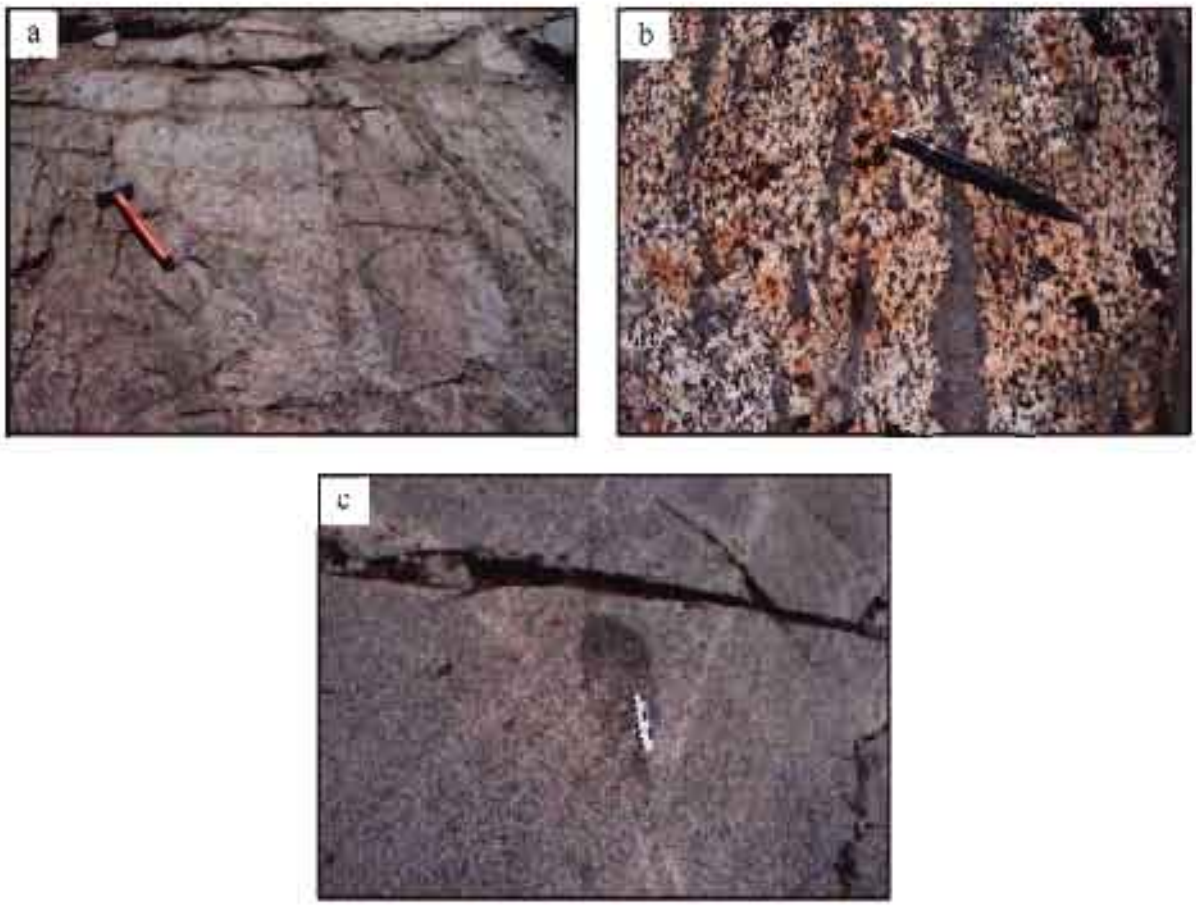

Figure 2.7: The central phase of the McDoogle pluton contains abundant mafic enclaves compared to the other phases. The photos shows the different types of mafic enclaves observed in each phase. a) Enclaves in the central phase are often located near the margins of wall-rock screens. The hammer is ~30 cm long. b) The aspect ratio of enclaves varies from ~ 2 to 20, and is usually higher in the central phase. These enclaves in the central phase have an aspect ration of ~5-10. The pencil is ~15 cm long. c) This enclave in the border phase has been cut by an internal intrusive contact. Enclaves in the border phase are typically coarser grained and have more diffuse boundaries. The scale card is 17 cm long.

Hornblende granodiorite (Khg)

Composition and texture

The hornblende granodiorite consists of 50-60% plagioclase, 15% quartz, 15% alkali feldspar, and 15% of biotite and hornblende combined (Mahan, 2000). The mafic minerals form glomerocrysts that give the rock a distinctive mottled texture. Mafic enclaves and modal layering are not present in the hornblende granodiorite. The hornblende granodiorite does not have a preferred orientation of minerals, but locally it is cut by mylonitic shear zones (1-5 cm thick) that strike NW.

Map distribution, age, and contact relations

The hornblende granodiorite mainly crops out in the southern portion of the map area. Xenoliths of the hornblende granodiorite are found within both the central and border phases. Hornblende granodiorite inclusions in the central phase are blocky and have sharp contacts without chilled margins. In some places, thin central-phase dikes separate large interlocking blocks of hornblende granodiorite. Bodies of the hornblende granodiorite both are contained within and separate the eastern border phase from the metasedimentary wall rocks along a portion of the contact. The concentration of Khg inclusions in the central phase increases to the south and east, where the central phase terminates against the hornblende granodiorite. The hornblende granodiorite is older than the central phase based on cross-cutting relationships that have been confirmed by geochronology. Mahan et al. (2003) reported a U-Pb zircon date of 97.6±0.4 Ma from a sample collected just west of Sawmill Lake.

Jurassic plutonic units

Woods Lake and Mule Lake plutons (Jwl and Jml)

Composition and texture

The Woods Lake and Mule Lake plutons were not foci of this study, and Moore (1963) described these rocks in more detail. The Woods Lake pluton is a coarse grained porphyritic granodiorite with ~1 cm alkali feldspar phenocrysts, and a color index of 10-15 (Moore, 1963). The Mule Lake pluton is equigranular granodiorite with a color index of 15-25 (?) (Moore, 1963). Both plutons contain abundant Jurassic Independence dikes.

Map distribution, age, and contact relations

The Woods Lake pluton is separated from the western border phase of the McDoogle pluton in the Sawmill Lake area by a thin screen of metasedimentary wall rock. Mahan (2000) reported that the border phase of the McDoogle intrudes the Woods Lake pluton in the most southern portion of the pluton. The Woods Lake pluton has not been mapped in detail, but appears not to contain either abundant wall-rock inclusions or significant lithologic variation . Chen and Moore (1982) reported a concordant U-Pb zircon age of 165±1 Ma for the Woods Lake pluton. The Mule Lake pluton is separated from the eastern border phase of the McDoogle pluton by a thin metasedimentary wall-rock screen. The Mule Lake pluton has not been dated by isotopic methods but it is intruded by many Independence dikes which limits the age to older than 148 Ma.

The granodiorite porphyry of Sawmill Lake (Jsl)

Composition and texture

Mahan (2000) first recognized and described the granodiorite porphyry of Sawmill Lake. It contains protomylonitic to mylonitic solid-state deformation. Locally it is well foliated and lineated, but less deformed varieties are dominated by penetrative lineation. Rotated plagioclase porphyroclasts are up to 6 mm long and as small as 0.5 mm, with a mean size of 1 mm. Annealing recrystallization has overprinted most of the mylonitic microstructures of the granodiorite porphyry of Sawmill Lake. The modal composition of the rock is 35-45% plagioclase, 10-25% alkali feldspar, 15-35% quartz, 10-15% biotite, 5-10% hornblende, 1-3% accessory and opaque minerals (Mahan, 2000).

Map distribution, age, and contact relations

The granodiorite porphyry of Sawmill Lake comprises < 5% of the map area. Locally, it is preserved as steeply dipping wall-rock screens within the McDoogle pluton that range in thickness from 1 meter to tens of meters. Mahan (2000) produced two ID-TIMS U-Pb ages from a sample north of the Sawmill Pass trail. Zircon yielded an age of 164±4 Ma, which is interpreted as the crystallization age. Titanite produced an age of 94.6±1.7 Ma, which is interpreted as the peak metamorphic age related to intrusion of the McDoogle pluton. The contacts where is it intruded by the McDoogle pluton are sharp and concordant with the overall trend of the pluton. Some areas of foliated granodiorite of Sawmill Lake are extensively intruded by dikes of McDoogle between 1 cm and 10 m thick. At certain localities, the McDoogle pluton and the granodiorite porphyry of

Sawmill Lake are so intermingled that they cannot be mapped separately at the 1:3000 scale.

Nonplutonic units

Metavolcanic rocks (Jmv, Jmm, Jfm)

Appearance, composition, and texture

The most voluminous wall rocks in the map area are felsic to intermediate metavolcanic rocks. The protoliths most likely ranged from rhyolite to andesite. Some contain relict feldspar phenocrysts up to 2 mm and lapilli up to 5 cm. The rocks are well foliated and locally weakly lineated. Most microstructures resulting from penetrative solid-state deformation of the metavolcanic rocks have been recrystallized (Mahan, 2000). The rocks are commonly stained orange.

Map distribution, age, and contact relations

Metavolcanic wall-rock screens are concentrated in the central phase of the pluton where they form elongate, tabular wall-rock screens that dip steeply. The overall strike of the wall-rock screens is concordant with the NNW strike of the pluton, but locally the screens are folded and strike perpendicular to the pluton. Screens range in thickness from centimeters to tens of meters. Small screens are concentrated near the margins of larger screens (Figure 2.2). Similar to the granodiorite porphyry of Sawmill Lake, the metavolcanic wall rocks are injected lit-par-lit by dikes of the McDoogle pluton down to the centimeter scale. The metavolcanic rocks are thought to be the Jurassic and

Cretaceous volcanic carapace that plutons later intruded (Longiaru, 1987). Longiaru (1987) mapped and dated the volcanic sequence in the Oak Creek pendant south and west of the McDoogle pluton. He reported Jurassic (165 Ma) felsic and intermediate ash flows that are unconformably overlain by Late Cretaceous (110 Ma) felsic and mafic tuffs.

Metasedimentary rocks (Pzms)

Appearance, composition, and texture

Marble and calc-silicate and siliciclastic rocks are all present in the Sawmill Lake area. All of the rocks are well foliated and weakly lineated and contain several generations of folds in some places. Unlike the metavolcanic rocks and granodiorite of Sawmill Lake, the metasedimentary wall rocks are not injected by McDoogle dikes. The metasedimentary rocks are also stained orange. The marble and garnet skarn outcrops are deeply weathered, whereas the siliciclastic and calc-silicate rocks form massive, less weathered outcrops.

Map distribution, age, and contact relations

Metasedimentary rocks are located near the margins of the pluton. Thin screens of wall rock separate the border phases of the McDoogle from the Woods Lake and Mule Lake plutons on both sides. The screen on the western margin consists of siliciclastic rocks and marble. This screen is the most continuous in the mapping area. The screen on the eastern margin consists of calc-silicate, skarn, and siliciclastic rocks. The metasedimentary units have been correlated to the stratigraphy of the White-Inyo

Mountains (Bateman, 1992). The stratigraphic units range from Precambrian to possibly Pennsylvanian-Permian(?) in age (Stevens and Greene, 1999). The contacts between the McDoogle pluton and metasedimentary wall rocks are concordant with the overall NNW strike of the pluton.

CHAPTER 3

STRUCTURAL GEOLOGY

Introduction

The structural geology of the McDoogle pluton and surrounding wall rocks was the main focus of Mahan's (2000) work. Mahan (2000) recognized the elongate McDoogle pluton as a subvertical sheeted intrusion (~12 x 2 km) with an overall strike of 320°. The pluton is entirely exposed near its ends in the Pinchot Pass and Sawmill Lake areas, whereas the middle is partially obscured by younger intrusions. The McDoogle pluton contains abundant wall-rock screens (~35 % by vol.) concentrated in the central phase. Paleozoic and Jurassic wall-rocks are concordant in and outside the pluton, which suggests the majority of screens define a "ghost" tectonostratigraphy, meaning that the screens are preserved in situ without significant rotation or translation.

At the outcrop scale, the McDoogle contains well developed planar (321/89°) and linear (146/80°) fabrics (Figure 3.1) defined by elongate mafic enclaves and mineral grains. The fabric has been interpreted to reflect magmatic flow. At the microscopic scale, the fabric is defined by aligned euhedral plagioclase, hornblende, and biotite. Mahan (2000) also observed undeformed quartz and feldspar that filled fractured

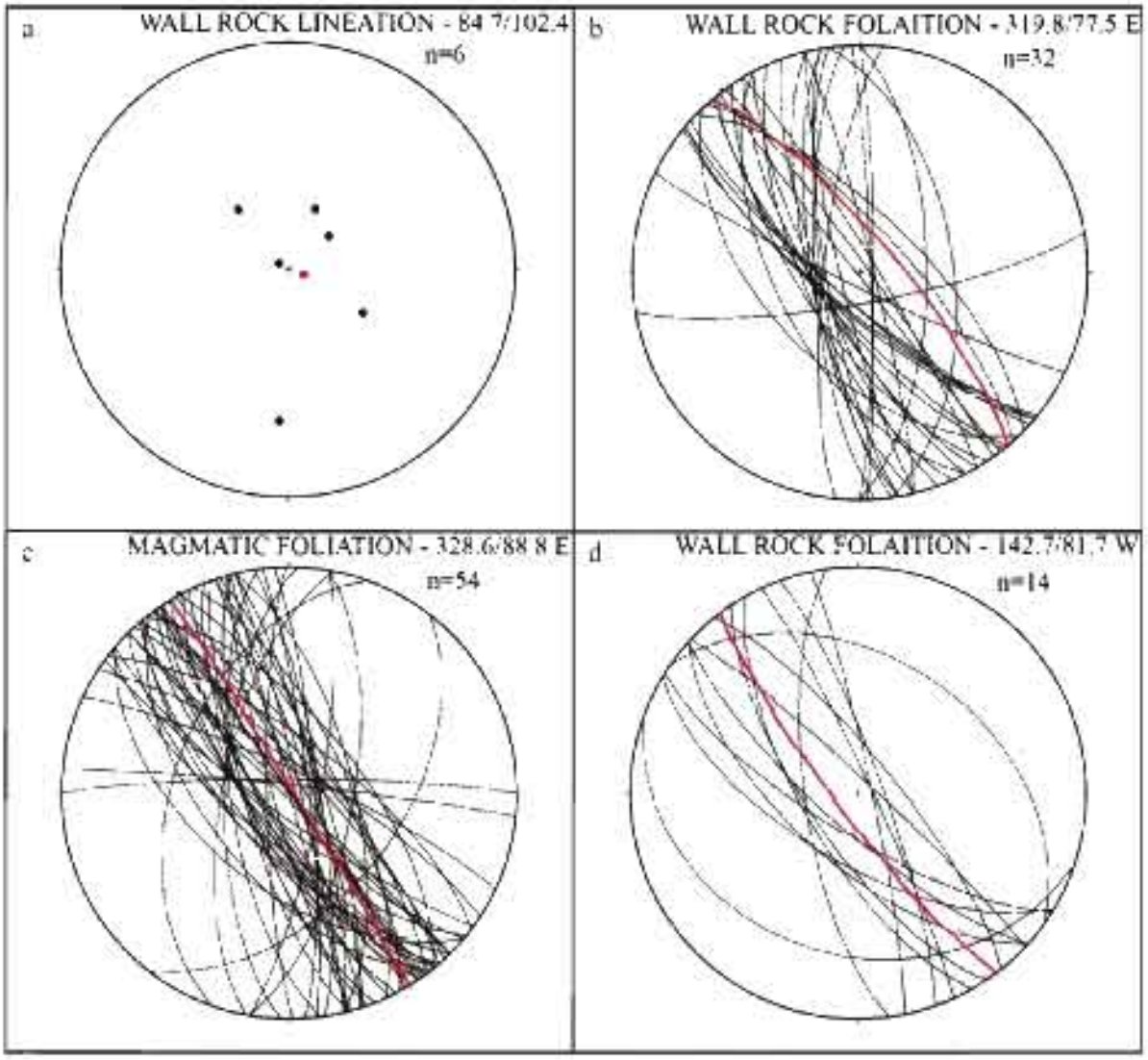

Figure 3.1: Equal-area stereonets showing fabric data (mean colored red) from the Sawmill Lake and Sawmill Meadow areas. a) lineation and b) foliation measurements of the wall rocks (Paleozoic metasedimentary units, metavolcanic units, and granodiorite porphyry of Sawmill Lake) near Sawmill Lake. c) Magmatic foliation measurements of the McDoogle pluton. d) Foliation measurements of the wall-rocks (Paleozoic metasedimentary units, Mule Lake pluton, and granodiorite porphyry of Sawmill Lake) near Sawmill Meadow.

plagioclase grains that he interpreted to reflect submagmatic brittle deformation in the presence of late-stage granitic melt.

Mahan (2000) recognized that strain was localized in the wall rocks in and immediately around the McDoogle pluton, and named this belt of focused strain the Sawmill Lake shear zone based on several lines of evidence. First, the metamorphic wall rocks in and around the McDoogle pluton are penetratively deformed, and the strain intensity increases from southwest to northeast. Second, the Jurassic intrusions bordering the McDoogle pluton are only locally cut by cm- to m-scale mylonitic shear bands, but are not penetratively deformed. Third, the metavolcanic rocks within the McDoogle pluton are more deformed than in the Oak Creek pendant, several kilometers away. The solid-state mean foliation (141/89°) and lineation (150/67°) (Figure 3.1) are parallel to the McDoogle and wall-rock fabric outside of the pluton. The Black Canyon hornblende granodiorite is not penetratively deformed. Blocks of this unit within the central phase of the McDoogle pluton are along strike with the most deformed rocks making it the oldest unit unaffected by the Sawmill Lake shear zone (Mahan, 2000).

Mahan (2000) focused on the Sawmill Lake porphyry to investigate emplacement related structures because its age (164±4 Ma) limits deformation and its coarse-grained character make it a good strain recorder. The Sawmill Lake porphyry is protomylonitic to mylonitic with porphyroclasts 1-3 mm in diameter. The fine-grained matrix has been statically recrystallized, wiping out the majority of mylonitic microstructures (Mahan, 2000).

Mahan (2000) recognized several scales (cm to m) of local folding and boudinage

of rocks in the Sawmill Lake shear zone. Mafic dikes are tightly folded along with the wall rocks that they intruded. The fold axes and stretching direction of boudinage are subvertical in the plane of the wall-rock foliation. Boudinage affects rocks as young as dikes of McDoogle granodiorite. The lack of a macroscopic fabric within the boudined McDoogle dikes and the presence of late-stage melt-filled microcracks in the granodiorite suggest that deformation was synintrusive.

Microscopic discontinuous shear bands (0.5 x ~1 mm) and multidomain quartz are the only solid-state deformation microstructures observed in the McDoogle pluton. More intense deformation is rare, but local ductile shear zones (1-20 cm thick) do occur in the McDoogle pluton. Overall the deformation suggests significant SW-NE contraction. The kinematics are locally ambiguous, but Mahan (2000) inferred a predominance of east-side up simple shear across the Sawmill Lake shear zone.

Magmatic structures

Mapping the McDoogle pluton at 1:3000 scale near Sawmill Lake allowed for a detailed investigation of map patterns and outcrop-scale structures. The border phases resemble dikes and terminate in sharp tips several kilometers southeast of Sawmill Lake. In the southern portion of the mapping area, the central phase terminates bluntly against the hornblende granodiorite (Khg). As Mahan (2000) observed, the southern end of the central phase commonly contains inclusions of the hornblende granodiorite that increase in concentration to the south and east. The inclusions commonly form interlocking blocks that are separated by dikes of McDoogle central phase. Only one screen of hornblende

granodiorite was observed in contact with the border phases.

Complex magmatic relationships

At the southern end of the central phase, magmatic and structural relationships become complex (Figure 3.2). The outcrop exposes several intrusive rock types and evidence of synintrusive shearing (Figure 3.2a, b). Basalt, aplite, and granodiorite are contained within a single dike which cross-cuts the McDoogle central phase (Figure 3.2a). The lack of a fabric in the sub-vertical shear zone and the absence of a sharp contact between the subhorizontal dike and the McDoogle exposed above it combine to suggest that the McDoogle central phase still contained a significant portion of partial melt when the subhorizontal dike intruded.

The contacts between each rock type within the subhorizontal dike are pillowed, and are interpreted to have been distorted by magmatic flow (Figure 3.2c, d). Where the subhorizontal dike contacts the earlier McDoogle above and the aplite feeder dikes below, material is pillowed out of the subhorizontal dike (Figure 3.2a, c). All of the aplite feeder dikes terminate at the subhorizontal dike and do not continue above it (Figure 3.2c). Basaltic, aplitic, and granodioritic magmas must have coexisted for the flow, pillowing, and mingling to occur, as well as to prevent dike propagation. The pillowing of magma from the subhorizontal dike may have occurred because of a pressure or viscosity differential between the different magmas.

Figure 3.3 illustrates two possible sequences of events based on cross-cutting relationships, fabric, and magmatic structural relations. First, the McDoogle central phase

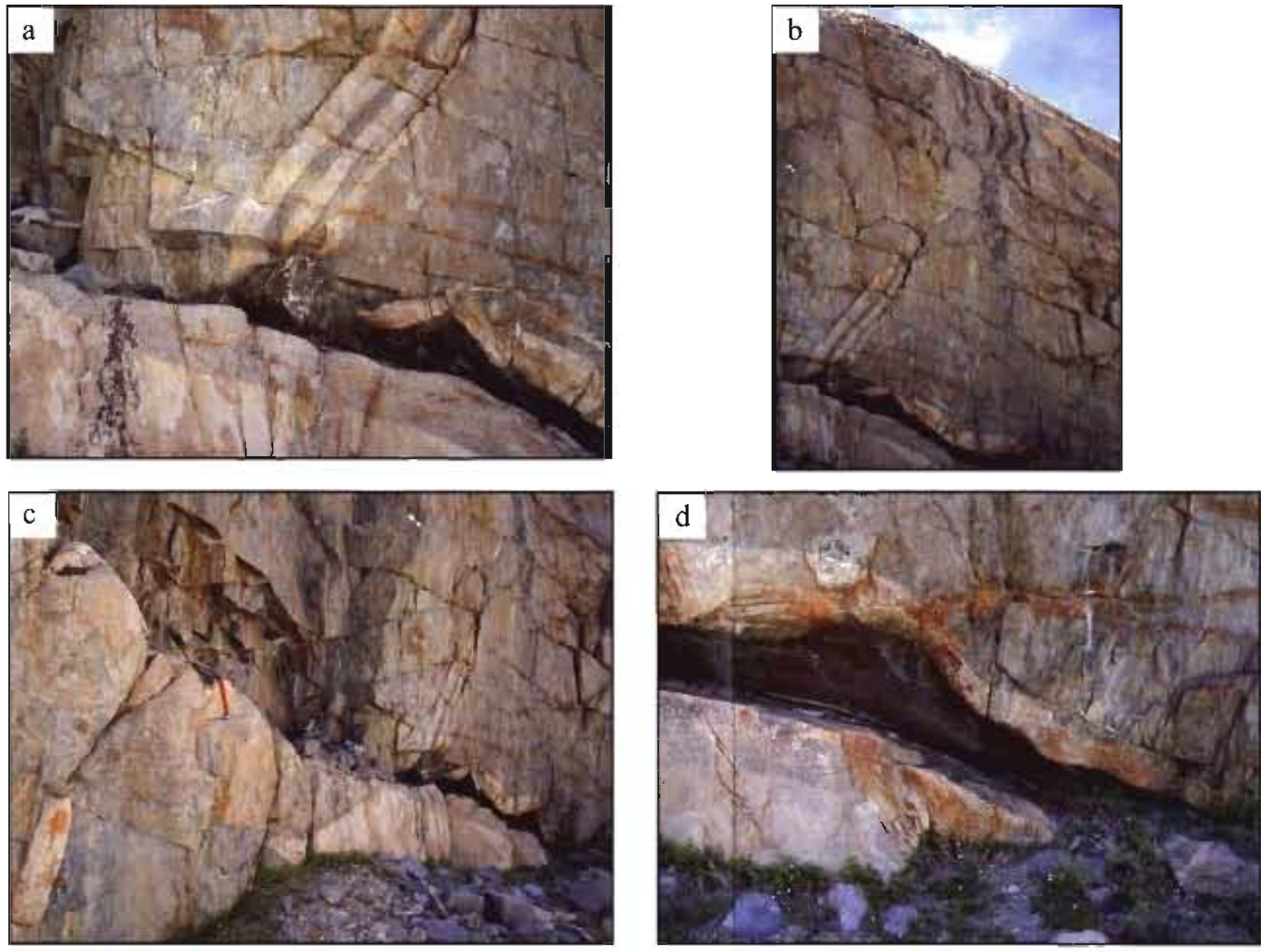

Figure 3.2: Photos of a complex outcrop at the southern end of the McDoogle central phase. Intrusive rock types include two ages of McDoogle central phase, aplite, and basalt. a) The junction of the normal-separation shear zone and the subhorizontal dike. b) Offset of the contact between older McDoogle and the metavolcanic rocks. c) An aplite feeder dike with pillowed aplite to the right. Hammer is approximately 30 cm. d). Mindgles aplite, basalt, and younger McDoogle within the subhorizontal dike.

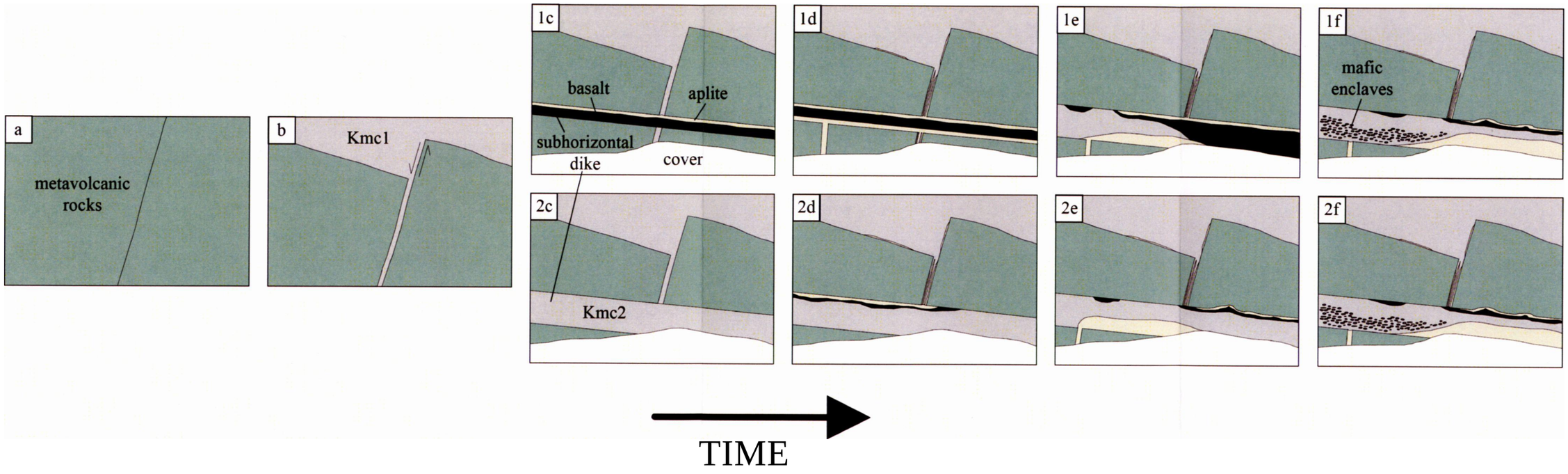

Figure 3.3: Illustration of two sequences that could have resulted in the observed outcrop. 1) The subhorizontal dike could have been basalt and aplite, and later the younger McDoogle central phase intruded the dike and pushed everything to the right. 2) The subhorizontal dike could have been McDoogle central phase flowing to the right carrying basalt and aplite, and later more aplite intruded the dike and was pushed to the right. Other sequences exist that could account for the observed relationships.

intruded the metavolcanic wall rock. The apparent normal offset of the contact between the McDoogle and metavolcanic blocks suggests that the rocks underwent extension during intrusion of the McDoogle central phase. Second, a subhorizontal dike intruded across the apparent normal-separation shear zone. The dike either contained basalt and aplite, or younger McDoogle central phase. Third, aplite was injected into the older McDoogle central phase through the normal-separation shear zone. Fourth, more aplite was pumped into the subhorizontal dike and pushed to the right by intrusion of more McDoogle granodiorite and flow within the dike.

Wall-rock screen patterns

The mapped distribution of wall-rock screens defines a complex but consistent pattern of folding. At several locations in the map area, multiple screens are folded together and mutually concordant through the fold. In these areas, the screens are deflected as much as 90° from the average strike of pluton and wall-rock screens. The scale of the folds is tens to hundreds of meters. Both the abundance of folds and the magnitude of deflections increase toward the southern end of the McDoogle pluton. At the southern end of the pluton, different types of wall rock exhibit different intrusion behaviors. The metavolcanic wall-rock screens are intruded concordantly along foliation planes. Near the termination of the central phase, the wall-rock inclusions mostly consist of hornblende granodiorite. These inclusions are in general equidimensional ranging from 1 m to tens of m in size. They record discordant intrusion along pre-existing fractures to form interlocking blocks separated by dikes of McDoogle. The central phase ends

southward against the main body of hornblende granodiorite, which is also injected by central-phase apophyses.

Solid-state structure

The McDoogle pluton is concentrated amongst the most deformed rocks of the Sawmill Lake shear zone (Mahan, 2000), but deformation related to the Sawmill Lake shear zone is more widespread than previously recognized. The Mule Lake pluton east of the McDoogle pluton is protomylonitic to mylonitic. The deformation in the Mule Lake pluton is localized in shear bands 10 cm to several meters thick which comprise ~50 % of the rock by volume. The Mule Lake pluton contains protomylonitic to mylonitic inclusions of Sawmill Lake porphyry that resemble inclusions within the Twin Lake pluton (Mahan, 2000). Locally, the fabric in the Sawmill Lake porphyry is cut by the fabric in the Mule Lake pluton, but generally the fabric (143/81°) is parallel in both units. Based on the inclusion and local cross-cutting relationships, the Sawmill Lake porphyry is slightly older than the Mule Lake and Twin Lakes plutons. The newly observed deformation is concentrated to the east of the main shear zone and may suggest a subsidiary strand exists to the east of the main shear zone. Locally, very small (1-3 cm thick) protomylonitic shear bands (322/86°) with ambiguous kinematics occur in the hornblende granodiorite.

Discussion

There are two possible causes for the pattern of folding in the central phase. First, the folding may have been caused by the emplacement of the 97.6±0.4 Ma (Mahan et al., 2003) hornblende granodiorite. This alternative implies that the McDoogle pluton intruded passively and preserved the pre-existing folds in the wall rock. Second, the folding was caused by the intrusion of the McDoogle pluton. Figure 3.4 shows how asymmetric incremental dike emplacement could fold the wall rocks.

If emplacement of the hornblende granodiorite caused folding, the deformation would be focused near the hornblende granodiorite. Rather, the intensity of folding increases over several kilometers toward the southern termination of the central phase. The spatial pattern of folding favors the asymmetric dike emplacement model (Figure 3.4) instead of folding caused by intrusion of the hornblende granodiorite. The change from metavolcanic rocks to hornblende granodiorite as the predominant wall-rock lithology could cause the transition from folding to injection at the south end of the central phase. The penetrative fabric caused the metavolcanic wall rocks to have anisotropic material properties. The hornblende granodiorite lacks both solid-state and magmatic fabrics and thus is isotropic.

The outcrop at the southern end of the central phase (Figure 3.2 and 3.3) exposes dikes of McDoogle central phase in different orientations. These orientations suggest dilation switched from horizontal to vertical. The orientation of dikes is governed by two combined stresses, far-field stress and magmatic overpressure (Delaney and Pollard, 1986; Parsons and Thompson, 1991). The principal stress directions may exert some

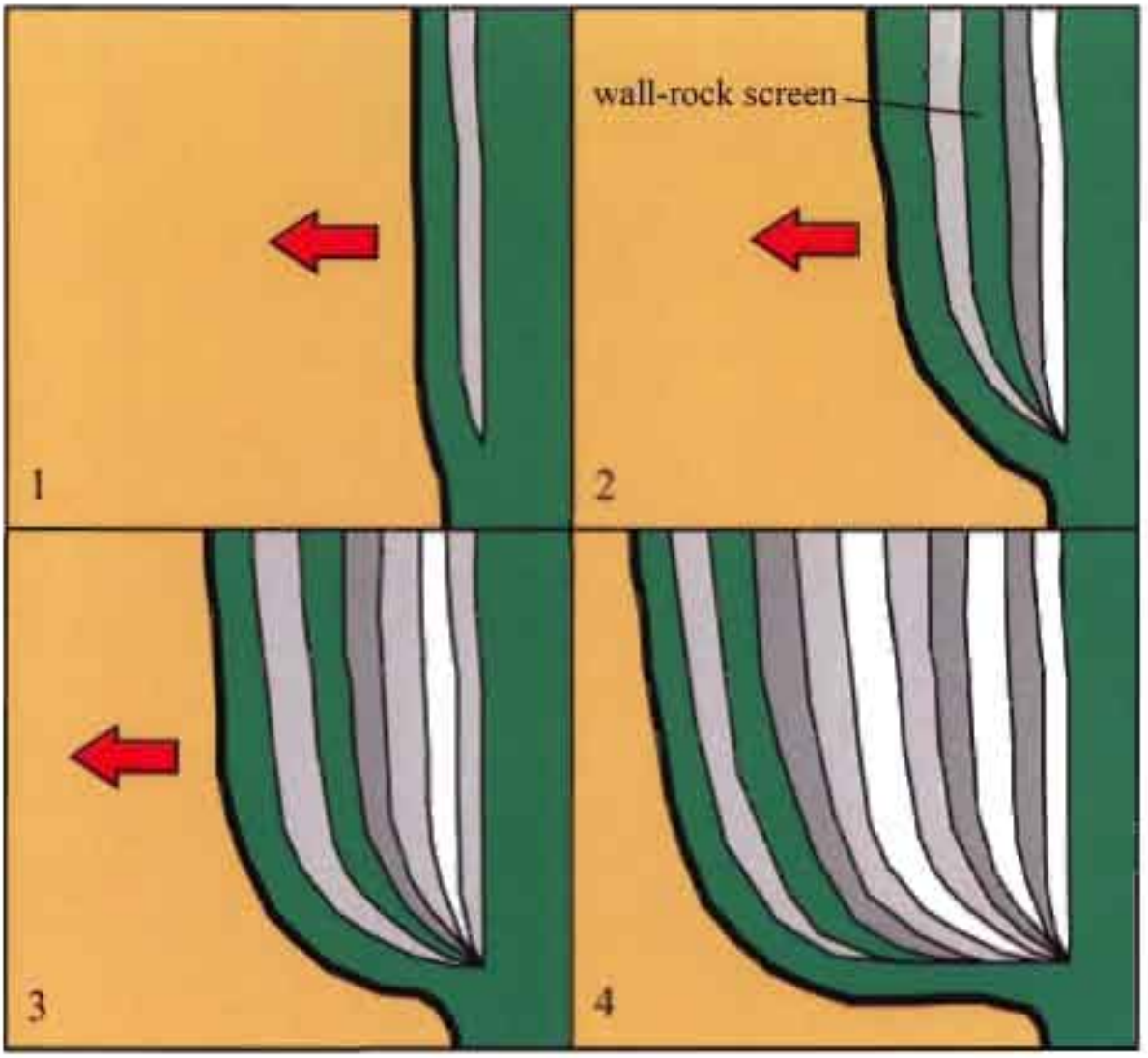

Figure 3.4: Model of dike intrusion that could create the observed pattern of folded wall-rock screens. Both the contact and the wall-rock screen are deflected nearly 90° by asymmetric incremental dilation. The tan and green rocks represent foliated wall rocks, and grey represents intruding dikes.

control the orientation of dike emplacement. Dikes emplaced in a system dominated by far-field stress are likely to be consistently oriented perpendicular to the minimum compressive stress. Conversely, overpressured magma will exploit pre-existing fractures in any orientation. Multiple dike orientations at the southern end of the map area suggest that magmatic overpressure contributed to emplacement of the McDoogle pluton.

The magmatic basalt, granodiorite, and aplite contained within a single subhorizontal dike (Figure 3.2 and 3.3) suggest that most magmas possibly be derived locally or from much deeper. petrologic The magma mingling within the subhorizontal dike may indicate that the majority of petrologic differentiation processes did not occur at the emplacement level. Rather, the magmatic relationships are more consistent with mechanical mingling in transit from the source region.

The lack of explicit cross-cutting relationships in the McDoogle pluton require age relationships to be inferred from map patterns. Two spatial problems arise if the border phases are older than the central phase. One, the border phases still would not have composed a single body if the central phase was not emplaced until later, because the abundant wall-rock screens in the central phase would have occupied space between the border phases. It seems improbable that two dike-like bodies would grow beside each other without intruding the foliated wall rock between them. Two, the central phase abruptly ends southward to the north of the border phase terminations. Undoing the dilation that accommodated the central phase would require both border phases to have been originally curved (Figure 3.5). Both border phases would then have been folded into

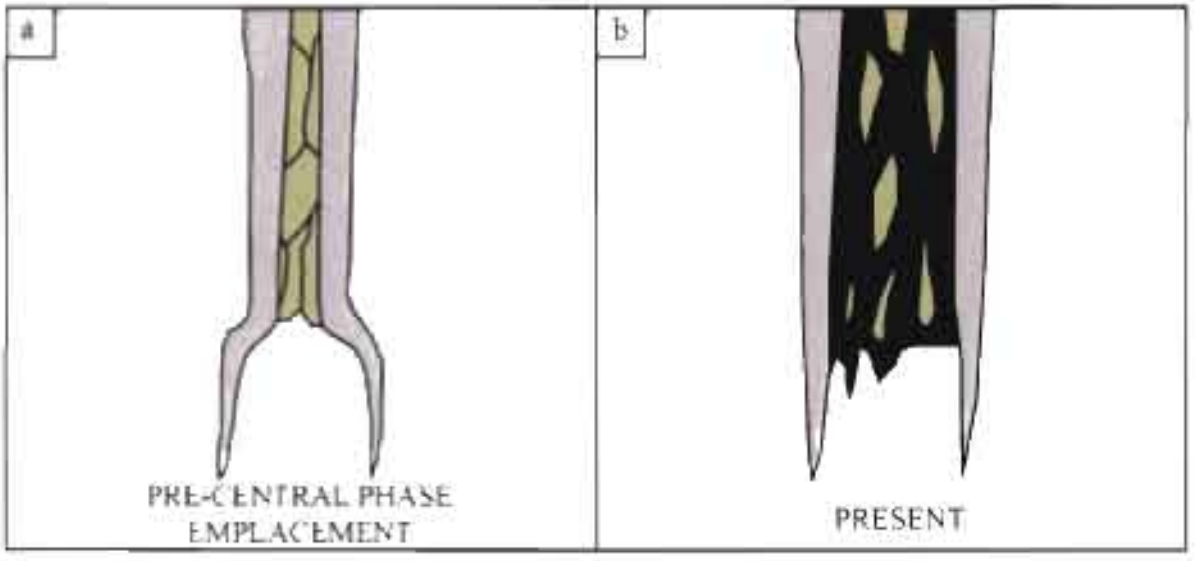

Figure 3.5. Hypothetical growth sequence and geometrical requirements if the border phases are younger than the central phase. a) The theoretical map pattern if the border phases are older than the central phase. The wall rocks between the phases and curvature are geometrically required by the b) existing map pattern of the pluton.

their current uncurved geometry by dilation to admit the central phase. It is thus possible, but unlikely, that the border phases are older than the central phase.

The different geometries of the border phases and central phase are interpreted to be related directly to the location of the hornblende granodiorite. The map patterns suggest that, during the emplacement of the McDoogle central phase, the wall rocks dilated to the width of the hornblende granodiorite. As the pluton transitioned from the intrusion of the central to the border phases, the mechanical effect of the hornblende granodiorite was eliminated. Without the hornblende granodiorite as a back stop, the border phases were free to extend southward as normal dike tips.

The structure of each phase is critical to understanding the emplacement of the entire McDoogle pluton. The sharp ends of the border phases suggest that they grew as dikes and that the strain associated with dilation was distributed in the wall rock toward the dike tips (Rubin, 1995). The termination of the central phase is structurally more complicated. The map pattern of wall-rock inclusions, folding, and the blunt termination suggests that the dilation was accommodated by an across-strike structure (Nicholson and Pollard, 1985) located at the blunt termination of the McDoogle central phase.

A metasedimentary interpluton screen separates the Woods Lake pluton from the McDoogle pluton to the west. Dilation along a discrete across-strike structure would offset passive markers like wall-rock screens. Thus, this structure would also have to extend into the wall rocks to the east because the screen on the western margin of the McDoogle has not been deflected. Reconnaissance mapping in these areas revealed no structure that could accommodate the dilation of the central phase. However, the

expected strain in the wall rocks to the east could be distributed across a diffuse zone instead of localized at a discrete plane, and thus it might be difficult to identify in the field.

CHAPTER 4

MAGNETIC SUSCEPTIBILITY OF THE MCDOOGLE PLUTON

Introduction

The magnetic properties of rocks have been useful for answering many geologic questions. Anisotropy of magnetic susceptibility has long been a focus of structural and igneous petrology investigations (Hrouda, 1982; Borradaile and Henry, 1997; Saint Blanquat et al., 2007). As internal contacts and structure were observed within plutons (Pitcher et al., 1972; McNulty et al., 2000; Mahan et al., 2003; Coleman et al., 2004; Glazner et al., 2004; Bartley et al., 2008), the need for a mapping technique that could distinguish subtle compositional variation became evident.

Several studies have successfully used field measurement of bulk magnetic susceptibility to map subtle compositional variations within plutons (Coleman et al., 2005; Gracely, 2007; Bartley et al., 2008). The ability to quantify the color index in the field also trains the eye of the worker to subtle compositional differences in the rock. Near Sawmill Lake, the McDoogle is compositionally heterogeneous, but sharp contacts and abrupt changes in lithology are rare. Lithologic differences tend to occur on the 10-100 m scale and are difficult to map by conventional methods that depend on discrete

rock units.

The relatively high bulk magnetic susceptibility of Sierran plutons (0.001-0.05 SI Units) has led to the assumption that the abundance of magnetite controls their bulk magnetic susceptibility. In addition to mapping of bulk magnetic susceptibility, this study investigates how well color index and rock composition are correlated to the bulk magnetic susceptibility in the McDoogle pluton.

Mapping instrumentation and method

The magnetic susceptibility was measured using a ZH Instruments SM-30 handheld meter. To measure the bulk rock value, at each station nine measurements were made on fresh planar surfaces within an area of ~1 m^2, in varied orientations to average out anisotropy (Appendix B). Individual magnetic susceptibility measurements ranged from < 1 x 10^{-3} to ~60 x 10^{-3} SI Units. From here forward, magnetic susceptibility values are reported as 10^{-3} SI units.

In the upper Sawmill Lake drainage, the McDoogle pluton is exposed on east-west elongate roche moutonnée that are separated by Quaternary alluvium, talus, and moraines (Chapter 2). Several east-west traverses were made as closely spaced as possible (~250 m). Station spacing within a traverse was ~50 m. Traverses in the Pinchot Pass area were impeded by rugged terrain, the younger Colosseum granodiorite, and significant groundcover. Wherever outcrop was sufficient, a 50-m station spacing was used. The arithmetic mean and 1-sigma standard deviation were calculated for each station and plotted in ArcGIS (Figure 4.1, 4.2, and 4.3, 4.4, respectively). The data were

then contoured using the inverse distance weighting (IDW) algorithm in ArcGIS. Input parameters for the IDW calculation were power = 2, stations in neighborhood = 12, and a variable neighborhood radius.

Mapping results

Sawmill Pass

Near Sawmill Lake at the southern end of the McDoogle pluton, BMS values were measured at 139 stations. Contouring the mean BMS value for each station produced a map that roughly reflects the geologic map (Figure 4.1). The central phase contains a tabular region of the highest BMS values. The tabular region is separated from the end of the central phase and the western border phase by an area with lower than average BMS (Chapter 2 and 3). The eastern border phase has a higher mean BMS value and varies more than the western border phase (Table 4.1). The two intermediate phases have a similar mean BMS values and standard deviations (Figure 4.2 and Table 4.1).

Pinchot Pass

Near Pinchot Pass at the northern end of the McDoogle pluton, 104 stations were measured. Contouring the mean BMS value for each station yielded a more complex and enigmatic map than near Sawmill Lake (Figure 4.3). Overall, BMS is lower at the northern end of the McDoogle pluton. A region of high BMS lies across a lithologic contact between the western border phase and the central phase. An extremely low BMS

a

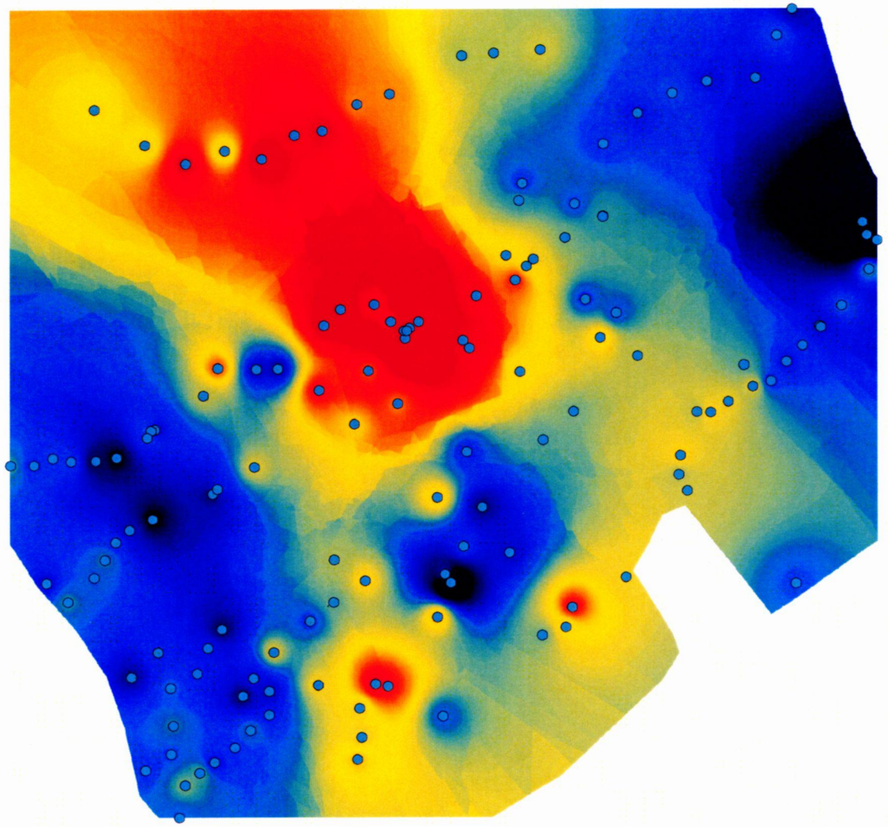

b

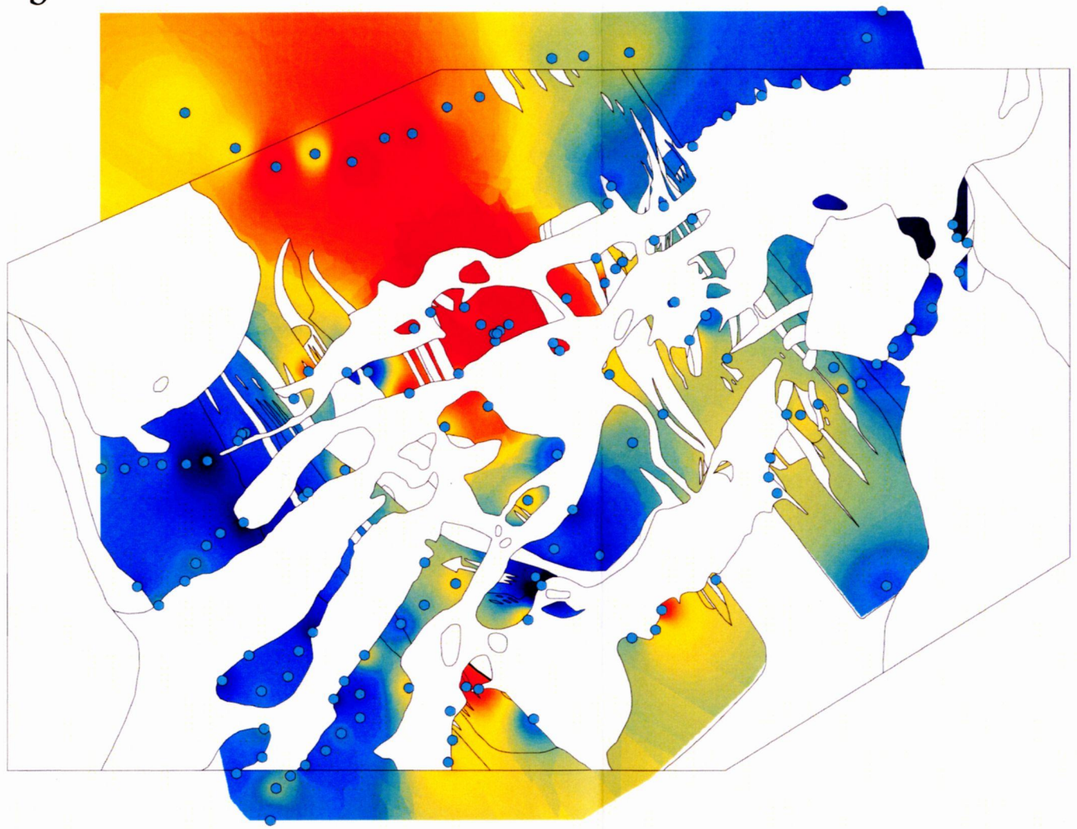

Figure 4.1: a) Map of the BMS near Sawmill Lake contoured by inverse distance weighting. Red represents regions of high BMS values and blue represents regions of low BMS values (~2 -45x10-3 SI units; Table 4.1). b) BMS map with the geologic map overlaid. Wall rocks and surficial units are white.

a

b

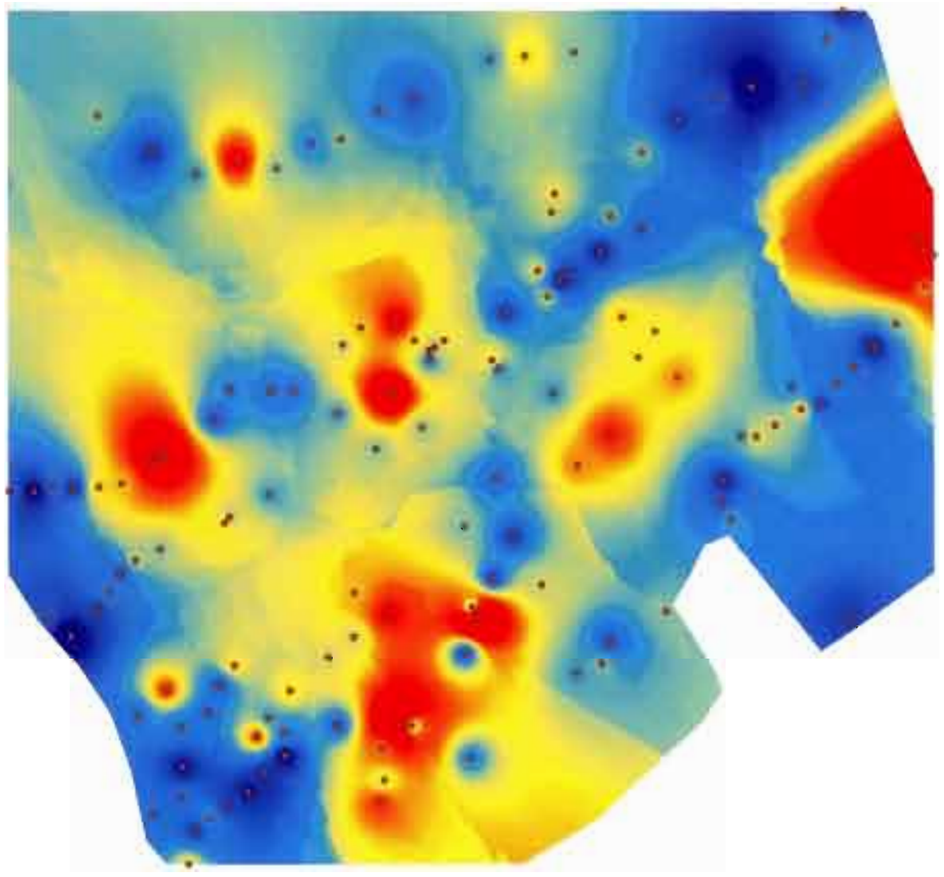

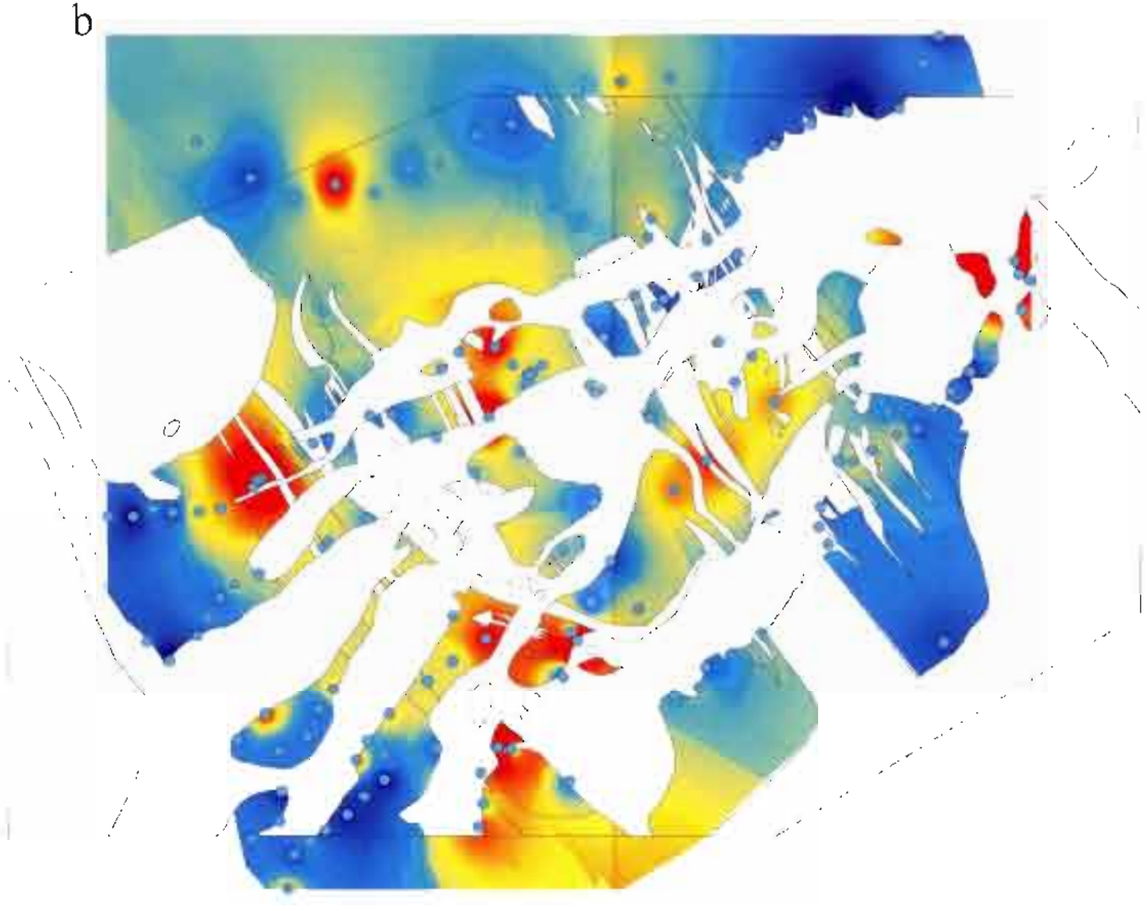

Figure 4.2: a) Map of 1 ⁻ standard deviation of the BMS near Sawmill Lake contoured by inverse distance weighting. Red represents regions of higher standard deviation and blue represents regions of lower standard deviation (~0 - 5). b) Map with the geologic map overlaid. Wall rocks and surficial units are white.

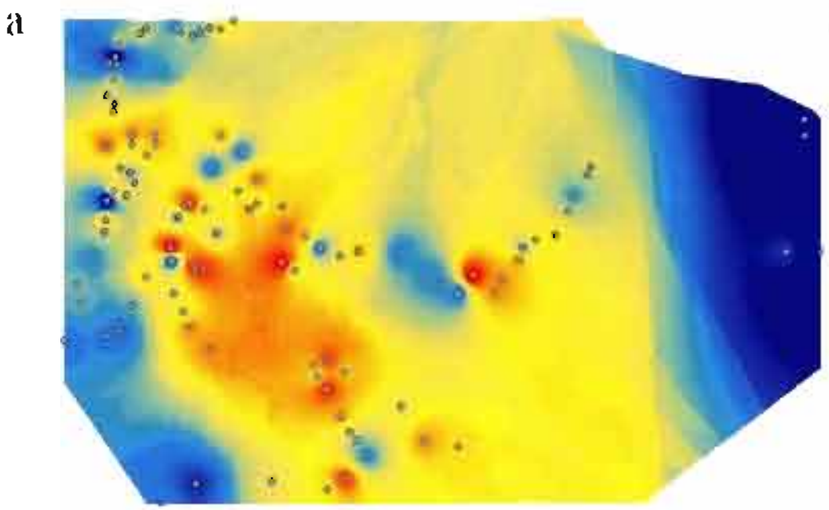

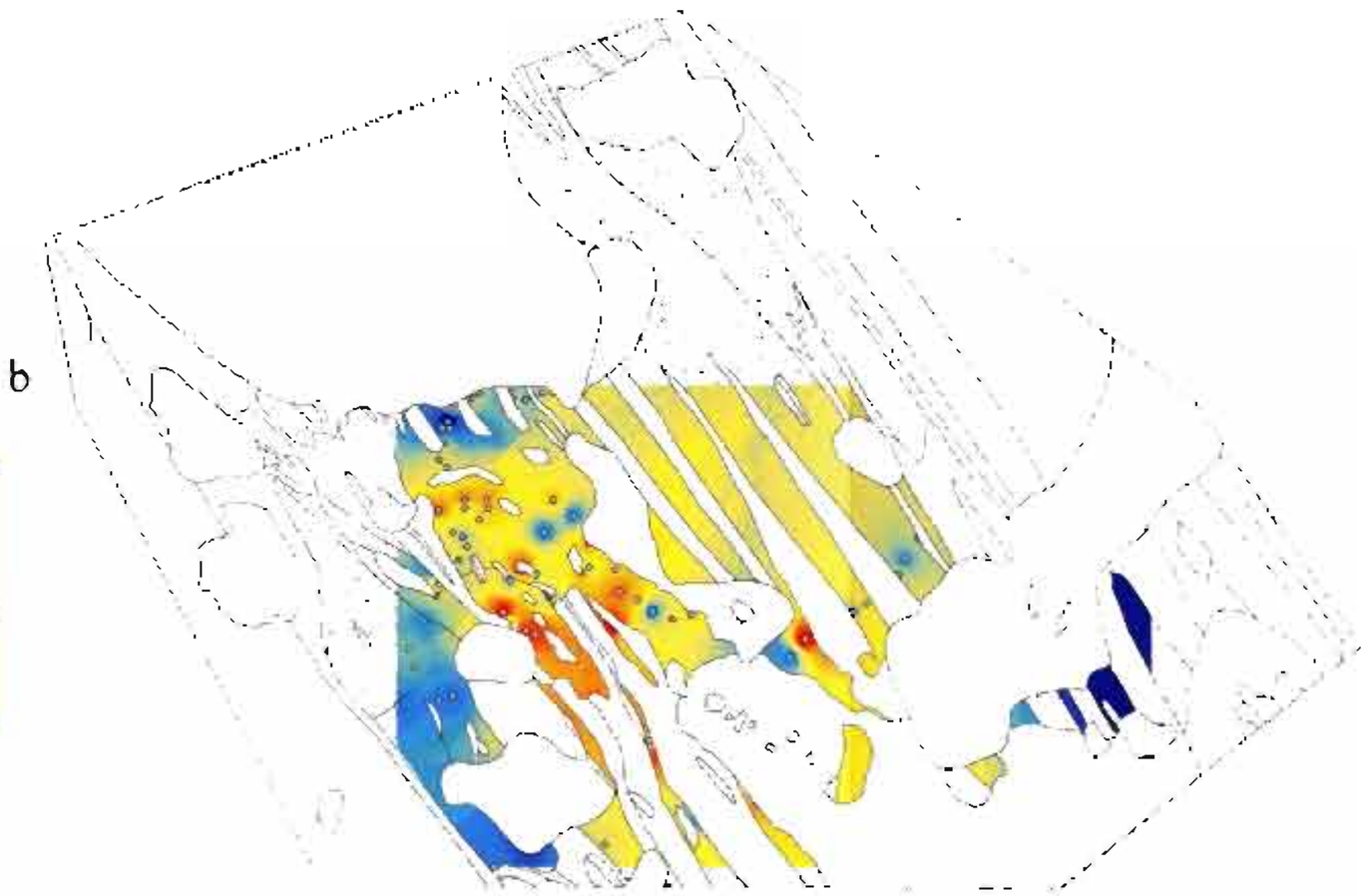

Figure 4.3. a) Map of the BMS near Pinchot contoured by inverse distance weighting. Red represents regions of high BMS values and blue represents regions of low BMS values (~0 - 35 x 10-3 SI units, Table 4.1). b) BMS map with the geologic map overlaid. Wall rocks and surficial units are white. The McDoogle pluton is hatched where not contoured.

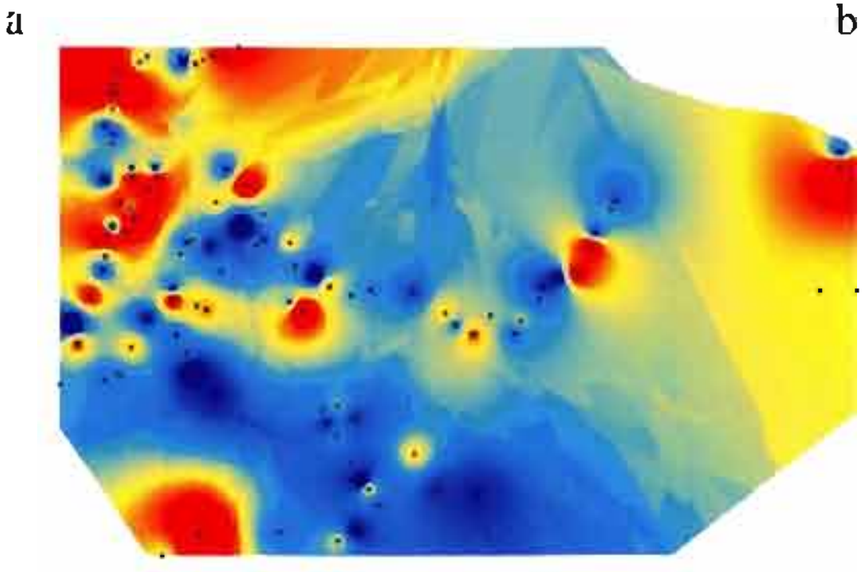

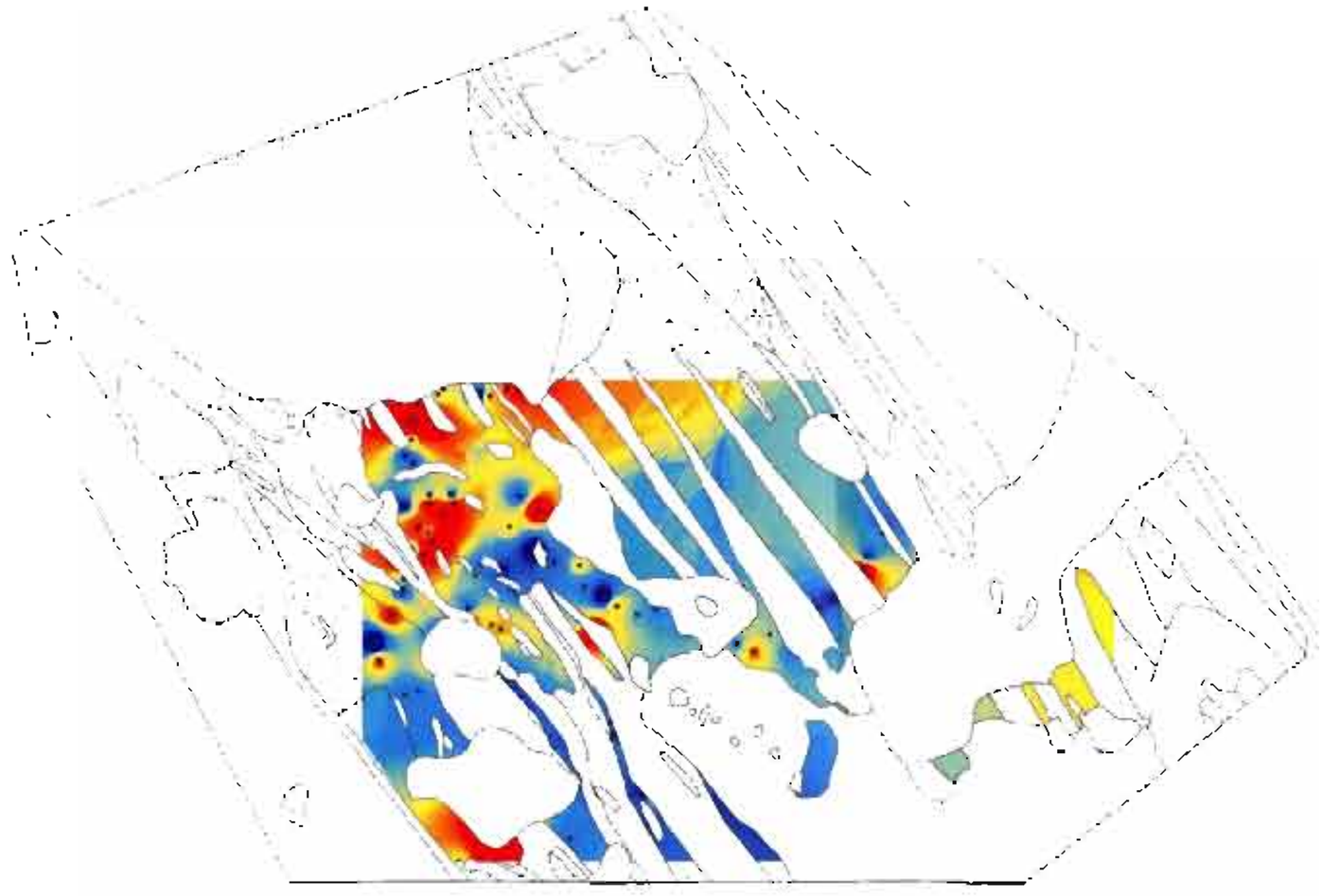

Figure 4.4 a) Map of 1 standard deviation of the BMS near Pinchot Pass contoured by inverse distance weighting. Red represents regions of higher standard deviation and blue represents regions of lower standard deviation (~0 - 5). b) Map with the geologic map overlaid. Wall rocks and surficial units are white. The McDoogle pluton is hatched where not contoured.

TABLE 4.1: BULK MAGNETIC SUSCEPTIBILITY* BY INTRUSIVE PHASE

Location	Phase	measurements (n)	mean	1-sigma	maximum	minimum
Sawmill Lake	western Kmb	37	18.14	2.947	25.07	12.22
	western Kmi	5	18.96	3.068	22.52	14.67
	Kmc	79	23.48	5.995	45.48	1.94
	eastern Kmi	2	19.93	3.239	22.22	17.64
	eastern Kmb	16	14.98	6.035	21.02	2.20
	all phases	139	20.84	6.101	45.48	1.94
Pinchot Pass	western Kmb	40	21.86	3.117	32.02	6.16
	Kmc	60	22.12	3.584	31.69	0.36
	eastern Kmb	4	3.92	0.714	13.62	0.19
	all phases	104	21.43	6.111	32.38	0.19

* all BMS values are shown in 10^{-3} SI units

region exists on the eastern margin of the pluton, but this is most likely due to late-stage oxidation indicated by a pervasive rust stain on rocks in this area.

Calibration of bulk magnetic susceptibility to color index

Method

Nine samples were collected near Sawmill Lake from outcrops that spanned the range of measured BMS values in the McDoogle pluton. Mineral modes were obtained by point counting two thin sections from each sample (Figure 4.5 and Table 2.1). Roughly 275 points were counted in each thin section for a total of ~550 points per sample. A grid spacing of 1.5 mm was used owing to the large grain size (1-5 mm) of the rocks (Solomon, 1963). From the mineral modes the color index (CI) was calculated:

$$\text{color index} = \frac{(mafic)}{(mafic + felsic)} * 100$$

The color index was compared to the BMS values of the nine samples (Figure 4.6a). With increasing BMS, the color index also increases but the correlation is poor (R^2 = 0.42) (Figure 4.6a). Further inspection of the thin sections in reflected and transmitted light and using electron microprobe analysis (EMPA) showed that magnetite and ilmenite are both present in rocks with lower susceptibilities (samples MS07-F2, F3, and F4). At higher magnetic susceptibilities magnetite is the only strongly magnetic phase. Magnetite (vol. k = 1.0-5.7 SI Units) generally contributes more to BMS than ilmenite (vol. k = 0.0022-3.800 SI Units) (Hunt et al., 1995) and thus a higher proportion of ilmenite should

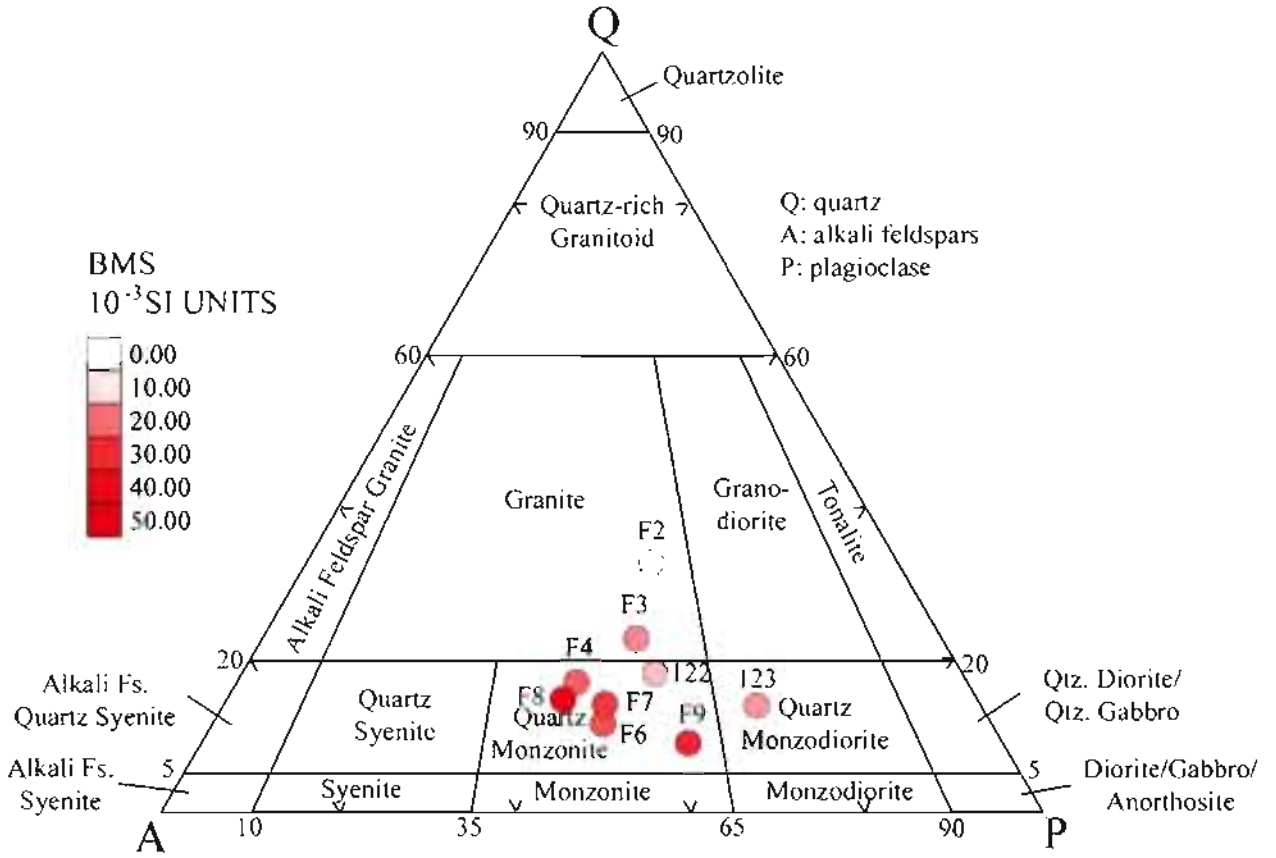

Figure 4.5: Quartz/alkali feldspar/plagioclase feldspar mineral modes plotted with IUGS classifications. Nine samples were collected from sites that spanned the range of observed BMS values. The color of the data corresponds to the mean BMS of the sample site.

a

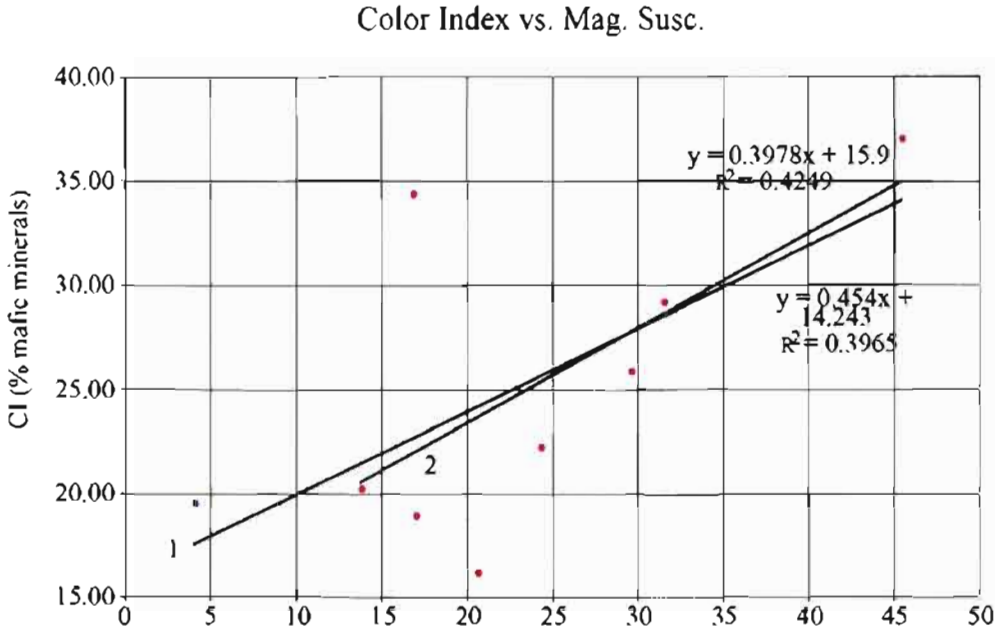

b

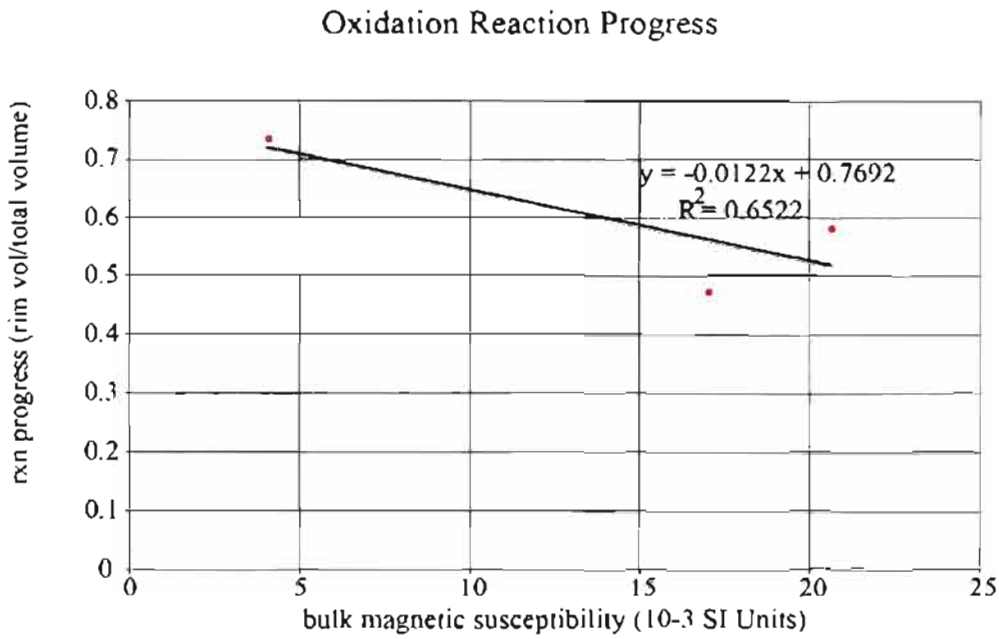

Figure 4.6: Plots showing the relationships between BMS, CI, and oxidation reaction progress. a) CI versus field BMS of nine samples. Regression line 1 includes all the data. Regression line 2 excludes sample MS07-F2 due to its high ilmenite proportion. b) Estimated reaction progress versus BMS of three samples. The negative slope of the regression line suggests that late-stage oxidation does

yield a lower BMS. Magnetite also occurred in several habits that range from euhedral to anhedral.

Some magnetite and ilmenite grains have titanite rims. Both the thickness of the titanite rim and the ratio of thickness to grain size varied throughout the samples. Simplified oxidation reactions that describe the overgrowth texture of ilmenite, based on the phases present in the rock, are:

Reaction 4.1: $\mathbf{4}CaFeSi_2O_6 + \mathbf{4}FeTiO_3 + \mathbf{7}O_2 = \mathbf{2}Fe_3O_4 + \mathbf{4}CaTiSiO_5 + \mathbf{4}SiO_2$

clinopyroxene ilmenite magnetite titanite quartz

Reaction 4.2: $\mathbf{6}Ca_2Fe_5Si_8O_{22}(OH)_2 + \mathbf{12}FeTiO_3 + \mathbf{7}O_2 = \mathbf{14}Fe_3O_4 +$

hornblende ilmenite magnetite

$\mathbf{12}CaTiSiO_5 + \mathbf{36}SiO_2 + \mathbf{6}H_2O$

titanite quartz

To estimate the degree of oxidation of samples containing ilmenite, reaction progress was estimated from the approximate volumes of grains and overgrowths by measuring the rim thickness and grain radius (i.e., reaction progress = (rim vol./grain vol.).

Both descriptive oxidation reactions produce magnetite, so it is necessary to check the correlation between estimated reaction progress and BMS (Figure 4.6b). As the BMS increases, reaction progress decreases ($R^2 = 0.65$). The negative correlation between reaction progress and BMS suggests that the signal is not controlled by late-stage oxidation of the pluton.

Qualitatively, the proportion of ilmenite decreases as BMS increases. Sample MS07-F2 has the highest amounts of ilmenite and systematically lower BMS than other samples. This samples were excluded from the second regression analysis based on the relationship between their ilmenite proportions and BMS. However, removal of MS07-F2 did not improve the correlation ($R^2 = 0.39$) (Figure 4.6a). Sample MS07-123 also has a systematically lower BMS than other samples, but contains only magnetite. Removing both outlier samples improved the correlation significantly ($R^2 = 0.89$).

The modal proportions of the oxides are important to understand the effect ilmenite has on the BMS. The relative proportions of magnetite and ilmenite were calculated by producing x-ray backscatter images on a scanning electron microscope (SEM). Oxide phases were identified using spot chemical analyses. The relative proportions were derived from the area of each oxide grain calculated by image analysis. The relative phase proportions were applied to the opaque accessory phase proportions obtained from point counting (Chapter 2).

Two problems exist with this method. One, the contrast of each oxide phase was too low to distinguish between different phases. Thus, each grain was only identified based on spot chemical analyses. The grains are more complicated internally. Exsolution laminae and composite grains are common in these phases (Price, 1980), and were not visible in backscatter x-ray imaging. The complicated magnetite grains probably contain a proportion of exsolved ilmenite. Thus, the volume proportions extrapolated from these images would likely have underestimated the proportion of ilmenite. Two, the modal proportions of opaque minerals obtained from point counting are not precise enough to

incorporate the calculated oxide proportions. The coarse grain size of the rocks dictated a larger grid spacing and fewer points per thin section. This led to imprecise modal proportions for the minor phases, like oxides. Often phases that can be found in transmitted light microscopy are not represented in the point-counted modal proportions.

Measuring BMS and CI at two drastically different volumes may result in a poor correlation. To address this concern the BMS of the thin-section billets from the nine samples were measured in the laboratory using a AGICO Kappabridge . The lab BMS measurements correlate poorly with the field data ($R^2 = 0.48$) (Figure 4.7a). Ideally the modal proportions and BMS data obtained from the same rock volume should have correlated well. This approach yielded data with significant outliers ($R^2 = 0.47$), most likely due to the large grain size of the McDoogle pluton (Figure 4.7b). The samples are commonly magnetically unrepresentative of the outcrop from which they were taken, and range both significantly higher and lower than mean outcrop value of sample location. To eliminate the effect of the large grain size of the McDoogle pluton it is necessary to obtain mineral modes and BMS from the same scale of sample volume. BMS measurements and modes from polished slabs may yield a better coupling.

Discussion

Mapping magnetic susceptibility in the two best exposed portions of the McDoogle pluton met with varied success. The relationship between the conventional geologic map and the BMS pattern near Pinchot Pass is unclear, and thus the significance

a

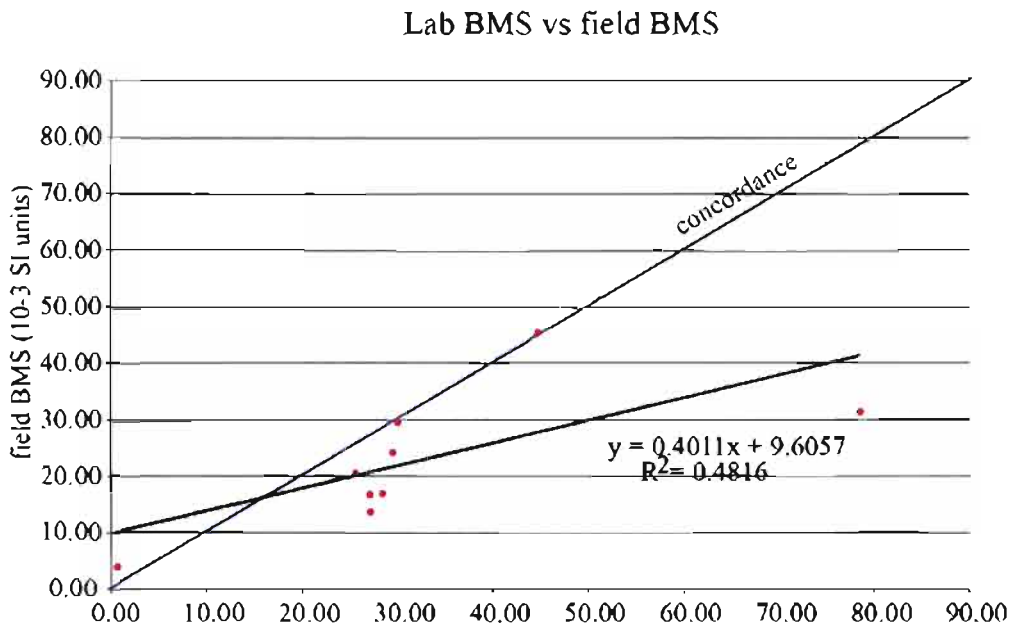

b

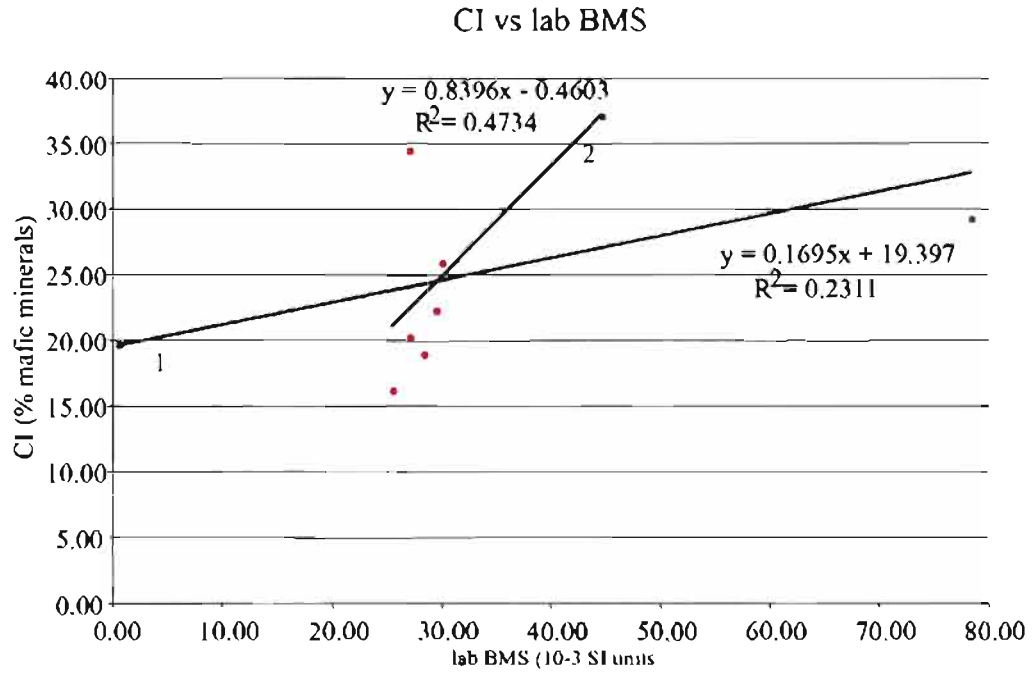

Figure 4.7: Plots showing the relationships between lab and field BMS, and lab BMS and CI. a) Field BMS versus lab BMS of nine samples. The blue line represents concordance between lab and field BMS measurements. The black line is a linear regression of all samples. b) CI versus lab BMS of nine samples. Regression line 1 includes all samples, and regression line 2 excludes

of the BMS variations is unclear. More data collected in a denser array might resolve the complexity of the BMS map.

Mapping BMS in the Sawmill Lake area was more successful. BMS correlates with outcrop-scale changes of CI in the McDoogle pluton and illuminates subtle petrologic variations that cannot be shown on the geologic map (Plate 1, in pocket). With more investigation, an additional mafic phase could likely be mapped within the central phase based on the BMS map. The low BMS area wrapping around the southern and western margins of the high BMS "mafic phase" supports the interpretation that the folding pattern observed in wall-rock screens at the southern end of the central phase resulted from intrusion of the central phase (Chapter 3). A denser dataset might also help clarify the structurally complex termination of the central phase, but denser sampling is not possible in some areas due to the Quaternary cover. Denser station spacing with the existing outcrop might resolve some of the complexities.

The mineralogical properties that control BMS in the McDoogle pluton are poorly understood. Ilmenite is present in sample with low BMS and seems to account for sample MS07-F2's higher than expected CI/BMS ratio. At higher BMS values, where ilmenite is absent, the correlation between CI and BMS seems to be controlled by other phases. Possibilities include abundance of magnetite relative to mafic phases and the presence sulfide phases like pyrite.

Several generations of both iron and titanium oxide phases suggest a complex crystallization history. If the oxygen fugacity of the magma is controlling the crystallization, ilmenite would have to begin crystallizing first (Buddington and Lindsley,

1964; Robinson and Miller, 1999). This is consistent with resorption textures of ilmenite. The crystallization of magnetite followed. Euhedral magnetite is observed to be included in other euhedral-subhedral crystals. This texture may be interpreted two ways. One, the euhedral magnetite may have begun crystallizing before the mineral that now encases it. Two, the magnetite may be euhedral because it has a strong preference for rational crystal faces, and may have grown in the solid state (Means and Park, 1994).

As the pluton cooled, the oxygen fugacity likely increased and reached a threshold at which the main titanium-bearing phase switched from ilmenite to titanite. This complex crystallization history suggests that the BMS of the rocks is not solely controlled by composition but also by the evolving oxygen fugacity of the cooling magma. In order to better understand the effect of ilmenite on the BMS signal, relative proportions of the ferro-ferrimagnetic phases must be known.

CHAPTER 5

U-Pb GEOCHRONOLOGY

Introduction

Uranium-lead (U-Pb) zircon geochronology is the preferred method for dating intrusive rocks because of the large range of age than can be dated accurately, the relatively high precision, and two independent decay series. Two unstable uranium isotopes, ^{235}U and ^{238}U, decay at different rates to produce two lead isotopes, ^{206}Pb and ^{207}Pb, respectively. Zircon is a refractory mineral that incorporates U and Th but excludes Pb from its crystal structure (Parrish and Noble, 2003). The closure temperature of zircon with respect to Pb diffusion is ~900°C (Cherniak and Watson, 2000), which is significantly higher than the solidus of granitoids. Thus, a zircon U-Pb age is interpreted to be the crystallization age of the zircon and, by extension, of the igneous rock that contains it. Recent advances in sample preparation technique, such as chemical abrasion (Mattinson ref.), have increased precision to ±~0.1%. Concordia diagrams (Wetherill, 1956) are a useful tool for evaluating the quality of U-Pb data. Samples that do not contain inherited Pb and have suffered no gains or losses of U and Pb will plot within error on concordia, producing concordant ages. A concordant age means that both ^{235}U

and ^{238}U decay series are in agreement and give the same calculated age. Inheritance of older zircon, improper common Pb correction, and Pb loss will each affect the pattern of data in a different way, but will generally lead to results that plot off concordia.

U-Pb zircon geochronology has been applied in regional studies of the Sierra Nevada batholith (Stern et al., 1981; Chen and Moore, 1982), as well as in many topical studies in the region (Carl, 2000; Mahan et al., 2003; Coleman et al., 2004). U-Pb zircon geochronology was used in this study to investigate age relationships among the different phases, and place limits on the growth duration of the McDoogle pluton.

Results

Zircons from all samples were colorless, euhedral, and had no visible overgrowths or cores. Cathodoluminescence was not used to image the grains. All ages are reported as the weighted mean of three or more equivalent fractions with 2σ errors. Equivalent fractions overlap within error and are statistically the same. Decay-constant errors have been ignored because this study compares data within the same decay systems. Shown with the ages are the mean squares of weighted deviates (MSWD) and the number of fractions (n) included in the weighted mean age (Figure 5.1, 5.2, and 5.3; Table 5.1). The ages reported here are not known with the highest confidence and should be treated as preliminary results. More work will be done on samples MS07-F8 and KM99-11B to increase the robustness and confidence level of the results. However, it is unlikely that further work will change the results significantly.

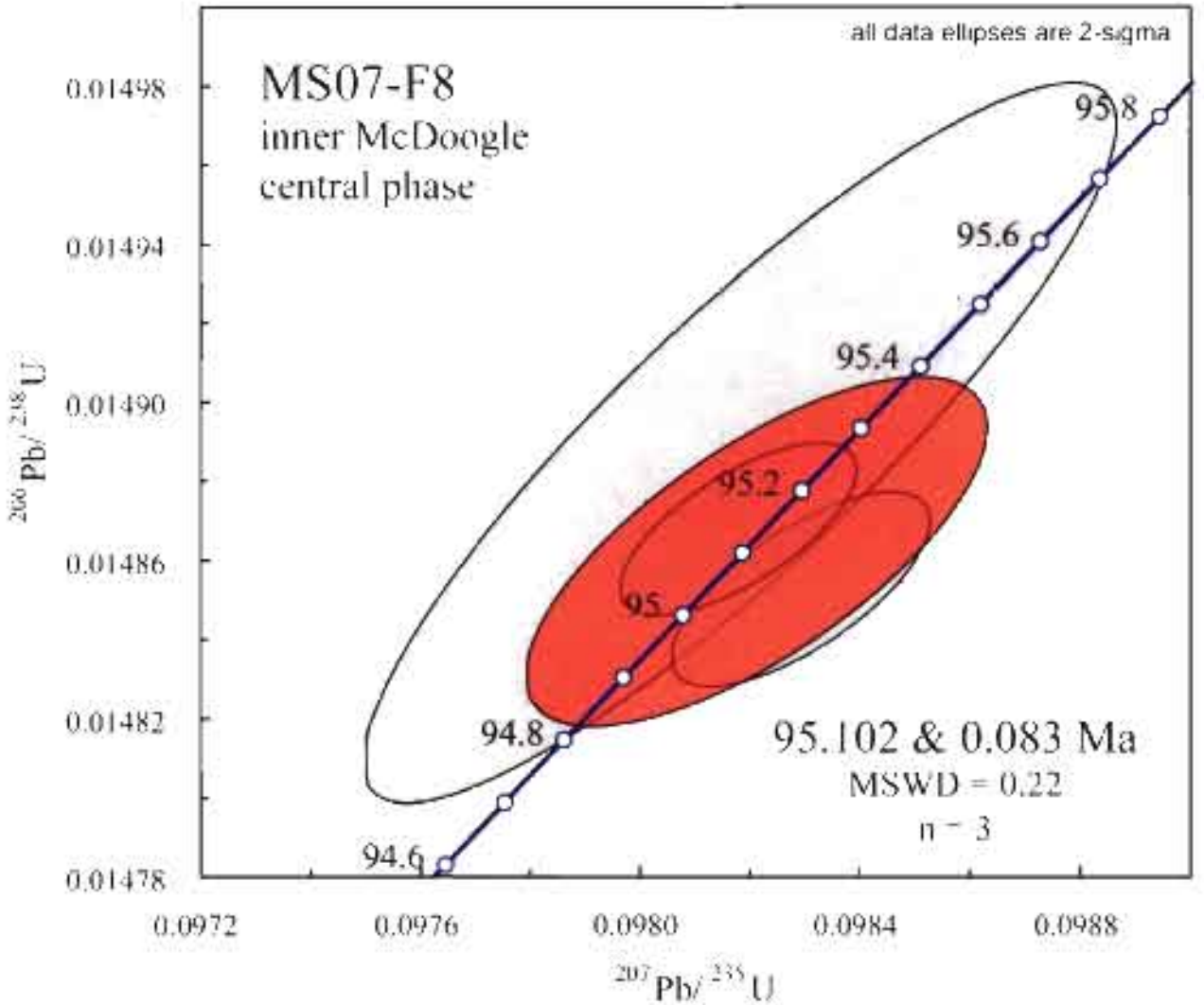

Figure 5.1: Concordia plot showing the mean age (red) of three fractions from sample MS07-F8. This sample was collected from the center of the McDoogle central phase west of Sawmill Lake.

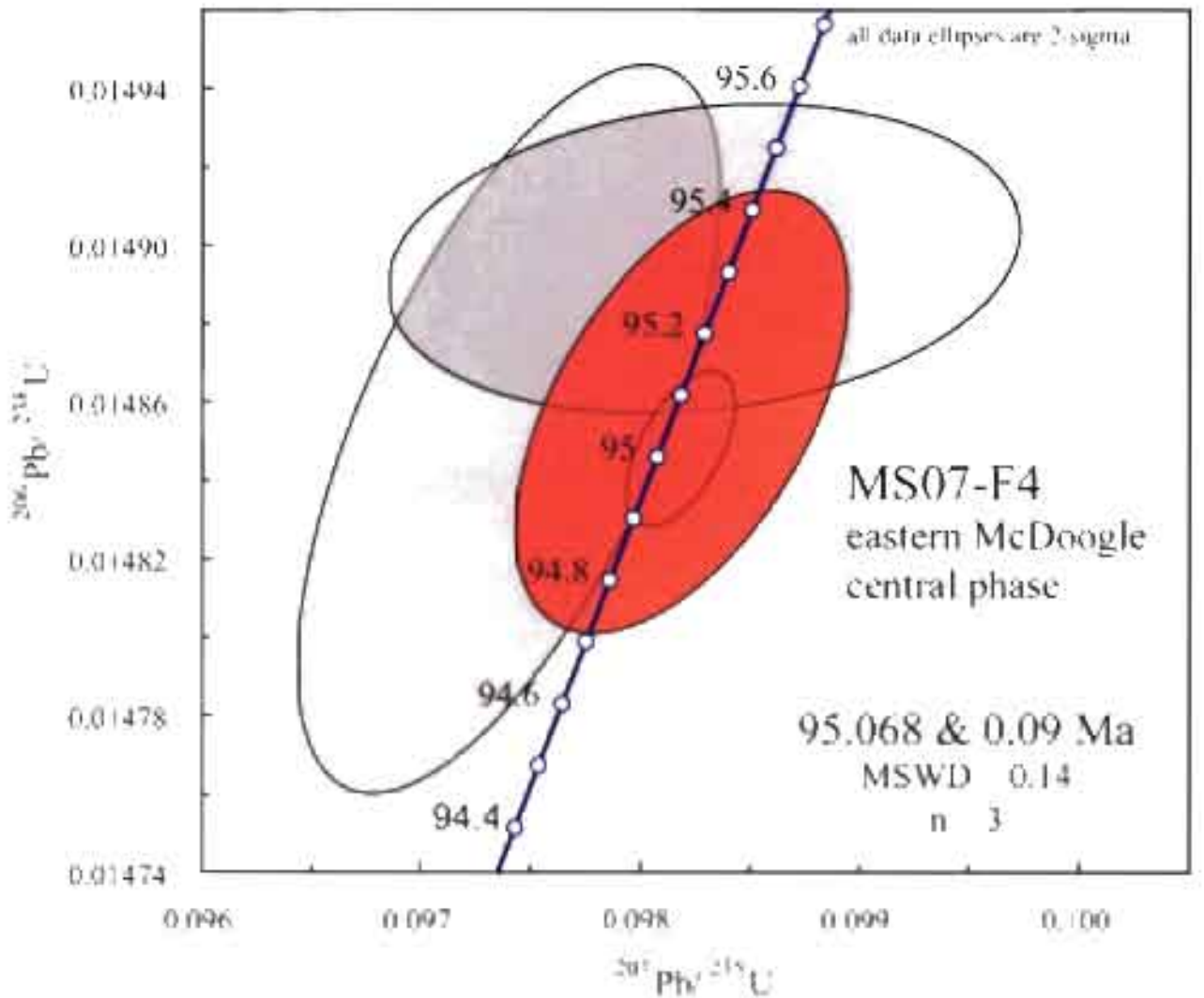

Figure 5.2. Concordia plot showing the mean age (red) of three fractions from sample MS07-F4. This sample was collected from the eastern margin of the McDoogle central phase west of Sawmill Lake

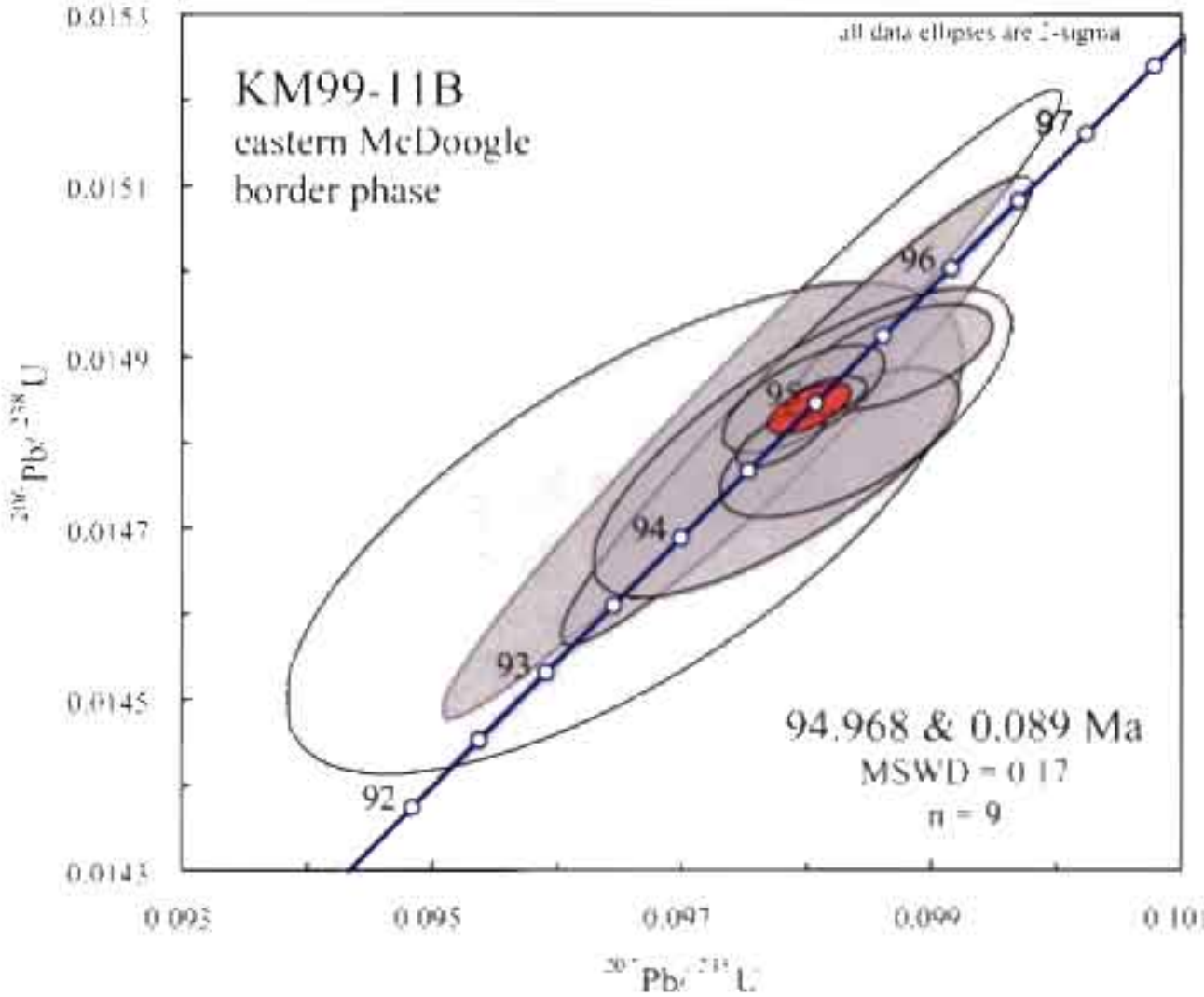

Figure 5.3 Concordia plot showing the mean age (red) of nine fractions from sample KM99-11B (Mahan et al., 2003). This sample was collected from the eastern border phase near Sawmill Lake.

TABLE 5.1: U-Pb FOR DATA FOR ROCKS OF THE SAWMILL LAKE AREA

		conc.	(ppm)	206Pb	206Pb	error	207Pb	error	207Pb	error	ages (Ma) 206Pb	207Pb	207Pb	corr.	total common
fraction (n)	weight (mg)	U	Pb*	204Pb	238U	(%)	235U	(%)	206Pb	(%)	238U	235U	206Pb	coef.	Pb (pg)
MS07-F8 McDoogle pluton - Km1 (UTM E 379180 N 4082993)															
z1 (2)	0.0139	764.1	12.63	749.33	0.01489	(0.50)	0.09818	(0.57)	0.04782	(0.27)	95.28	95.09	90.41	0.88	13.8
z2 (2)	0.0180	447.8	7.17	2605.53	0.01487	(0.12)	0.09817	(0.18)	0.04789	(0.13)	95.14	95.09	93.91	0.69	3.0
z3 (2)	0.0203	574.6	9.04	4474.64	0.01485	(0.14)	0.09829	(0.20)	0.04799	(0.14)	95.04	95.19	99.04	0.70	2.5
MS07-F4 McDoogle pluton - Km2 (UTM E 379597 N 4083232)															
z3 (1)	0.0222	458.4	7.70	967.03	0.01485	(0.51)	0.09739	(0.81)	0.04756	(0.62)	95.04	94.36	77.27	0.65	10.1
z4 (1)	0.0320	397.3	6.18	2790.14	0.01485	(0.11)	0.09818	(0.21)	0.04796	(0.17)	95.01	95.09	97.25	0.56	4.3
z7 (1)	0.0250	125.0	1.96	1061.04	0.01490	(0.22)	0.09828	(1.21)	0.04785	(1.19)	95.32	95.19	92.05	0.19	2.8
KM99-11B McDoogle pluton - Kmb (UTM E 380170 N 4082950)															
z2 (2)	0.0074	332.6	5.42	431.89	0.01485	(2.03)	0.09756	(2.08)	0.04766	(0.44)	95.00	94.52	82.41	0.98	5.6
z3 (2)	0.0088	285.3	4.31	633.83	0.01485	(0.35)	0.09797	(0.54)	0.04784	(0.40)	95.04	94.90	91.58	0.67	3.9
z4 (1)	0.0083	392.4	6.66	375.79	0.01484	(1.51)	0.09792	(1.58)	0.04786	(0.44)	94.95	94.85	92.43	0.96	8.6
z5 (2)	0.0103	429.3	6.73	1437.40	0.01481	(0.19)	0.09779	(0.29)	0.04791	(0.22)	94.74	94.74	94.69	0.67	2.9
z7 (2)	0.0034	825.7	13.38	3509.81	0.01485	(0.13)	0.09816	(0.27)	0.04793	(0.23)	95.05	95.07	95.67	0.52	0.8
z9 (1)	0.1600	306.9	5.40	456.40	0.01480	(0.48)	0.09826	(0.80)	0.04815	(0.62)	94.70	95.20	107.00	0.63	ND
z10 (1)	0.0840	361.5	7.00	254.00	0.01490	(0.34)	0.09871	(0.64)	0.04800	(0.52)	95.40	95.60	99.30	0.59	ND
z11 (3)	0.0880	243.9	4.20	486.60	0.01470	(1.60)	0.09653	(2.30)	0.04754	(1.70)	94.20	93.60	76.50	0.70	ND
z12 (1)	0.0400	361.5	5.90	881.60	0.01480	(1.00)	0.09796	(1.40)	0.04794	(0.89)	94.80	94.90	96.30	0.77	ND

note: additional analytical and statistical data included in Appendix C

* Radiogenic

Three samples were analyzed. Samples (MS07-F8 and MS07-F4, Figure 5.4) were collected from the center and eastern margin of the central phase, respectively. Additional zircons from the Mahan et al. (2003) sample from the eastern border phase (KM99-11B, Figure 5.4) were analyzed using updated techniques to improve the precision of their original 94.8±0.6 Ma age. The inner central phase sample (MS07-F8) yielded an age of 95.102±0.083 Ma (Figure 5.1). One reversely discordant fraction from this sample was discarded. The reverse discordance of the fraction was most likely due to an inappropriate common lead correction. The eastern central phase sample (MS07-F4) yielded an age of 95.068±0.09 Ma (Figure 5.2). This sample yielded a complex population of fractions that spread for 1.6 Ma along concordia. The spread is interpreted to reflect zircon recycling from previous increments of the McDoogle pluton and does not represent the "crystallization age" of the sample. The oldest fraction was not equivalent to the other fractions. This date is interpreted to reflect inheritance and therefore it was excluded from the calculation. Two fractions from MS07-F8 were reversely discordant and interpreted to also reflect an inappropriate common lead correction. The addition of new fractions to the Mahan et al. (2003) dataset yielded a new age of 94.968±0.089 Ma (Figure 5.3). Two reversely discordant fractions were discarded due to an inappropriate common lead correction. One discordant fraction does not define a meaningful discordia line, and was interpreted to be inherited and discarded.

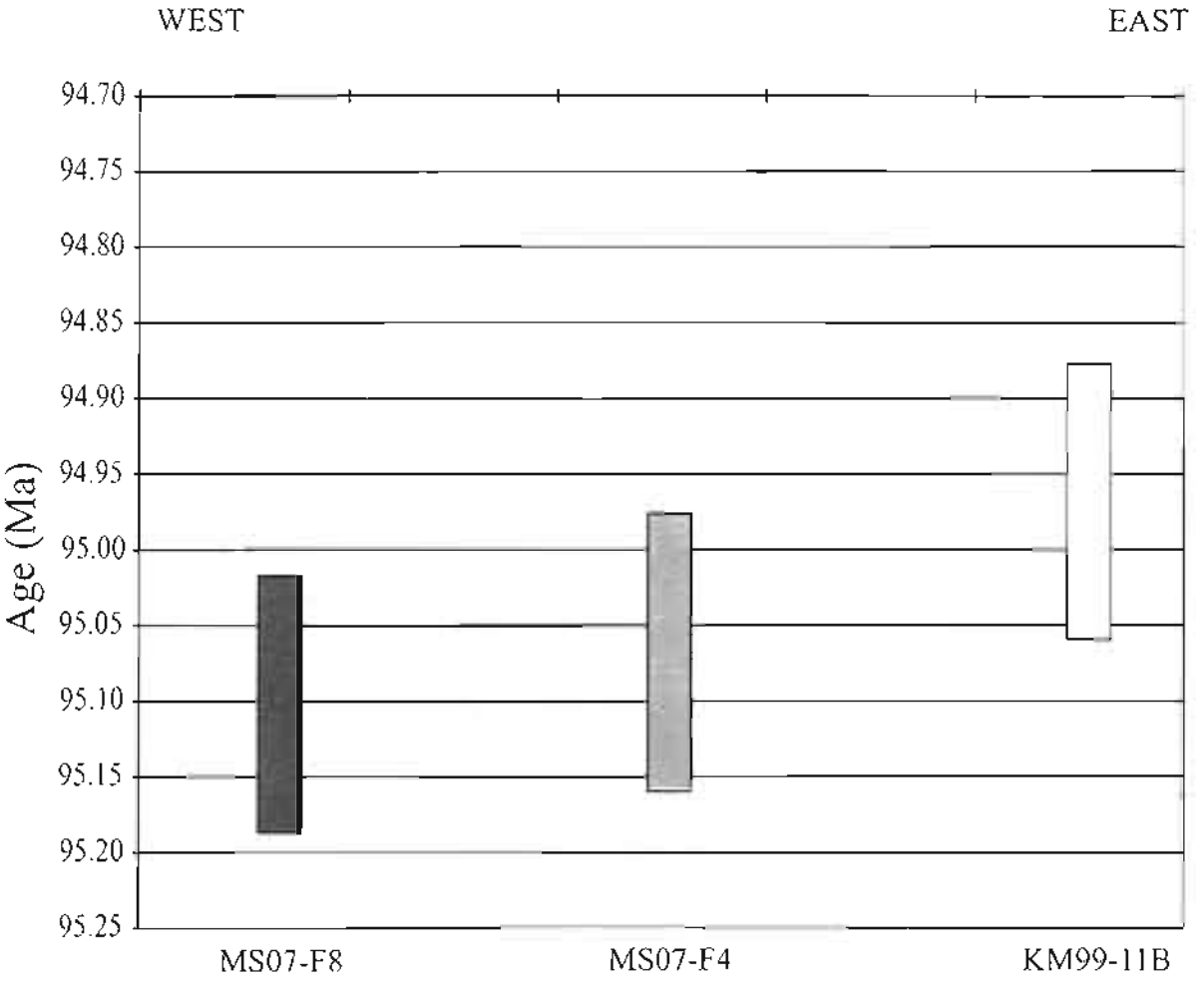

Figure 5.4: The growth duration of the McDoogle pluton. Each bar is a single U-Pb zircon age, and the length of the bar is the 2-sigma error of the date. Each date is statistically equivalent, so the growth duration is a minimum.

Discussion

All three ages overlap within analytical error and are statistically equivalent. The preliminary U-Pb data suggest that the McDoogle pluton rapidly intruded the Sawmill Lake shear zone. The data suggest that the central phase is older than the border phase, but the measured age difference is not statistically meaningful. Howver, this age relationship is consistent with the relationship based on map interpretations in Chapter 3.

Dike intrusion rates are controlled by two driving forces: far-field stresses and magmatic overpressure. The tabular shape of the McDoogle pluton allows a simple intrusive rate to be calculated based on the wall-rock dilation required by the width of the pluton. Near Sawmill Lake, the McDoogle pluton is ~1325 m thick, excluding wall-rock screens. The maximum growth duration based on the preliminary U-Pb age data is 306,000 yrs. This requires a minimum local wall-rock dilation rate of ~4.5 mm/yr. Further north in the John Muir Intrusive Suite (JMIS), Gracely's (2007) results from the Lamarck granodiorite in Dusy Basin define a similar maximum growth duration (Figure 5.5) and minimum dilation rate (~3.5 mm/yr). Long-term local displacement rates in a continental setting are usually ~1-2 mm/yr (e.g., Leeder et al., 2008), although short-term local geodetic rates can be as high as ~10 mm/yr. The minimum local rate of ~4.5 mm/yr over 10^5 yr time scale thus suggests that magmatic overpressure contributed significantly to making space for the intrusion.

Delaney et al. (1986) demonstrated that dike systems dominated by far-field stresses will be similarly oriented, and systems dominated by magmatic overpressure will tend to have more random orientations due to the exploitation of pre-existing fractures.

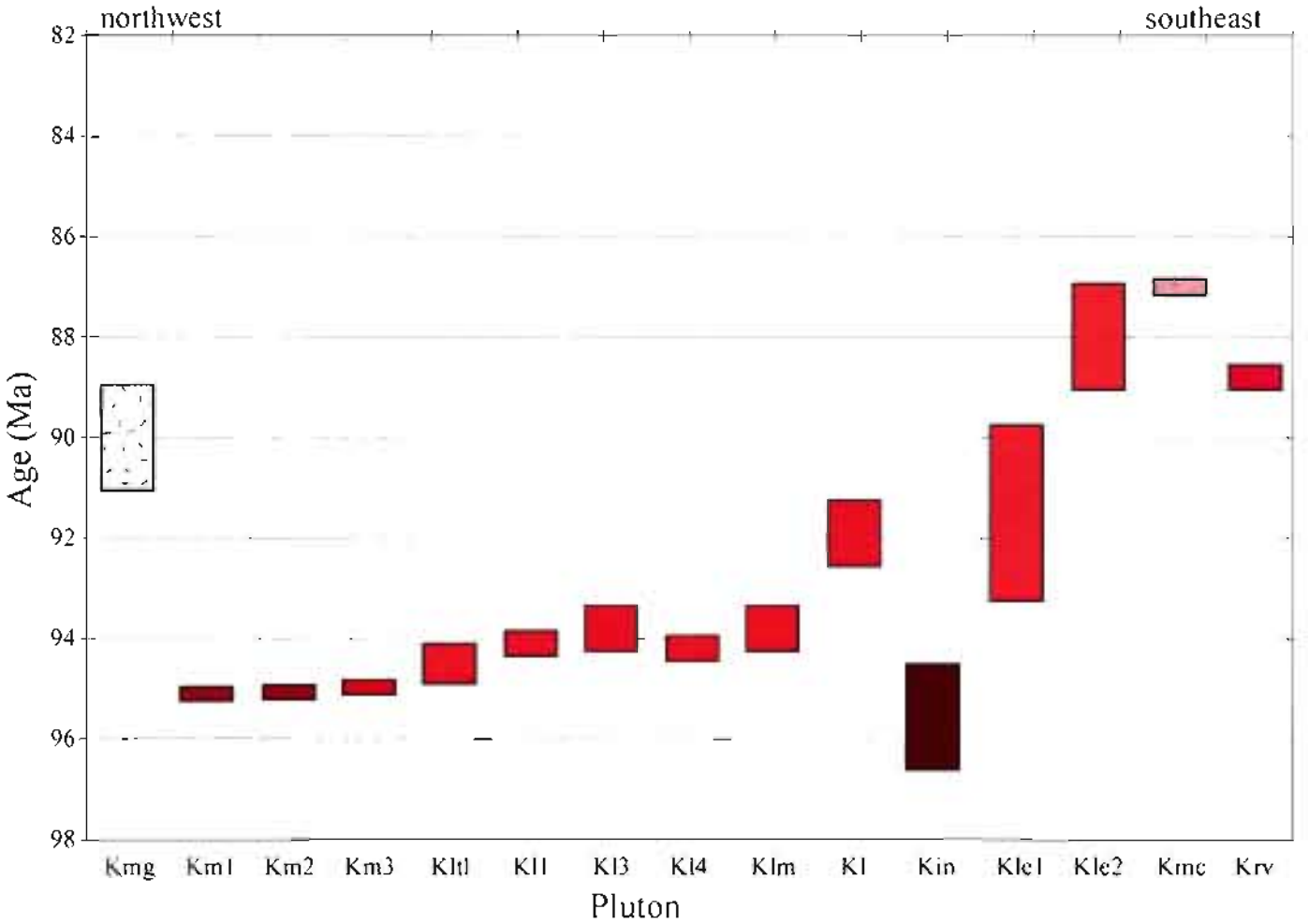

Figure 5.5: The growth duration of the John Muir Intrusive Suite (JMIS). Each bar is a single U-Pb zircon age, and the length of the bar is the 2-sigma error of the date. The JMIS grew over nearly 10 Myr. Data from Gracely (Klk1, Klk3, Klk4, Klkm, Kin; 2007), Tobisch et al. (Kmg and Kle; 1995), Coleman et al. (Klk; 1992), Gaschnig et al. (Krc, Kmc, and Krv; 2006). Figure adapted from Gracely, 2007.

These geometric predictions are useful for investigating any system constructed by diking such as the McDoogle pluton. However, Delaney et al. (1986) assumed that the wall rock is relatively isotropic, like the hornblende granodiorite (Khg) at the southern end of the central phase. Dikes that intrude anisotropic rock, such as strongly foliated rocks in a ductile shear zone, may have similar orientations controlled by the pre-existing anisotropy, even if magmatic overpressure dominated the system..

The uniform orientation of dikes in most of the McDoogle pluton may reflect either control by far-field stress or by the pre-existing anisotropy of rocks in the Sawmill Lake shear zone. However, McDoogle dikes that intrude the hornblende granodiorite (Khg) exploit random pre-existing fractures. This observation, coupled with the elevated wall-rock displacement rate determined above, suggest that magmatic overpressure was an important driving force during the intrusion of the McDoogle pluton.

CHAPTER 6

DISCUSSION

The previous chapters reported and briefly discussed the results of geologic mapping, structural analysis, bulk magnetic susceptibility mapping and calibration, and U-Pb geochronology conducted to investigate the internal anatomy and assembly of the McDoogle pluton. This chapter synthesizes the results to better understand the McDoogle pluton and the early growth period of intrusive suites like the John Muir Intrusive Suite.

The McDoogle pluton was amalgamated from hundreds of dikes intruded into the Sawmill Lake ductile shear zone during a period of relaxed crustal contraction. This interpretation is suggested by the overall dike-like shape, the large number of in-situ wall-rock screens in the central phase (Mahan, 2000), and the scarcity of solid-state deformation of the McDoogle pluton. Interactions between intruding dikes, the existing wall rocks, and synintrusive deformation shaped the overall system and evolved over time (Figure 6.1). As dikes began to intrude the Sawmill Lake shear zone, the wall rocks were relatively cold and well foliated. The foliation guided dikes into the shear zone (Pitcher and Berger, 1972; Mahan et al., 2003; Gaffney et al., 2007). As the pluton grew antitaxially, hundreds of wall-rock screens were isolated by dikes anastamosing between

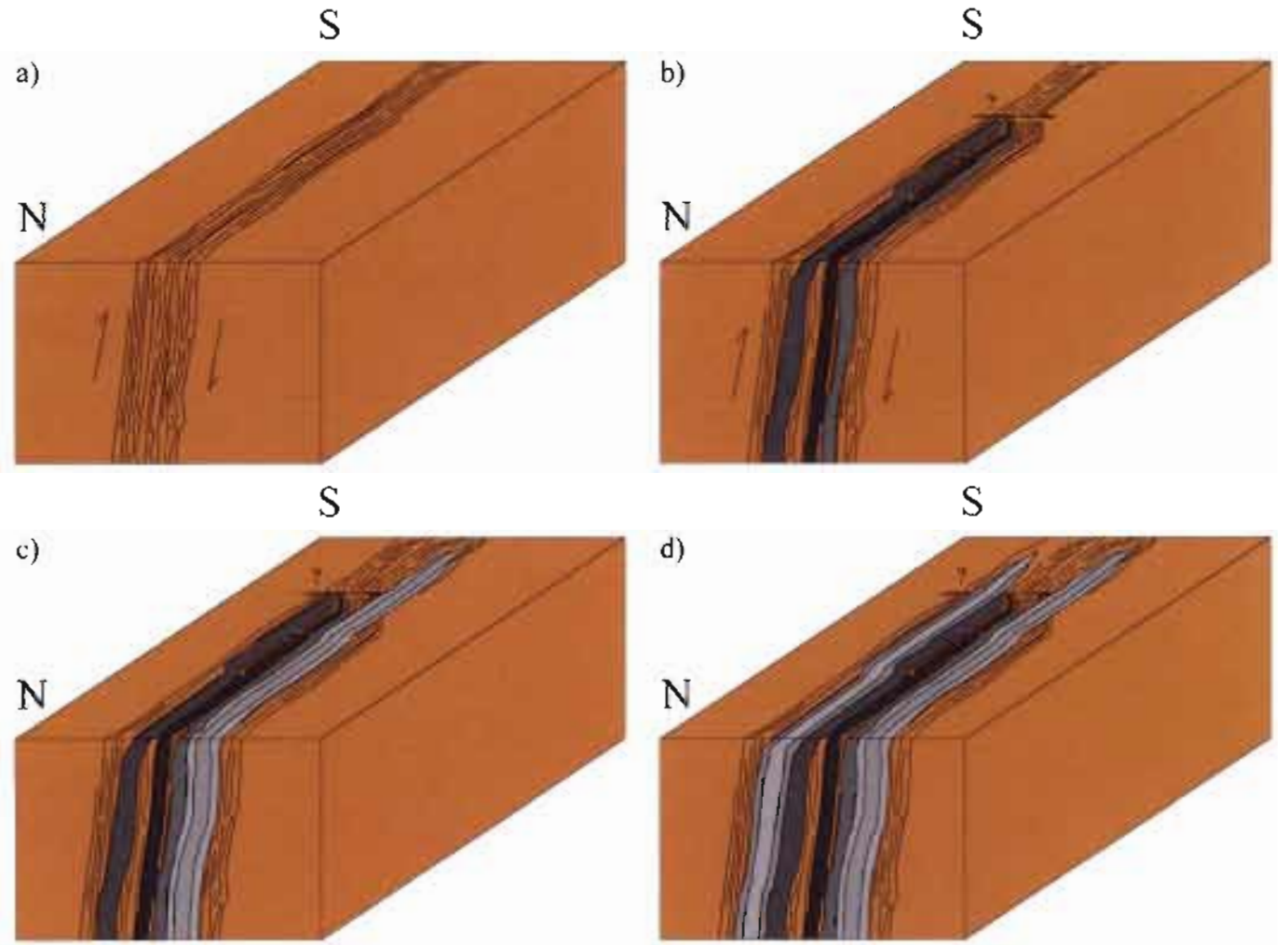

Figure 6.1: Block diagrams showing the inferred growth sequence of the McDoogle pluton. a) East-side-up movement across the steeply east-dipping SLSZ. b) Antitaxial growth of the central phase and movement across an accommodating shear zone (?). c,d) Syntaxial growth of the border phases, extending south with dike-like tips.

foliation planes (Bartley et al., 2008).

At some point during the assembly of the pluton, the growth mechanism shifted from antitaxial to syntaxial (Chapter 3). The switch from antitaxial to syntaxial growth requires the preferred fracture location to switch from outside or at the margin of the dike to within an existing dike. Mahan (2000) reported static recrystallization of wall rocks in the Sawmill Lake shear zone, and attributed it to the heat from the McDoogle pluton. The relations between static recrystallization of the wall rocks and four material properties could trigger the change from antitaxial to syntaxial growth. The distribution of lowered strength, focused stress, or both could control the preferred fracture location for new dikes. One, thermal contraction after a dike crystallizes could focus stress within the dike. Two, contrasts in tensile strength owing to grain size differences might make the dike weaker than its wall rocks. Three, the anisotropy of elastic strength during cooling could lower the strength of the wall rocks perpendicular to foliation. Four, partial melt within the dike could serve as a weakness for new intrusions to exploit. These four phenomena could operate, and possibly mutually reinforce one another, to focus stress or reduce strength to control the fracture location for the next intruding dike.

As a dike cools, the crystallizing magma undergoes a negative volume change. The change causes internal stresses in the dike that are likely focused at grain boundaries, effectively decreasing the tensile strength. Over time, the internal stresses statically recover through mechanisms such as fracturing and healing, grain boundary migration, subgrain boundary formation, and dislocation creep (Covery-Crump, 1997). New intrusions will exploit the presence of pre-existing flaws (Karihaloo and Huang, 1991) if

they have not recovered. The wall rocks began to recover once movement across the shear zone ceased, and recovery was aided by the heat from each new dike. If this mechanism controls dike intrusion, during antitaxial growth the time scale of a dike's recovery would be shorter than the time between dike intrusions. Syntaxial growth would require the opposite relationship.

If all else is equal, rocks with larger grains have a lower tensile strength than rocks with smaller grains (Knudsen, 1959). This effect is controlled by pervasive cracks along grain boundaries. Coarser-grained rocks have longer intergrain cracks (along grain boundaries) because the length and aperture are proportional to the grain size. The tendency for a crack to propagate is proportional to the length of the crack and thus materials with longer cracks are weaker than those with short cracks (Segall, 1984). The McDoogle pluton intruded a shear zone that had undergone significant grain size reduction, and therefore the wall rocks likely were stronger than dikes.

Each new dike that intruded the Sawmill Lake shear zone cooled and contracted along with the surrounding wall rocks. The wall rocks are weakened perpendicular to foliation and stress is focused in thermally contracting dikes. Fractures related to cooling that develop parallel to the dike margins (Prinz and Bentley, 1964) could be exploited by the next intruding dike if the wall rocks are less anisotropic or stronger than the dike.

Residual melt inside a cooling dike would cause a zone of weakness that could localize the next intruding dike. Average dike cooling times vary by orders of magnitude depending on the dike thickness. The average thicknesses of dikes comprising the McDoogle pluton is 1-5 m. A 1 m dike will solidify in ~1 day and a 10 m dike ~1 week

(Delaney and Pollard, 1982). If the McDoogle pluton was constructed over its maximum growth duration (~300,000 yrs) entirely of 1-10 m dikes, the time between intrusions would be ~250 to 25 years. Thus, it is unlikely that remaining melt in the centers of dikes controlled the fracture location because of the disparity between the timescale of the existence of melt and diking frequency.

These four mechanisms suggest that antitaxial growth requires well-foliated wall rock. Once enough heat is added to statically recrystallize the wall rocks and reduce the anisotropy, a threshold is reached and the system continues to grow syntaxially. The pattern of antitaxial followed by syntaxial growth is seen in several plutons and intrusive suites. The earlier phases of many plutons and intrusive suites most likely grew antitaxially, including the Treasure Lakes phase of the Lamarck granodiorite (Clemons and Bartley, 2008), the Kuna Crest-Glen Aulin phases of the Tuolumne Intrusive Suite, the border phase of the Alta stock (Vogel et al., 2001; Bartley et al., 2008), Jackass Lakes pluton (McNulty et al., 1996), the Mesozoic granites of the Ruby Mountains, Nevada (Lee et al., 2003), and the Main Donegal granite (Pitcher and Berger, 1972). As each pluton grew, a mechanical threshold was reached after which syntaxial growth was preferred. This transition is expected based on the previous discussion. Antitaxial growth does not persist because annealing recrystallization owing to heat introduced by earlier intrusive increments suppresses the mechanical anisotropy of foliated wall rocks. The short duration of antitaxial growth and focusing of dikes by syntaxial growth ultimately leads to the formation of tabular plutons rather than dike swarms.

The inferences below are speculative and meant to explore some possible

implications of the research. The rate at which the McDoogle pluton grew seems to be controlled by both local tectonic dilation rates and magmatic overpressure. If growth rates are equal, the size of a pluton dictates its growth duration. The McDoogle pluton is a relatively small pluton and U-Pb geochronology yielded a short growth duration (< 300,000 yr). Big plutons like the Half Dome granodiorite possibly yielded much longer growth durations (~ 5 Myr) (Coleman et al., 2004) because the plutons are proportionally larger. This duration-size relationship may suggest that plutons are be constructed of similar sized increments. If the sizes of dikes in the early antitaxial growth phases are representative of increments for entire intrusions, the average increment size is ~1-5 wide.

The outcrop geometry of the Sawmill Lake porphyry suggests that, before it was deformed and intruded, it was a tabular body similar to the McDoogle pluton. Within the McDoogle, bodies of granodiorite porphyry of Sawmill Lake are separated by metavolcanic and metasedimentary rocks. These metavolcanic and metasedimentary rocks were likely wall-rock screens within the granodiorite porphyry of Sawmill Lake before the intrusion of the McDoogle, and may suggest that a portion of the granodiorite porphyry of Sawmill Lake grew antitaxially. This location within the batholith, now occupied by the granodiorite porphyry of Sawmill Lake and the McDoogle pluton, has focused dike intrusion for ~70 Myr (Bartley et al., 2008).

CHAPTER 7

CONCLUSIONS

Incremental emplacement and assembly has become the best explanation for many laboratory and field observations regarding the anatomy and assembly of plutons around the world. The McDoogle pluton has emerged as a classic example of the antitaxial growth process and the early growth phase of intrusive suites. There are still many unanswered questions regarding pluton emplacement process. This study emphasized the utility of simple anatomical and temporal relationships between the components of a pluton and its wall rocks. These relationships provide key insights into how the McDoogle pluton was assembled.

The McDoogle pluton grew from the center outward, switching from antitaxial growth of the central phase to syntaxial growth of the border phases. The more mafic central phase and felsic border phases are arranged in a reversely zoned pattern. Magmatic differentiation at the emplacement level would have produced a trend of mafic to felsic rocks towards the center of the pluton. The reverse zonation suggests that magma differentiation occurred below the emplacement level, and possibly in the source region. The zonation of the McDoogle was entirely controlled by the assembly process.

The strong wall-rock foliation in the shear zone that hosts the pluton controlled whether the McDoogle pluton grew antitaxially or syntaxially. When the foliation was overprinted by static recrystallization, the growth mechanism switched from antitaxial to syntaxial. The intrusion rate controls the timing and rate of static recrystallization. Magma overpressure probably accounts for the rapid intrusion rate of the McDoogle pluton (> 4.5 mm/yr). The rapid intrusion rate could have caused the growth mechanism to change earlier in the assembly of the pluton.

BMS roughly correlates to color index for the McDoogle pluton, but the mineralogical variations that govern BMS are complex and heterogeneous through the range of BMS values. In addition to variations in bulk Fe content that correlate with color indew, the initial fO_2 or the bulk oxidation ratio of the magma can control BMS. BMS mapping is useful for gathering spatial data coverage quickly and showing subtle petrologic trends that cannot be expressed on a traditional geologic map. Patterns in the BMS map of the Sawmill Lake area are consistent with structural interpretations made from the lithologic map. However, all large BMS surveys should investigate what controls the BMS and if BMS variations correlate with CI.

APPENDIX A

ELECTRON MICROPROBE ANALYTICAL DATA

TABLE A1. MICROPROBE ANALYSES OF FELDSPARS FROM SELECTED SAMPLES

	Kmc												
	MS07-F8											MS07-F4	
	1a-core	1b-rim	2a-core	2b-rim	3a-core	4a-core	4b-rim	5a-core	5b-rim	6a-core	6b-rim	1a-core	1b-rim
Cation													
Na	0.10	0.11	0.13	0.06	0.10	0.09	0.11	0.11	0.07	0.10	0.08	0.07	0.45
Al	1.05	1.04	1.04	1.04	1.03	1.02	1.03	1.01	1.03	1.03	1.05	1.03	1.16
Si	2.97	2.97	2.97	2.98	2.98	2.99	2.99	2.99	2.99	2.99	2.97	2.98	2.85
K	0.87	0.88	0.85	0.90	0.89	0.88	0.87	0.88	0.89	0.87	0.89	0.91	0.40
Ca	0.00	0.00	0.01	0.00	0.00	0.00	0.00	0.00	0.00	0.00	0.00	0.00	0.13
Fe	0.00	0.01	0.00	0.00	0.00	0.00	0.00	0.00	0.00	0.00	0.00	0.00	0.00
Total	4.99	5.00	5.00	4.98	4.99	4.98	4.99	5.00	4.97	4.99	5.00	5.00	5.00
Feldspar composition													
Ab	10.60	10.62	12.84	6.24	9.77	9.19	10.86	10.99	7.31	10.42	8.63	7.53	45.76
Or	89.40	89.32	86.37	93.76	90.19	90.81	89.14	89.00	92.69	89.58	91.37	92.43	40.80
An	0.00	0.06	0.79	0.00	0.04	0.00	0.01	0.02	0.00	0.00	0.00	0.04	13.44

TABLE A1 (continued)

	Kmc			Kmb			
	MS07-F4			MS07-F2			
	1c-rim	2a-core	2b-rim	1a-core	1b-rim	2a-core	2b-rim
Cation							
Na	0.46	0.12	0.08	0.14	0.07	0.12	0.11
Al	1.15	1.03	1.03	1.03	1.01	1.03	1.02
Si	2.85	2.98	2.98	2.98	3.00	2.98	2.99
K	0.41	0.87	0.90	0.84	0.90	0.87	0.86
Ca	0.13	0.00	0.00	0.01	0.00	0.00	0.00
Fe	0.00	0.00	0.00	0.00	0.00	0.00	0.01
Total	5.01	5.00	5.00	4.99	4.98	5.00	4.99
Feldspar composition							
Ab	46.07	12.02	8.43	13.81	7.15	11.69	11.01
Or	40.81	87.97	91.58	85.59	92.86	88.13	89.00
An	13.12	0.01	0.00	0.60	0.00	0.17	0.00

TABLE A2. MICROPROBE ANALYSES OF MINERALS FROM SELECTED SAMPLES

	ilmenite			ilmenite	magnetite	ilmenite	ilmenite	magnetite	allanite	magnetite	amphibole	titanite
	Kmc			Kmb								
	MS07-F3	MS07-F4		MS07-F2								
	1	1		1	2	3	4	5	6	7	8	9
Wt. % Oxides			Wt. % Oxides									
SiO2	0.021	0	SiO2	0.04	0.02	0.07	0.03	0.01	37.42	0.00	45.88	30.09
TiO2	46.71	47.165	TiO2	49.38	0.08	47.18	52.05	0.03	0.08	0.01	0.45	37.55
Al2O3	0	0	Al2O3	0.00	0.06	0.00	0.00	0.05	23.50	0.01	8.17	1.69
FeO	38.753	36.609	FeO	44.32	89.36	47.73	43.02	92.35	11.71	90.19	19.25	2.44
Cr2O3	0.029	0.035	Cr2O3	0.00	0.32	0.05	0.02	0.06	0.00	0.07	0.01	0.02
Fe2O3	8.89	7.411	ZnO	0.00	0.14	0.12	0.02	0.03	0.00	0.00	0.02	0.05
MnO	2.882	5.508	NiO	0.00	0.03	0.00	0.00	0.00	0.02	0.01	0.00	0.00
V2O3	1.704	2.003	MnO	3.78	0.34	1.74	4.24	0.05	0.09	0.03	0.42	0.06
MgO	0.193	0.135	MgO	0.02	0.00	0.00	0.06	0.00	0.00	0.00	10.32	0.00
CaO	0.017	0.058	CaO	0.09	0.02	0.16	0.03	0.02	22.73	0.13	11.75	27.35
Nb2O3	0.294	0.329	Na2O	0.05	0.01	0.01	0.00	0.01	0.01	0.03	0.91	0.03
Total	99.493	99.253	Total	97.69	90.37	97.06	99.48	92.62	95.54	90.48	97.17	99.26

TABLE A2 (continued)

	magnetite		?	magnetite	magnetite	ilmenite	titanite	augite
	Kmb			Kmc				
	MS07-F2			MS07-F3				
	1	2	3	1	2	3	4	5
Wt. % Oxides								
SiO2	4.21	#	19.96	0.02	0.03	0.05	30.62	47.05
TiO2	0.14	#	0.16	0.02	0.01	49.20	38.72	0.71
Al2O3	0.03	#	2.13	0.06	0.02	0.00	1.41	6.95
FeO	72.67	#	49.08	91.32	91.03	43.57	1.19	17.29
Cr2O3	0.00	#	0.02	0.22	0.27	0.04	0.01	0.05
ZnO	0.07	#	0.02	0.05	0.05	0.06	0.03	0.05
NiO	0.00	#	0.00	0.01	0.02	0.00	0.00	0.00
MnO	0.02	#	0.17	0.04	0.03	6.36	0.06	0.46
MgO	0.17	#	3.93	0.00	0.00	0.09	0.00	11.53
CaO	0.22	#	4.56	0.01	0.11	0.04	27.92	11.75
Na2O	0.04	#	0.27	0.02	0.01	0.00	0.01	1.03
Total	77.56	#	80.29	91.78	91.57	99.41	99.98	96.88

APPENDIX B

BULK MAGNETIC SUSCEPTIBILITY DATA

TABLE B1: MAGNETIC SUSCEPTIBILITY DATA FOR ROCKS OF THE SAWMILL LAKE AND PINCHOT PASS AREAS

waypoint	1	2	3	4	5	6	7	8	9	mean	1 sigma
1	15.40	13.10	16.10	17.40	13.10	15.90	12.70	16.20	15.10	15.00	1.65
2	14.10	13.10	12.80	9.75	7.71	12.40	15.20	12.00	13.30	12.26	2.27
3	11.10	11.60	13.00	12.10	14.10	12.30	15.60	18.70	15.30	13.76	2.44
4	20.30	20.00	19.80	18.30	17.40	19.10	19.10	19.50	16.00	18.83	1.39
5	19.00	17.30	21.20	17.00	16.40	17.80	17.80	19.00	21.90	18.60	1.88
6	18.10	18.60	18.60	17.00	16.50	16.80	17.20	19.20	17.40	17.71	0.94
7	21.60	23.90	19.10	20.70	20.80	21.10	19.00	20.80	16.50	20.39	2.04
8	18.10	17.40	16.50	15.40	16.40	17.70	13.20	15.50	17.10	16.37	1.50
9	19.90	20.40	21.00	20.70	19.70	19.30	19.60	19.40	21.30	20.14	0.73
10	21.00	20.30	19.10	18.30	21.50	17.10	16.50	20.00	19.90	19.30	1.71
11	21.80	18.30	20.40	14.80	19.50	21.80	22.10	21.00	22.00	20.19	2.40
12	17.30	20.60	17.00	18.80	18.90	15.70	20.20	16.70	20.00	18.36	1.75
13	17.50	18.80	12.60	17.90	16.80	17.00	14.90	15.90	12.10	15.94	2.33
14	10.80	11.80	13.10	10.80	11.10	10.40	15.40	14.10	12.50	12.22	1.71
15	26.50	25.00	24.60	25.10	21.10	22.50	22.10	20.60	20.00	23.06	2.31
16	15.10	19.30	14.80	13.20	14.90	17.20	14.40	16.70	17.20	15.87	1.87
17	18.80	17.40	17.00	16.30	17.60	18.90	17.20	18.60	16.70	17.61	0.95
18	19.20	21.50	18.60	21.20	18.40	21.10	19.50	17.80	21.60	19.88	1.48
19	17.10	17.20	19.10	16.50	18.80	20.30	18.40	18.50	18.40	18.26	1.16
20	20.20	16.20	18.00	16.30	15.90	15.50	16.30	16.00	16.00	16.71	1.48
21	19.60	23.00	16.60	24.40	22.70	24.20	20.00	18.00	20.60	21.01	2.74
22	20.50	21.40	21.10	21.00	24.80	19.40	24.00	20.50	19.40	21.34	1.88
23	24.20	21.10	19.30	19.70	14.90	15.30	17.20	18.70	17.70	18.68	2.89
24	18.40	16.20	16.40	19.30	20.30	20.20	16.00	15.70	17.30	17.76	1.84
25	22.10	21.10	22.40	21.30	18.00	22.80	17.80	19.20	19.00	20.41	1.93

TABLE B1 (continued)

waypoint	1	2	3	4	5	6	7	8	9	mean	1 sigma
26	18.40	21.60	18.50	20.90	19.80	21.00	18.90	20.50	21.10	20.08	1.22
27	19.10	18.80	22.60	18.40	21.20	16.80	20.10	16.10	18.60	19.08	2.02
28	16.50	19.40	18.50	15.70	16.10	18.20	16.60	21.60	19.60	18.02	1.96
29	17.70	21.00	18.80	18.30	20.70	17.50	22.70	18.80	19.00	19.39	1.72
30	15.60	14.40	11.10	13.20	18.60	13.20	13.90	16.20	11.00	14.13	2.43
31	19.50	18.70	18.80	15.50	15.70	18.50	21.20	19.30	13.70	17.88	2.38
32	21.10	25.30	21.00	21.50	28.80	18.00	21.60	20.80	21.90	22.22	3.09
33	23.30	21.20	21.50	19.50	18.60	16.90	19.70	24.20	30.00	21.66	3.86
34	23.40	20.00	25.50	22.00	21.20	23.50	22.60	19.10	16.70	21.56	2.65
35	20.20	27.40	28.10	27.90	26.30	23.90	26.80	26.80	24.20	25.73	2.55
36	27.40	20.80	29.70	29.10	23.20	22.80	28.80	27.30	28.00	25.79	2.99
37	34.80	27.00	37.00	33.50	28.30	24.80	25.90	30.80	32.00	30.46	4.22
38	30.10	27.80	31.70	21.70	32.30	31.70	32.10	29.10	29.00	29.50	3.33
39	26.10	27.80	36.20	28.20	39.20	31.20	31.40	34.40	33.20	31.97	4.25
40	20.00	26.20	22.90	13.70	18.40	28.80	20.30	32.10	23.50	22.88	5.60
41	29.90	24.30	38.70	30.10	28.60	30.80	31.20	28.60	29.80	30.22	3.77
42	20.00	20.90	22.80	23.70	24.80	24.70	25.50	23.20	24.60	23.36	1.86
43	23.30	18.10	22.00	29.10	25.70	23.90	26.40	22.00	22.50	23.67	3.15
44	16.40	16.50	17.50	15.70	20.10	18.10	18.10	15.00	15.40	16.98	1.63
45	24.20	25.20	28.90	24.60	26.90	30.50	35.40	32.00	27.60	28.37	3.74
46	32.20	30.20	33.40	26.40	30.20	3.60	30.40	26.30	21.70	26.04	9.14
47	26.90	32.90	34.20	27.30	32.20	29.30	28.70	33.20	29.50	30.47	2.70
48	28.10	22.70	26.30	26.50	26.10	25.20	25.20	32.60	19.80	25.83	3.51
49	26.40	27.50	30.90	34.30	25.40	31.80	24.50	26.80	26.50	28.23	3.31
50	16.40	19.00	17.40	18.80	16.00	16.70	19.30	16.30	14.80	17.19	1.55
51	19.90	20.20	17.20	22.20	17.00	18.30	19.00	17.80	16.40	18.67	1.85
52	16.70	16.20	17.00	16.90	16.70	17.20	16.40	18.00	16.50	16.84	0.53
53	15.30	17.00	16.20	16.10	18.50	17.50	14.90	18.10	18.70	16.92	1.38

TABLE B1 (continued)

waypoint	1	2	3	4	5	6	7	8	9	mean	1 sigma
54	19.00	18.90	16.10	14.30	20.90	20.30	18.00	19.00	19.30	18.42	2.06
55	13.60	15.80	15.00	16.50	15.20	13.70	14.50	16.30	14.00	14.96	1.09
56	4.66	3.71	1.60	0.92	2.57	1.27	4.48	5.75	3.23	3.13	1.67
57	28.30	18.90	20.60	17.80	15.40	20.20	22.90	24.40	20.70	21.02	3.80
58	19.20	20.10	15.10	16.90	18.70	22.80	22.60	20.50	17.00	19.21	2.60
59	18.30	17.80	17.90	18.60	15.70	15.40	15.90	14.60	15.70	16.67	1.49
60	22.30	16.60	21.10	16.60	20.00	17.00	18.40	18.10	17.60	18.63	2.05
61	17.90	16.50	20.60	16.50	13.00	16.20	16.40	17.20	17.10	16.82	1.97
62	20.00	20.30	17.30	16.80	15.80	17.00	16.20	17.60	17.80	17.64	1.56
63	22.90	25.80	21.40	17.50	19.80	18.80	18.90	21.60	19.90	20.73	2.52
64	27.90	22.30	21.50	27.40	26.90	19.70	21.00	20.70	18.00	22.82	3.64
65	29.00	19.00	26.20	20.70	24.10	23.10	18.70	21.90	22.40	22.79	3.32
66	29.60	27.40	22.60	22.00	22.20	26.80	20.80	18.00	21.30	23.41	3.71
67	21.10	23.80	22.60	22.00	22.20	26.80	20.80	18.00	18.40	21.74	2.68
68	22.40	24.30	26.00	22.90	22.50	24.30	20.20	23.10	25.00	23.41	1.71
69	21.50	22.20	20.20	19.80	25.50	19.30	19.60	23.30	22.60	21.56	2.06
70	19.30	21.70	26.60	20.70	21.50	19.20	23.20	26.20	20.10	22.06	2.76
71	27.10	21.30	20.20	28.30	24.60	21.90	22.20	19.50	20.50	22.84	3.13
72	29.80	27.10	26.20	34.20	29.90	28.70	25.20	26.10	28.70	28.43	2.74
73	22.00	22.50	22.40	24.40	24.50	20.80	31.00	23.90	20.30	23.53	3.17
74	19.20	21.30	18.40	21.40	26.30	20.60	20.20	22.20	17.00	20.73	2.64
75	21.70	21.40	17.40	17.00	15.20	19.20	17.50	19.30	19.10	18.64	2.10
76	34.70	30.20	23.60	29.00	24.80	27.50	22.20	28.30	30.50	27.87	3.88
77	33.70	21.20	66.90	31.40	26.60	21.20	26.00	22.90	22.30	30.24	14.44
78	24.00	20.30	22.30	23.70	21.20	18.10	25.50	31.00	16.60	22.52	4.27
79	24.70	20.40	30.20	18.70	21.40	20.60	22.20	19.60	24.50	22.48	3.54
80	26.50	22.20	21.10	28.20	22.90	35.30	25.20	28.20	16.00	25.07	5.45
82	18.40	23.60	24.90	17.30	20.90	21.10	18.80	19.50	16.50	20.11	2.80

TABLE B1 (continued)

waypoint	1	2	3	4	5	6	7	8	9	mean	1 sigma
83	14.40	16.30	18.80	17.90	21.20	19.90	22.60	16.40	18.30	18.42	2.56
84	22.90	21.50	19.20	21.00	19.20	20.90	19.20	22.50	22.30	20.97	1.48
85	17.50	16.20	14.70	13.00	18.30	16.90	21.70	19.50	20.70	17.61	2.80
86	21.00	21.20	18.20	18.70	23.40	17.40	16.00	24.90	21.60	20.27	2.91
87	27.80	25.80	24.80	25.80	16.80	25.10	28.80	21.10	21.00	24.11	3.79
88	24.00	22.10	26.30	20.90	23.70	21.40	20.60	20.00	22.90	22.43	2.00
89	23.90	27.80	27.50	24.50	36.40	24.70	31.10	29.20	23.60	27.63	4.18
90	31.50	30.00	28.70	26.80	28.20	28.70	25.20	24.00	28.90	28.00	2.33
91	26.90	25.00	29.40	22.90	21.80	23.20	32.10	35.70	26.50	27.06	4.61
92	29.10	21.20	28.80	24.10	16.70	21.30	30.00	26.10	28.90	25.13	4.61
93	38.50	35.20	27.40	32.30	23.70	26.50	17.70	17.70	26.30	27.26	7.17
94	33.60	27.40	22.80	41.00	34.80	28.40	37.00	28.20	29.90	31.46	5.61
95	32.70	34.30	24.40	26.60	36.60	31.30	34.80	26.50	27.40	30.51	4.38
96	15.90	18.60	15.10	16.00	13.90	18.10	15.30	13.80	17.20	15.99	1.70
97	29.50	19.50	29.20	29.60	25.80	26.20	24.60	27.20	28.80	26.71	3.25
98	24.20	20.90	20.70	21.60	22.40	22.60	17.60	21.60	25.20	21.87	2.18
99a	14.10	14.10	12.80	21.70	21.30	21.40	19.80	15.20	20.70	17.90	3.74
99b	16.10	10.90	16.40	18.30	11.60	11.70	16.50	16.00	24.50	15.78	4.20
100	15.00	7.80	9.71	15.80	18.60	11.50	16.60	20.90	12.10	14.22	4.27
101a	34.50	20.20	15.40	22.40	16.00	15.60	21.20	27.10	19.00	21.27	6.23
101b	14.20	14.40	11.30	15.10	16.80	15.50	13.20	17.00	14.50	14.67	1.76
102a	22.40	15.20	19.70	23.50	22.50	19.00	13.80	10.80	17.30	18.24	4.34
102b	16.40	15.40	17.20	17.70	12.20	19.70	17.20	17.50	19.50	16.98	2.24
103	18.30	15.50	19.70	12.20	14.90	14.90	15.90	11.70	15.60	15.41	2.54
104	14.50	16.10	20.00	15.20	17.10	19.30	19.40	20.70	21.20	18.17	2.49
105	28.00	22.70	19.80	26.60	22.20	20.90	21.80	20.00	20.60	22.51	2.90
106	25.50	27.50	28.50	21.40	27.40	24.40	17.90	22.10	23.40	24.23	3.43
107	17.00	19.90	17.20	18.90	10.20	20.40	19.90	19.50	19.90	18.10	3.20

TABLE B1 (continued)

waypoint	1	2	3	4	5	6	7	8	9	mean	1 sigma
108	19.00	19.60	13.40	15.50	22.80	17.90	19.40	15.60	22.20	18.38	3.12
109	20.10	30.30	23.30	18.80	24.20	18.20	18.10	24.30	18.90	21.80	4.08
110	27.40	23.50	25.90	16.40	28.30	29.90	23.70	22.90	21.20	24.36	4.10
111	25.40	29.30	20.60	20.10	18.70	13.70	24.20	16.50	19.60	20.90	4.75
112	16.30	22.40	25.60	12.50	22.10	19.60	23.40	21.00	21.90	20.53	3.96
113	18.20	19.40	13.00	18.20	17.30	16.20	12.70	14.40	16.10	16.17	2.38
114	19.70	21.10	18.90	17.80	17.60	19.10	18.70	16.90	15.90	18.41	1.55
115	26.10	26.60	23.40	17.80	26.80	23.40	30.40	24.50	23.90	24.77	3.43
116	14.90	14.50	16.60	15.00	14.80	14.30	15.60	12.00	14.40	14.68	1.23
117	18.10	18.70	13.80	16.30	16.50	18.30	18.70	17.40	20.10	17.54	1.83
118	19.70	23.50	22.00	19.80	26.60	27.10	27.30	23.50	21.60	23.46	2.98
122	15.20	14.10	13.70	15.30	18.80	11.00	15.40	9.06	11.80	13.82	2.88
123	17.30	14.10	19.40	13.30	19.10	17.10	18.20	17.10	16.30	16.88	2.07
124	25.30	24.30	21.70	27.00	18.00	16.90	27.20	26.40	19.40	22.91	4.02
125	15.10	15.50	14.70	20.60	16.40	18.90	19.30	20.60	21.90	18.11	2.72
126	23.50	16.30	25.10	18.40	18.10	19.00	22.00	20.00	23.20	20.62	2.96
127	24.70	26.00	28.00	28.60	21.40	24.40	26.40	24.70	22.00	25.13	2.43
128	1.00	1.04	1.19	2.17	3.62	2.34	2.28	2.98	0.88	1.94	0.98
129	17.50	17.60	17.70	17.70	14.30	20.20	14.40	15.70	14.10	16.58	2.07
130	30.10	26.90	29.60	23.40	20.50	27.60	21.30	16.90	15.00	23.48	5.46
131	19.90	22.40	18.40	23.30	22.90	21.50	26.20	18.90	19.90	21.49	2.49
132	12.20	13.70	17.20	17.40	12.50	14.90	11.60	9.96	13.10	13.62	2.49
133	0.62	0.60	0.38	0.58	0.60	0.72	0.64	0.57	0.80	0.61	0.11
134	1.41	1.02	1.14	1.10	1.17	0.94	1.44	1.06	2.24	1.28	0.40
135	0.19	0.21	0.21	0.14	0.19	0.21	0.21	0.18	0.17	0.19	0.02
136	23.60	23.50	23.20	24.70	23.50	17.40	19.00	25.40	19.70	22.22	2.79
137	16.90	24.10	18.60	25.60	20.90	21.70	17.40	20.50	16.70	20.27	3.18
138	17.30	17.90	15.30	20.30	20.80	16.30	17.80	22.50	17.50	18.41	2.31

TABLE B1 (continued)

waypoint	1	2	3	4	5	6	7	8	9	mean	1 sigma
139	21.20	17.30	14.30	22.10	17.60	33.30	19.70	23.80	17.40	20.74	5.53
140	31.60	20.30	37.10	19.90	20.50	26.00	24.30	19.10	21.80	24.51	6.15
141	25.20	25.30	27.50	26.50	21.30	24.10	22.10	22.00	20.70	23.86	2.43
142	19.80	17.70	15.80	22.00	18.40	17.40	16.90	21.80	19.00	18.76	2.13
143	30.50	23.90	24.70	26.10	27.50	23.90	18.80	30.20	28.60	26.02	3.70
144	23.60	21.40	25.50	29.20	25.70	15.80	26.00	23.30	20.50	23.44	3.88
145	29.10	32.60	24.00	27.90	27.80	19.70	19.40	26.60	25.70	25.87	4.29
146	21.80	23.20	31.90	28.10	25.30	27.30	28.20	23.00	21.70	25.61	3.50
147	22.10	31.10	36.80	26.80	38.00	28.30	35.30	34.70	32.10	31.69	5.20
148	19.40	20.20	19.90	14.90	11.10	17.70	15.70	17.70	11.50	16.46	3.43
149	16.80	21.70	16.60	16.50	15.20	20.00	15.20	22.00	19.60	18.18	2.68
150	18.70	18.60	24.80	21.00	15.90	16.30	14.70	15.00	15.30	17.81	3.36
151	16.20	15.20	20.40	17.20	16.50	14.90	20.80	17.10	19.80	17.57	2.22
152	22.10	31.10	23.50	25.20	26.50	27.30	26.70	18.20	25.70	25.14	3.62
153	17.00	22.80	25.50	29.10	19.40	22.50	21.60	20.70	22.00	22.29	3.47
154	12.50	18.20	21.90	22.20	13.90	15.60	17.30	14.80	16.90	17.03	3.34
155	26.40	27.50	23.10	25.30	22.00	25.50	26.70	22.60	26.00	25.01	1.96
156	27.40	30.50	30.90	19.10	28.00	26.60	29.00	22.40	27.90	26.87	3.82
157	26.80	24.90	20.60	23.40	24.30	29.40	16.40	22.80	31.90	24.50	4.60
158	25.50	22.00	20.70	20.70	18.40	22.90	19.90	23.20	27.60	22.32	2.87
159	29.10	25.70	24.70	27.80	28.70	29.00	23.90	30.60	16.80	26.26	4.19
160	16.50	22.80	19.20	11.20	14.70	20.20	18.50	9.65	24.20	17.44	4.93
161	25.60	25.70	27.70	26.20	29.30	21.50	21.00	21.10	28.80	25.21	3.27
162	21.40	15.80	12.50	17.70	20.60	18.00	12.30	15.90	16.20	16.71	3.14
163	25.00	23.10	25.40	25.50	24.00	22.90	22.30	22.60	24.70	23.94	1.25
164	30.30	21.90	28.30	25.90	24.20	23.30	26.20	19.90	30.40	25.60	3.65
165	26.90	29.30	31.80	28.50	25.80	33.00	36.40	41.00	28.90	31.29	4.88
166	24.20	18.80	19.00	29.50	31.70	31.70	13.50	18.10	19.00	22.83	6.70

TABLE B1 (continued)

waypoint	1	2	3	4	5	6	7	8	9	mean	1 sigma
167	30.50	26.90	22.10	33.60	32.40	31.10	22.30	26.10	23.40	27.60	4.45
168	23.90	27.70	22.80	21.10	20.90	24.80	23.10	25.20	29.90	24.38	2.95
169	21.80	22.50	29.20	16.80	19.00	25.30	22.10	17.70	26.00	22.27	4.08
170	23.20	24.00	26.20	20.50	28.70	23.10	28.40	28.40	28.20	25.63	3.02
171	24.60	22.50	26.20	19.70	25.90	20.60	26.60	26.50	27.00	24.40	2.78
172	31.60	14.70	17.30	25.40	16.60	22.70	27.40	25.10	23.00	22.64	5.53
173	25.50	23.20	36.00	27.40	23.30	18.20	27.30	20.20	16.80	24.21	5.80
174	26.60	17.90	18.60	17.30	25.30	19.80	26.40	14.00	27.30	21.47	4.95
175	18.40	13.40	20.80	15.30	19.40	15.00	21.50	20.40	23.80	18.67	3.45
176	16.30	17.60	20.60	18.00	17.90	16.90	26.10	21.00	28.00	20.27	4.17
177	23.70	22.50	22.80	23.50	18.90	20.70	21.60	21.50	25.10	22.26	1.83
178	16.10	17.00	20.30	16.90	14.10	16.70	18.80	13.00	21.10	17.11	2.65
179	24.10	20.90	16.70	24.10	22.40	22.30	20.10	13.50	21.00	20.57	3.48
180	17.80	19.70	20.60	24.80	21.40	30.30	20.80	24.40	19.40	22.13	3.80
181	21.10	25.40	15.10	24.10	30.00	20.70	27.80	28.10	15.30	23.07	5.43
182	0.32	0.55	0.58	0.36	0.56	0.90	-	-	-	0.54	0.20
183	14.70	13.50	16.10	15.00	24.80	18.40	11.90	13.20	13.30	15.66	3.92
184	19.20	18.40	10.60	13.30	14.00	19.40	26.00	25.40	22.00	18.70	5.32
185	19.70	27.90	27.80	23.70	21.10	20.60	16.70	24.00	20.90	22.49	3.72
186	19.90	19.80	25.80	19.50	20.00	24.00	21.10	26.20	21.20	21.94	2.67
187	25.00	24.60	19.70	22.70	19.80	19.40	17.50	23.20	20.60	21.39	2.58
188	23.00	18.60	24.20	18.00	29.80	24.80	25.10	24.30	27.50	23.92	3.77
189	28.00	27.30	29.00	22.70	22.00	27.40	30.20	30.00	25.70	26.92	2.95
190	24.80	35.70	25.60	23.00	24.10	29.50	29.30	25.30	27.50	27.20	3.89
191	27.30	27.20	15.90	25.00	27.20	27.90	25.20	23.30	13.10	23.57	5.39
192	19.50	15.90	26.90	27.60	21.50	17.60	12.50	29.30	24.70	21.72	5.79
193	27.20	26.30	26.30	26.30	28.50	29.20	22.10	25.60	18.80	25.59	3.24
194	25.40	21.10	20.10	27.80	18.30	27.70	37.80	18.30	26.30	24.76	6.22

TABLE B1 (continued)

waypoint	1	2	3	4	5	6	7	8	9	mean	1 sigma
195	16.20	18.90	27.40	33.90	23.00	31.50	28.30	18.60	23.50	24.59	6.11
196	14.20	14.10	19.80	23.10	19.40	22.80	15.90	17.20	19.70	18.47	3.35
197	24.20	29.90	24.40	23.40	25.20	20.80	29.10	24.50	27.40	25.43	2.88
198	16.30	16.70	20.80	30.90	31.80	26.90	26.00	13.60	16.50	22.17	6.87
199	25.70	29.60	27.70	18.30	25.00	17.20	17.50	19.50	15.80	21.81	5.18
200	4.98	3.65	7.42	5.15	9.09	7.85	3.49	5.68	8.13	6.16	2.03
201	25.70	23.00	26.30	24.60	35.20	22.20	21.30	23.40	26.90	25.40	4.13
202	21.20	23.50	16.90	22.60	19.30	24.10	20.20	21.50	17.50	20.76	2.52
203	13.50	21.40	16.50	24.90	12.60	22.20	18.30	15.90	16.20	17.94	4.13
204	19.80	19.70	18.30	19.00	21.10	18.20	20.00	22.50	20.30	19.88	1.35
205	22.00	25.50	20.70	16.30	20.30	11.10	17.70	22.70	19.40	19.52	4.16
206	15.30	16.10	21.50	17.40	15.40	12.00	17.10	15.80	17.20	16.42	2.50
207	17.50	21.10	17.70	15.90	15.30	15.00	19.10	20.80	14.90	17.48	2.42
208	18.40	15.50	11.90	18.70	16.70	12.80	15.40	16.10	14.90	15.60	2.26
209	25.10	17.30	20.20	16.50	13.90	24.80	17.40	19.50	18.70	19.27	3.70
210	27.80	20.40	21.50	29.10	23.80	24.60	24.50	25.10	24.20	24.56	2.71
211	7.30	12.40	12.40	16.50	14.20	18.10	12.20	17.60	17.20	14.21	3.52
212	30.70	28.60	35.70	34.60	30.70	34.90	34.00	35.60	23.40	32.02	4.10
213	19.00	17.20	21.50	23.30	16.30	19.00	16.90	14.10	22.10	18.82	3.02
215	23.60	26.50	22.00	30.30	30.60	28.10	24.90	27.90	22.80	26.30	3.17
216	35.30	37.10	29.60	28.40	31.70	29.80	22.20	25.90	24.00	29.33	4.92
217	21.20	20.30	24.60	22.40	22.10	24.60	28.10	20.70	21.20	22.80	2.52
218	19.00	21.80	18.00	22.90	22.20	21.80	22.40	18.10	14.30	20.06	2.88
219	36.90	18.40	29.80	28.40	30.10	24.20	33.20	24.10	29.00	28.23	5.44
220	25.70	25.10	22.40	27.90	34.10	30.00	40.80	23.50	32.10	29.07	5.88
221	24.70	23.50	17.40	19.20	20.40	25.70	19.40	25.10	21.70	21.90	2.98
222	22.80	18.90	25.10	25.80	22.70	19.20	21.10	27.30	26.90	23.31	3.16
223	27.40	23.00	26.00	25.60	28.00	29.00	23.80	23.20	26.60	25.84	2.15

TABLE B1 (continued)

waypoint	1	2	3	4	5	6	7	8	9	mean	1 sigma
225	30.30	28.00	29.50	22.90	24.90	25.50	24.00	22.00	27.30	26.04	2.90
226	26.60	32.70	33.30	39.70	31.50	32.60	30.60	29.10	35.30	32.38	3.73
227	23.50	29.80	29.50	20.60	22.90	20.50	23.10	28.40	24.30	24.73	3.62
228	25.90	21.80	25.60	22.10	20.40	22.80	22.90	29.10	21.90	23.61	2.72
229	26.50	28.40	28.80	31.60	23.50	32.80	23.60	29.40	36.60	29.02	4.26
230	26.60	24.10	25.60	24.00	20.70	22.70	26.70	32.50	27.30	25.58	3.35
231	21.80	21.80	23.60	23.20	21.40	26.60	20.80	23.80	21.70	22.74	1.78
232	20.80	18.00	22.10	22.80	20.90	18.00	10.90	18.70	20.60	19.20	3.55
233	19.70	13.90	16.60	18.60	18.80	21.10	15.10	17.20	16.10	17.46	2.30
234	28.50	24.30	27.70	26.30	23.60	29.00	31.90	32.40	29.00	28.08	3.02
235	25.60	26.50	25.20	28.30	16.70	18.30	25.30	21.10	26.70	23.74	4.05
236	21.50	18.90	19.40	18.40	20.00	25.50	22.30	23.60	27.00	21.84	3.03
237	12.00	17.00	10.20	21.70	9.02	13.40	9.80	12.90	9.40	12.82	4.18
238	13.60	17.00	15.10	14.80	21.60	19.00	19.00	18.60	12.00	16.74	3.09
239	11.00	12.10	12.80	8.90	10.30	12.60	8.60	13.80	12.30	11.38	1.80
242	2.49	3.29	1.62	1.35	3.13	2.57	1.24	2.77	1.31	2.20	0.82
243	3.28	4.69	7.87	3.15	2.98	4.82	3.86	4.31	1.92	4.10	1.69
244	15.50	17.60	16.50	17.90	15.50	16.80	18.90	17.80	16.80	17.03	1.13
245	23.10	19.80	21.80	20.50	20.70	20.50	17.80	21.40	20.20	20.64	1.46
247	22.50	24.80	25.20	24.30	26.60	25.10	21.60	23.80	25.00	24.32	1.51
248	29.00	37.10	30.10	27.00	23.10	38.90	27.20	25.10	29.10	29.62	5.23
250	50.90	43.00	48.30	50.20	47.70	39.00	38.30	43.70	48.20	45.48	4.67
251	30.10	35.40	26.00	35.50	33.40	26.10	34.60	36.50	26.10	31.52	4.47
252a	16.70	18.70	12.90	10.20	17.30	9.32	12.60	14.60	10.00	13.59	3.44
252b	46.80	53.10	60.80	42.40	43.30	30.30	52.10	54.50	44.40	47.52	8.86
258	22.60	25.10	23.20	24.90	23.40	20.80	25.40	24.60	21.50	23.50	1.64

APPENDIX C

GEOCHRONOLOGY SAMPLE PREPARATION

Two samples were prepared for U-Pb zircon geochronology at the Department of Geologic Sciences, University of North Carolina at Chapel Hill, under the guidance of Dr. Drew Coleman. Jesse Davis, Michael Tappa, and Ayumi Shimokawa completed some steps of the sample preparation. The samples were first crushed and disc-milled to a fine powder. The powder was separated using a Rogers ™ Table, heavy liquid (methylene iodide), and a Franz ™ Magnetic Barrier Laboratory Separator (Krogh, 1982). The magnetic separator was set to an initial current of 0.25 mA and, in successive sample passes, the current was increased in 0.25 mA increments to 1.5 mA. This removed almost every mineral (mainly hornblende and titanite) except zircon that lacked ferromagnetic mineral inclusions. Roughly a hundred zircon grains were picked based on clarity, shape, and size. These grains were thermally annealed in a furnace at 900 °C for 48 hours. Eight fractions then were hand-picked. Single grain fractions were chosen when the grains were large enough. The fractions were chemically abraded in a mixture of HF and HNO_3 acid for 12 hours at 180 °C to mitigate effects of Pb loss and inheritance (Mundil et al., 2004; Mattinson, 2005). Each fraction was spiked with a ^{205}Pb-^{236}U-^{233}U solution (Krogh and Davis, 1975; Parrish and Krogh, 1987) and dissolved directly in HF and HNO_3 for 72 hours at 220 °C. Uranium and lead were eluted from the fractions using anion column chemistry (Parrish and Krogh, 1987). Isotope ratios were measured by TIMS using a VG Sector 54 mass spectrometer using Tripoli computer software. Data were reduced using PbMacDat2, written by Drew Coleman and modified by Clark Isachsen. The decay constants used were $^{238}U = 0.155125 \times 10^{-9}\ a^{-1}$ and $^{235}U = 0.98485$ x

10^{-9} a^{-1} (Steiger and Jäger, 1977). All weights were known within 10% and errors are reported in percent at the 2σ confidence interval.

APPENDIX D

PLATE 1

GEOLOGIC MAP CD-ROM

This CD-ROM contains a detailed geologic map of the McDoogle pluton near Sawmill Lake, central Sierra Nevada, California. Adobe Reader® is required to view the file.

REFERENCES

Ague, J.J., and Brimhall, G.H., 1988, Magmatic arc asymmetry and distribution of anomalous plutonic belts in the batholiths of California; effects of assimilation, crustal thickness, and depth of crystallization: Geological Society of America Bulletin, v. 100, p. 912-927.

Bartley, J.M., Coleman, D.S., and Glazner, A.F., 2008, Incremental pluton emplacement by magmatic crack-seal: Transactions of the Royal Society of Edinburgh: Earth Sciences, v. 97, p. 383-396.

Bateman, P.C., 1992, Plutonism in the central part of the Sierra Nevada batholith: US Geological Survey Professional Paper 1483, 186 p.

Borradaile, G.J., and Henry, B., 1997, Tectonic applications of magnetic susceptibility and its anisotropy: Earth Science Reviews, v. 42, p. 49-93.

Bradford, K.J., 1995, Petrology of a mafic intrusive suite in the central Sierra Nevada, California [M.S. Thesis]: Chapel Hill, NC, University of North Carolina, 63p.

Buddington, A.F., and Lindsley,D.H., 1964, Iron-Titanium oxide minerals and synthetic equivalents: Journal of Petrology, v. 5, p. 310-357.

Burchfiel, B.C., Cowan, D.S., and Davis, G.A., 1992, Tectonic overview of the Cordilleran orogen in the western United States, *in* Burchfiel, B.C., Lipman, P.W., and Zoback, M.L., eds., The Cordilleran Orogen: Conterminous U.S.: Boulder, Colorado, Geological Society of America, v. G-3, p. 9-56.

Carl, B.S., 2000, Structure, Intrusion, and Tectonic Origin of the Independence Dike Swarm, Eastern California [Ph.D. dissertation]: Chapel Hill, NC, University of North Carolina, 269 p.

Carl, B.S., and Glazner, A.F., 2002, Extent and significance of the Independence dike swarm, eastern California: Geological Society of America Bulletin, v. 195, p. 117-130.

Chen, J.H., and Moore, E.F., 1982, Uranium-lead isotopic ages from the Sierra Nevada batholith: Journal of Geophysical Research, v. 87, p. 4761-4784.

Cherniak, D.J., and Watson, E.B., 2000, Pb diffusion in zircon: Chemical Geology, v. 172, p. 5-24.

Clemens, J.D., and Mawer, C.K., 1992, Granitic magma transport by fracture propagation: Tectonophysics, v. 204, p. 339-360.

Clemens, J.D., 1998, Observations on the origins and ascent mechanisms of granitic magmas: Journal of the Geological Society, v. 155, p. 843-851.

Clemons, K.M., and Bartley, J.M., 2008, Field and petrofabric relations of the Long Lake shear zone and the Treasure Lakes phase, Lamarck granodiorite, Central Sierra Nevada, California: Geological Society of America Abstracts with Programs, v. 40, p. 52.

Coleman, D.S., Glazner, A.F., Miller, J.S., Bradford, K.J., Frost, T.P., Joye, J.L., and Bachl, C.A., 1995, Exposure of the late Cretaceous layered mafic-felsic magma system in the central Sierra Nevada batholith, California: Contributions to Mineralogy and Petrology, v. 120, p. 129-136.

Coleman, D.S., Carl, B.S., Glazner, A.F., and Bartley, J.M., 2000, Cretaceous dikes within the Jurassic Independence dike swarm in eastern California: Geological Society of America Bulletin, v. 112, p. 504-511.

Coleman, D.S., Gray, W., and Glazner, A.F., 2004, Rethinking the emplacement and evolution of zoned plutons: Geochronologic evidence for incremental assembly of the Tuolumne Intrusive Suite, California: Geology, v. 32, p. 433-436.

Covey-Crump, S.J., 1997, The high temperature static recovery and recrystallization behaviour of cold-worked Carrara marble: Journal of Structural Geology, v. 19, p. 225-241.

Culey, A.G. and Joplin, G.A., 1937, Evidence of magmatic stoping in a dyke at Hartley, N.S.W.: Journal and Proceedings of the Royal Society of New South Wales, v. 70, p. 327-331.

Dalziel, I.W.D., 1991, Pacific margins of Laurentia and East Antarctica-Australia as a conjugate rift pair: Evidence and implications for an Eocambrian supercontinent: Geology, v. 19, p. 598-601.

Delaney, P.T. and Pollard, D.D., 1982, Solidification of basaltic magma during flow in a dike: American Journal of Science, v. 282, p. 856-885.

Delaney, P.T., Pollard, D.D., Ziony, J.I., and McKee, E.H., 1986, Field relations between dikes and joints: Emplacement processes and paleostress analysis: Journal of Geophysical Research, v. 91, p. 4920-4938.

Engebretson, D.C., Gordon, R.G., and Cox, A., 1985, Relative motions between oceanic and continental plates in the Pacific Basin: Geologic Society of America Special Paper 206, 59 p.

Gaffney, E.S., Damjanac, B., Valentine, G.A., 2007, Localization of volcanic activity: 2. Effects of pre-existing structure: Earth and Planetary Science Letters, v. 263, p. 323-338.

Glazner, A.F. and Bartley, J.M., 2006, Is stoping a volumetrically significant pluton emplacement process?: Geological Society of America Bulletin, vol. 118, p. 1185-1195.

Glazner, A.F., Bartley, J.M., Coleman, D.S., Gray, W., and Taylor, R.Z., 2004, Are plutons assembled over millions of years by amalgamation from small magma chambers: GSA Today, v. 14, p. 4-11.

Glazner, A.F., 2007, Thermal limitations on incorporation of wall rock into magma: Geology, v. 35, p. 319-322.

Hoffman, P.F., 1988, United Plates of America, The Birth of a Craton: Early Proterozoic Assembly and Growth of Laurentia: Annual Reviews in Earth and Planetary Sciences, v. 16, p. 543-603.

Hrouda, F., 1982, Magnetic anisotropy of rocks and its application in geology and geophysics: Surveys in Geophysics, v. 5, p. 37-82.

Hunt, C.P., Moskowitz, B.M., and Banejee, S.K., 1995, Magnetic properties of rocks and minerals: Rock Physics and Phase Relations, A Handbook of Physical Constants, American Geophysical Union, p. 189-203.

Hutton, D.H.W., Dempster, T.J., Brown, P.E., Becker, and Becker, S.D., 1990, A new mechanism of granite emplacement: intrusion in active extensional shear zones: Nature, v. 343, p. 452-455.

Hutton, D.H.W., 1982, A tectonic model for the emplacement of the Main Donegal Granite, NW Ireland: Journal of the Geologic Society, London, v. 139, p. 615-631.

Hutton, D.H.W., 1992, Granite sheeted complexes: evidence for the dyking ascent mechanism: Transactions of the Royal Society of Edinburgh; Earth Sciences, v.

83, p. 377-382.

Karihaloo, B.L. and Huang, X., 1991, Tensile response of quasi-brittle materials: Pageoph, v. 137, p. 461-487.

Knudsen, F.P., 1959, Dependence of mechanical strength of brittle polycrystalline specimens on porosity and grain size: Journal of the American Ceramic Society, v. 42, p. 376-387.

Krogh, T.E., and Davis, D.L., 1975, The production and preparation of 205Pb for the use as a tracer of isotopic dilution analysis: Yearbook – Carnegie Institute of Washington 74, p. 619-623.

Krogh, T.E., 1982, Improved accuracy of U-Pb dating by selection of concordant fractions using a high gradient magnetic separation technique: Geochemica et Cosmochimica Acta, v. 46, p. 631-636.

Lee, S.U., Barnes, C.G., Snoke, A.W., Howard, K.A., and Frost, C.D., 2003, Petrogenesis of Mesozoic, Peraluminous Granites in the Lamoille Canyon area, Ruby Mountains, Nevada, USA: Journal of Petrology, v. 44, p. 713-732.

Leeder, M.R., Mack, G.H., Brasier, A.T., Parrish, R.R., McIntosh, W.C., Andrews, J., and Duermeijer, C.E., 2008, Late-Pliocene timing of Corinth (Greece) rift-margin fault migration: Earth and Planetary Science Letters, v. 274, p. 132-141.

Longiaru, S., 1987, Tectonic evolution of the Oak Creek volcanic roof pendant, eastern Sierra Nevada [Ph.D. dissertation]: Santa Cruz, University of California, 205 p.

Ludwig, K.R., 1989, PbDAT for MSDOS: A computer program for IBM-PC compatibles for processing raw Pb-U-Th isotope data, version 1.06, U.S. Geological Survey Open-File Report 88-542, 40 p.

Ludwig, K.R., 1990, ISOPLOT: A plotting and regression program for radiogenic isotope data, for IBM-PC compatible computers, version 2.02, U.S. Geological Survey Open-File Report 88-557

Mahan, K.H., Bartley, J.M., Coleman, D.S., Glazner, A.F., and Carl, B.S., 2003, Sheeted intrusion of the synkinematic McDoogle pluton, Sierra Nevada, California: Geological Society of America Bulletin, v. 115, p. 1570-1582.

Mahan, K.H., 2000, Wallrock deformation and emplacement of the McDoogle Pluton, Central Sierra Nevada, California [M.S. Thesis]: Salt Lake City, University of Utah, 134 p.

Marsh, B.D., 1982, On the mechanics of igneous diapirism, stoping, and zone melting: American Journal of Science, v. 282, p. 808-940.

Mattinson, J.M., 2005, Zircon U-Pb chemical abrasion ("CA-TIMS") method: Combined annealing and multi-step partial dissolution analysis for improved precision and accuracy of zircon ages: Chemical Geology, v. 220, p. 47-66.

McNulty, B.A., Tobisch, O.T., Cruden, A.R., and Gilder, S., 2000, Multistage emplacement emplacement of the Mount Givens pluton, Central Sierra Nevada batholith, California: Geological Society of America Bulletin, v. 112, p. 119-135.

McNulty, B.A., Tong, W., and Tobisch, O.T., 1996, Assembly of dike-fed magma chamber: The Jackass Lakes pluton, central Sierra Nevada, California: Geological Society of America Bulletin, v. 106, p. 926-940.

Means, W.D. and Park, Y., 1994, New experimental approach to understanding igneous texture: Geology, v. 22, p. 323-326.

Moore, J.G., 1963, Geology of the Mount Pinchot Quadrangle, southern Sierra Nevada, California: U.S. Geological Survey Bulletin 1130, 152 p.

Moore, J.G. and Hopson, C.A., 1961, The Independence dike swarm in eastern California: American Journal of Science, v. 259, p. 241-259.

Mundil, R., Ludwig, K.R., Metcalfe, I., and Renne, P.R., 2004, Age and timing of the Permian mass extinctions; U/Pb dating of closed-system zircons: Science, v. 305, p. 1760-1763.

Nicholson, R. and Pollard, D.D., 1985, Dilation and linkage of echelon cracks: Journal of Structural Geology, v. 7, p. 583-590.

Park, Y. and Means, W.D., 1996, Direct observation of deformation processes in crystal mushes: Journal of Structural Geology, v. 18, p. 847-858.

Parrish, R.R. and Krogh, T.E., 1987, Synthesis and purification of 205Pb for U-Pb geochronology: Chemical Geology, v. 66, p. 103-110.

Parrish R.R. and Noble, S.R., 2003, Zircon U-Th-Pb geochronology by isotope dilution; thermal ionization mass spectrometry (ID-TIMS): Reviews in Mineralogy and Geochemistry, v. 53, p. 183-213.

Parsons, T. and Thompson, G.A., 1991, The role of magma overpressure in suppressing earthquakes and topography; worldwide examples: Science, v. 253, p. 1399-1402.

Petford, N., Cruden, A.R., McCaffery, K.J.W., and Vigneresse, J.L., 2000, Granite magma formation, transport, and emplacement in the Earth's crust: Nature, v. 408, p. 669-673.

Pignotta, G.S., and Paterson, S.R., 2007, Voluminous stoping in the Mitchell Peak Granodiorite, Sierra Nevada Batholith, California, USA: The Canadian Mineralogist, v. 45, p. 87-106.

Pitcher, W.S., Berger, A.R., Spencer, M.O., 1972, The geology of Donegal; A Study of Granite Emplacement and Unroofing: New York, Wiley Interscience, 435 p.

Poole, F.G., Stewart, J.H., Palmer, A.R., Sandberg, C.A., Madrid, R.J., Ross, R.J., Jr., Hintze, L.F., Miller, M.M., and Wrucke, C.T., 1992, Latest Precambrian to latest Devonian time; Development of a continental margin, *in* Burchfiel, B.C., Lipman, P.W., and Zoback, M.L., eds., The Cordilleran Orogen: Conterminous U.S.: Boulder, Colorado, Geological Society of America, v. G-3, p. 9-56.

Price, G.D., 1980, Exsolution microstructures in titanomagnetites and their magnetic signiture: Physics of the Earth and Planetary Interiors, v. 23, p. 2-12.

Prinz, M. and Bentley, R.D., 1964, Cylindrical columnar jointing in dolerite dikes, Beartooth Mountains, Montana-Wyoming: Geological Society of America Bulletin, v. 75, p. 1165-1168.

Ramberg, H., 1972, Theoretical models of density stratification and diapirism in the Earth: Journal of Geophysical Research, v. 77, p. 877-889.

Ramsey, J.G., 1980, The crack-seal mechanism of rock deformation: Science, v. 284, p. 135-139.

Renne, P.R., Tobisch, O.T., and Saleeby, J.B., 1993, Thermochronologic record of pluton emplacement, deformation, and exhumation at Courtright shear zone, central Sierra Nevada, California: Geology, vol. 21, 331-334.

Robinson, D.M. and Miller, C.F., 1999, Record of magma chamber processes preserved in accessory mineral assemblages: American Mineralogist, v. 84, p. 1346-1353.

Rubin, A.M., 1995, Propagation of magma-filled cracks: Annual Review of Earth and Planetary Sciences, v. 23, p. 287-336.

de Saint Blanquat, M. and Tikoff, B., 1997, Development of magmatic to solid-state fabrics during syntectonic emplacement of the Mono Creek granite, Sierra Nevada batholith, *in* Bouchez, J.L., Stephens, W.E., Hutton, D., eds., Granite: From Segregation of Melt to Emplacement Fabrics, Dordrecht, Kluwer Academic,

p. 231-252.

de Saint Blanquat, M., Habert, G., Horsman, E., Morgan, S.S., Tikoff, B., Launeau, P., and Gleizes, G., 2006, Mechanisms and duration of non-tectonically assisted emplacement in the upper crust; the Black Mesa Pluton, Henry Mountains, Utah: Tectonophysics, v. 428, p. 1-31.

Saleeby, J.B. and Busby-Spera, C., 1992, Early Mesozoic tectonic evolution of the western U.S. Cordillera, *in* Burchfiel , B.C., Lipman, P.W., and Zoback, M.L., eds., The Cordilleran Orogen: Conterminous U.S.: Boulder, Colorado, Geological Society of America, v. G-3, p. 107-168.

Saleeby, J.B., Kistler, R.W., Longiaru, S., Moore, J.G., and Nockleberg, W.J., 1990, Middle Cretaceous silicic metavolcanic rocks in the Kings Canyon area, central Sierra Nevada, California, *in* Anderson, J.L., ed., The nature and origin of Cordillern magmatism: Bouler, Colorado, Geologic Society of America, p. 251-270.

Segall, P., 1984, Formation and growth of extensional fracture sets: Geological Society of America Bulletin, vol. 95, p. 454-462.

Sisson, T.W., Grove, T.L., and Coleman, D.S., 1996, Hornblende gabbro sill complex at Onion Valley, California, and a mixing origin for the Sierra Nevada batholith: Contributions to Mineralogy and Petrology, v. 126, p. 81-108.

Solomon, M., 1963, Counting and sampling errors in modal analysis by point counting: Journal of Petrology, vol. 4, p. 367-382.

Steiger, R.H. and Jager, E., 1977, Subcommission on geochronology: Convention on the use of decay constants in geo- and cosmochronology: Earth and Planetary Science Letters, v. 36, p. 359-362.

Stern, T.W., Bateman, P.C., Morgan, B.A., Newell, M.F., and Peck, D.L., 1981, Isotopic U-Pb ages of zircon from the granitoids of the central Sierra Nevada: U.S. Geological Survey Professional Paper 185, 17 p.

Stevens, C.H. and Greene, D.C., 1999, Stratigraphy, depositional history, and tectonic evolution of Paleozoic continental-margin rocks in roof pendants of the eastern Sierra Nevada, California: Geological Society of America Bulletin, v. 111, p. 919-933.

Tikoff, B. and Teyssier, C., 1992, Crustal-scale, en echelon "P-shear" tensional bridges: A possible solution to the batholithic room problem: Geology, v. 20, p. 927-930.

Umhoefer, P.J., 2003, A model for the North America Cordillera in the Early Cretaceous: Tectonic escape related to arc collision of the Guerrero terrane and a change in North America plate motion, *in* Johnson, S.E., Paterson, S.R., Fletcher, J.M., Girty, G.H., Kimbrough, D.L., and Martin-Barajas, A., eds., Tectonic evolution of northwestern Mexico and the southwestern USA: Geological Society of America Special Paper 374, p. 117-134.

Vogel, T.A., Cambray, F.W., and Constenius, K.N., 2001, Origin and emplacement of igneous rocks in the central Wasatch Mountains, Utah: Rocky Mountain Geology, v. 36, p. 119-162.

Wetherill, G.W., 1956, Discordant uranium-lead ages, I: Eos Transactions, v. 37, p. 320-326.